

«ELECTRICAL ENGINEERING & ELECTROMECHANICS»

SCIENTIFIC & PRACTICAL JOURNAL

Journal was founded in 2002 by

National Technical University «Kharkiv Polytechnic Institute»

Co-Founder – State Institution «Institute of Technical Problems of Magnetism of the NAS of Ukraine»



INTERNATIONAL EDITORIAL BOARD

- Klymenko B.V.** Editor-in-Chief, Professor, National Technical University "Kharkiv Polytechnic Institute" (NTU "KhPI"), Ukraine
Sokol Ye.I. Deputy Editor, Professor, Corresponding member of NAS of Ukraine, rector of NTU "KhPI", Ukraine
Rozov V.Yu. Deputy Editor, Professor, Corresponding member of NAS of Ukraine, Director of State Institution "Institute of Technical Problems of Magnetism of the NAS of Ukraine"(SI "ITPM NASU"), Kharkiv, Ukraine
- Batygin Yu.V.** Professor, Kharkiv National Automobile and Highway University, Ukraine
Bíró O. Professor, Institute for Fundamentals and Theory in Electrical Engineering, Graz, Austria
Bolyukh V.F. Professor, NTU "KhPI", Ukraine
Doležel I. Professor, University of West Bohemia, Pilsen, Czech Republic
Féliachi M. Professor, University of Nantes, France
Gurevich V.I. Ph.D., Honorable Professor, Central Electrical Laboratory of Israel Electric Corporation, Haifa, Israel
Kildishev A.V. Associate Research Professor, Purdue University, USA
Kuznetsov B.I. Professor, SI "ITPM NASU", Kharkiv, Ukraine
Kyrylenko O.V. Professor, Member of NAS of Ukraine, Institute of Electrodynamics of NAS of Ukraine, Kyiv, Ukraine
Podoltsev A.D. Professor, Institute of Electrodynamics of NAS of Ukraine, Kyiv, Ukraine
Rainin V.E. Professor, Moscow Power Engineering Institute, Russia
Rezynkina M.M. Professor, SI "ITPM NASU", Kharkiv, Ukraine
Rožanov Yu.K. Professor, Moscow Power Engineering Institute, Russia
Shkolnik A.A. Ph.D., Central Electrical Laboratory of Israel Electric Corporation, member of CIGRE (SC A2 - Transformers), Haifa, Israel
Yufarov V.B. Professor, National Science Center "Kharkiv Institute of Physics and Technology", Ukraine
Vinitzki Yu.D. Professor, GE EEM, Moscow, Russia
Zagirnyak M.V. Professor, Corresponding member of NAES of Ukraine, rector of Kremenchuk M.Ostrohradskyi National University, Ukraine
Zgraja J. Professor, Institute of Applied Computer Science, Lodz University of Technology, Poland

НАЦІОНАЛЬНА РЕДАКЦІЙНА КОЛЕГІЯ*

- Клименко Б.В.** головний редактор, професор, НТУ "ХПІ"
Сокол Є.І. заступник головного редактора, член-кор. НАНУ, ректор НТУ "ХПІ"
Розов В.Ю. заступник головного редактора, член-кор. НАНУ, директор ДУ "ІТПМ НАНУ"
Гречко О.М. відповідальний секретар, к.т.н., НТУ "ХПІ"
Баранов М.І. д.т.н., НДПКи "Молнія" НТУ "ХПІ"
Боев В.М. професор, НТУ "ХПІ"
Веприк Ю.М. професор, НТУ "ХПІ"
Гриб О.Г. професор, НТУ "ХПІ"
Гурин А.Г. професор, НТУ "ХПІ"
Данько В.Г. професор, НТУ "ХПІ"
Жемеров Г.Г. професор, НТУ "ХПІ"
Кравченко В.І. професор, директор НДПКи "Молнія" НТУ "ХПІ"
Мілих В.І. професор, НТУ "ХПІ"
Михайлов В.М. професор, НТУ "ХПІ"
Омельяненко В.І. професор, НТУ "ХПІ"
Пуйло Г.В. професор, ОНТУ, Одеса
Резинкін О.Л. професор, НТУ "ХПІ"
Рудаков В.В. професор, НТУ "ХПІ"
Сосков А.Г. професор, ХНУМГ імені О.М. Бекетова, Харків
Ткачук В.І. професор, НУ "Львівська Політехніка"
Шинкаренко В.Ф. професор, Національний технічний університет України "Київський політехнічний інститут"

* Члени національної редакційної колегії працюють у провідних українських наукових, освітніх та дослідницьких установах

NATIONAL EDITORIAL BOARD*

- Klymenko B.V.** Editor-in-Chief, professor, NTU "KhPI"
Sokol Ye.I. Deputy Editor, corresponding member of NAS of Ukraine, rector of NTU "KhPI"
Rozov V.Yu. Deputy Editor, corresponding member of NAS of Ukraine, Director of SI "ITPM NASU"
Grechko O.M. Executive Managing Editor, Ph.D., NTU "KhPI"
Baranov M.I. Dr.Sc. (Eng.), NTU "KhPI"
Boev V.M. Professor, NTU "KhPI"
Vepryk Yu.M. Professor, NTU "KhPI"
Gryb O.G. Professor, NTU "KhPI"
Guryn A.G. Professor, NTU "KhPI"
Dan'ko V.G. Professor, NTU "KhPI"
Zhemerov G.G. Professor, NTU "KhPI"
Kravchenko V.I. Professor, NTU "KhPI"
Milykh V.I. Professor, NTU "KhPI"
Mikhaylov V.M. Professor, NTU "KhPI"
Omel'yanenko V.I. Professor, NTU "KhPI"
Puilo G.V. Professor, Odessa National Polytechnic University
Rezynkin O.L. Professor, NTU "KhPI"
Rudakov V.V. Professor, NTU "KhPI"
Soskov A.G. Professor, O.M. Beketov National University of Urban Economy in Kharkiv
Tkachuk V.I. Professor, Lviv Polytechnic National University
Shynkarenko V.F. Professor, National Technical University of Ukraine "Kyiv Polytechnic Institute"

* Members of National Editorial Board work in leading Ukrainian scientific, educational and research institutions

Адреса редакції / Editorial office address:

Кафедра "Електричні апарати", НТУ "ХПІ", вул. Кирпичова, 21, м. Харків, 61002, Україна
Dept. of Electrical Apparatus, NTU "KhPI", Kyrpychova Str., 21, Kharkiv, 61002, Ukraine

тел. / phone: +380 57 7076281, +380 67 3594696, e-mail: a.m.grechko@gmail.com (Гречко Олександр Михайлович / Grechko O.M.)

ISSN (print) 2074-272X

ISSN (online) 2309-3404

© National Technical University «Kharkiv Polytechnic Institute», 2016

© State Institution «Institute of Technical Problems of Magnetism of the NAS of Ukraine», 2016

Printed 29.08.2016. Format 60 x 90 1/8. Paper – offset. Laser printing.

Edition 200 copies. Order no.66/172-04-2016.

Design of cover by Vyrovets L.P. e-mail: vsv_2007@ukr.net

Printed by Printing house «Madrid Ltd» (11, Maksymilianivska Str., Kharkiv, 61024, Ukraine)



2016/4

TABLE OF CONTENTS

Electrical Engineering. Great Events. Famous Names

Baranov M.I. An anthology of the distinguished achievements in science and technique. Part 33: electromagnetic compatibility and protection from action of powerful electromagnetic interference of radioelectronic, electrical engineering and electric power equipment 3

Electrical Machines and Apparatus

Vaskovskiy Yu.M., Melnyk A.M., Tytko O.I. Electromagnetic vibration disturbing forces at the eccentricity of rotor of turbogenerator 16

Pantelyat M.G., Doležel I. Finite element technique for solution of thermo-contact problems and its application in numerical analysis of devices working with induction heating 22

Shevchenko V.V. Influence of manufacturing quality of laminated core on a turbogenerator exploitation term..... 28

Electrotechnical Complexes and Systems. Power Electronics

Budashko V.V. Increasing control's efficiency for the ship's two-mass electric drive..... 34

Tugay D.V. Three-phase energy supply systems simulation for the total power losses components assessment..... 43

High Electric and Magnetic Field Engineering. Cable Engineering

Batygin Yu.V., Chaplygin E.A., Sabokar O.S. Magnetic-pulse car body panels flattening. Theoretical aspects and practical results 54

Shchebeniuk L.A., Antonets T.Yu. Investigation of losses in insulation of high-voltage power cables with XLPE insulation 58

Power Stations, Grids and Systems

Zaitsev R.V., Kyrychenko M.V., Kholod A.V., Zaitseva L.V., Prokopenko D.S., Khrypunov G.S. Calculation of operating parameters of high-voltage power take-off system for the photovoltaic facility 63

Information

Petrushin V.S. Methodics, software and laboratory equipment for an innovative electrical engineering discipline 69

M.I. Baranov

AN ANTHOLOGY OF THE DISTINGUISHED ACHIEVEMENTS IN SCIENCE AND TECHNIQUE. PART 33: ELECTROMAGNETIC COMPATIBILITY AND PROTECTION FROM ACTION OF POWERFUL ELECTROMAGNETIC INTERFERENCE OF RADIOELECTRONIC, ELECTRICAL ENGINEERING AND ELECTRIC POWER EQUIPMENT

Purpose. Implementation of brief analytical review of basic scientific and technical achievements in area of electromagnetic compatibility (EMC) and protection from destabilizing and striking action of powerful electromagnetic interference (PEMI) of natural and artificial origin of radioelectronic, electrical engineering and electric power equipment. Methodology. Scientific methods of collection, analysis and analytical treatment of scientific and technical information in a sphere EMC and such areas of knowledge's as radioelectronics, electrical engineering and electric power engineering. Results. A brief scientific and technical review is resulted modern positions problems EMC and protection of equipment from action on them PEMI. It is shown that PEMI can result in failures in-process and death of examined equipment. Annual harm in the industrially developed countries of the world from the striking affecting of PEMI modern equipment with integral microcircuits and semiconductor devices can make ten of milliards of USD. The basic methods of protection of equipment are resulted from PEMI and protective devices (PD), intended for the increase of effectiveness of modern equipment to the action of external PEMI. Principles of work of the resulted PD and their basic technical descriptions are described. Originality. On the basis of materials of scientific monographs, journal publications, normative documents and internet-reports systematization of basic PD, in-use presently in an area EMC and protection of different equipment from the hazard agency of external PEMI is executed. Practical value. Popularization of scientific and technical knowledge's in an area EMC and protection of modern equipment from a dangerous action on them PEMI. Formulation of important for society scientific and technical problems and tasks, arising up in an area EMC and providing of the reliable functioning of modern equipment in power electromagnetic interference. References 50, figures 25.

Key words: electromagnetic compatibility, equipment, powerful electromagnetic interference, protection of equipment from electromagnetic interference, protective devices, review.

Приведен краткий аналитический обзор основных научно-технических достижений в области электромагнитной совместимости технических средств, методов и устройств защиты радиоэлектронного, электротехнического и электроэнергетического оборудования от внешнего воздействия на него мощных импульсных электромагнитных помех, содержащих высокие напряжения, большие токи и сильные электромагнитные поля. Библи. 50, рис. 25.

Ключевые слова: электромагнитная совместимость, технические средства, мощная электромагнитная помеха, защита технических средств от электромагнитных помех, помехозащитные устройства, обзор.

Introduction. Uninterrupted operation of the modern diversified electronic, electrical and power equipment, to provide linking practical implementation are important for a variety of industrial production and technologies, strategic military-technical objects and everyday citizens of any country in the world electrotechnological processes are directly related to the implementation of strict requirements for its *electromagnetic compatibility* (EMC) and protection from destabilizing the second and the harmful effect of external *powerful electromagnetic interference* (PEMI) of natural and artificially origin [1-3]. It is necessary to remind the reader that is currently under the EMC of equipment refers to the ability to operate the vehicle with a given quality at a given electromagnetic environment (EME) and not cause harmful on the amplitude-time parameters (ATP) of electromagnetic interference with other equipment [3]. We point out that in the field of EMC, the term «*electromagnetic interference*» means one or other electromagnetic process, which impairs or may impair the functioning of the equipment, as well as adversely affect the vital functions of the living organism [3]. As for the equipment concepts, then under it in the EMC field refers equipment, apparatus, product, component parts, the functioning of which is based on the known laws of such on-scientific and technical disciplines like electrical

engineering, radio engineering, electricity and electronics, which in its composition contains various electronic components and circuits that perform the following functions: generation, conversion, transmission, reception, storage and switching magnetic and electrical quantities [3]. It should be noted that in the field of EMC the *interference immunity* of the equipment means the ability of the equipment to maintain a given quality of operation when subjected to external electromagnetic interference with regulated values of ATP, given the relevant regulations [3]. Under electromagnetic resistance (*interference resistance*) of equipment in the solution in the EMC field applications means the ability of the vehicle to provide a predetermined quality function and its operation only until certain ATP levels affecting it PEMI specified in the relevant national (international) standards and published scientific and technical literature [4-14]. Continuously expanding worldwide scope of application in the equipment highly sensitive to the effects of PEMI microprocessor devices for control, registration parameters, information exchange and automation of technological processes objectively lead to increased relevance of EMC problems in modern technology [3].

1. Main sources and types of PEMI. First of all, we note that [5, 15, 17] under PEMI refers to such

© M.I. Baranov

electromagnetic interference, the impact of which on the vehicle is the absence in them interference funds not related to the principles of action and the construction of protected device violation of their normal functioning, temporary glitch device operation (reversible failure) or failure (irreversible failure). Sources occurrence PEMI are divided into two main classes: *the first class* – the sources of natural origin; *the second class* - the sources of artificial origin [5, 15]. The main types of PEMI caused sources of natural origin, are [2, 3, 7, 10, 13-17]: *lightning discharges (lightning)* in the atmosphere, characterized in the microsecond time domain amplitude of current flowing in the dozens (hundreds) kA; a powerful *electromagnetic pulse (EMP)*, formed in the Earth's atmosphere by a high-channel lightning and changing in the microsecond time range; *discharges of static electricity* at its potentials tens (hundreds) of kV, occurring in the initial stage in the nanosecond time range. The main types of PEMI caused by man-made sources, according to [4-9, 11-15, 17-19] include: *switching overvoltage* amplitude of tens kV and *short-circuit currents* amplitude of tens kA, resulting in the millisecond time range in industrial electrical network frequency (50/60) Hz and the contact networks of railway and urban electric transport; discharge *large pulse currents* amplitudes in the tens (hundreds) kA and *high electromagnetic fields* with electric field strength up to (10^2 - 10^4) kV/m and magnetic field strength up to (0.3-30) kA/m generated in the nano- and microsecond timeframes by high (extrahigh) voltage electrical installations intended for scientific and electrotechnological purposes; a powerful EMP generated in the Earth's atmosphere by a nuclear explosion, and changing in the nanosecond time range; a powerful EMP generated in the microwave range of the new type of weapon - electromagnetic weapons, based on non-traditional physical principles of its construction and use.

2. Main methods of devices protection from PEMI. According to [2, 15, 17, 18], the main methods of protection from the action on modern devices PEMI are: first, the *structural method* and, secondly, the *method of circuit*. We emphasize that these methods of protection of devices against PEMI not affect the principles of operation and construction of the devices itself. With their practical use of all the device protection from external electromagnetic disturbances are outside the protected electronic components and electrical circuits of devices. Internal «interference» in the vehicle to be protected in the application of such methods to protect them from the action of external PEMI does not happen. The most common methods of practical implementation of the structural protection of the devices from PEMI the method is the use of *electromagnetic screens* located around the device protected and *grounding devices (GD)* which discharge occurring interfering electrical potentials and currents in the ground [3-5, 7, 15]. The method of circuits for protection of devices from PEMI involves the use in hazardous areas and the approach paths to the following electrical equipment protected [1-7, 15, 18-21]: *protection dischargers; surge arresters; varistors; clamping diodes; combined circuits; protective filters; interference compensation devices; devices for*

electromagnetic isolation of circuits; resistive circuits. Here below the technical features and capabilities of these methods and modern safety devices of the PEMI impact on devices.

3. Electromagnetic screens utilization for the equipment protection against PEMI. Microelectronic and microprocessor technology, communication devices, control systems, information processing and transmission, as well as generating a voltage pulse device (currents) and electromagnetic fields (EMF) special forms and ATP and low-current low-voltage converter equipment are shielded from the effects of external PEMI using metal shells of rectangular, cylindrical, spherical and other geometric shapes [3-7]. Theory of device shielding from external electric and permanent magnetic fields and pulsed EMF variables currently developed for metal shells at a high level [3, 21-23]. The main parameter characterizing the electromagnetic shielding effectiveness of the device when exposed to EMF screen attenuation A_e is defined in decibels according to the following expression [5, 15, 21]:

$$A_e = 20 \lg(E_0 / E_i) = 20 \lg(H_0 / H_i), \quad (1)$$

where E_0 , H_0 are respectively the strengths of electrical and magnetic fields acting from outside on the screen and device protected by it; E_i , H_i are respectively the strengths of electrical and magnetic fields penetrated through wall of the screen into its internal area (screening area against EMF) and acting directly on the protected device.

As a rule, the value of strengths E_0 and H_0 presenting in (1) are set. The strength values E_i and H_i can be determined from the calculated ratios, given, for example, for the quasi-stationary mode of penetration of low- and high-frequency EMF different spatial orientation in the non-magnetic and flat, cylindrical and spherical screens in [3, 21-23]. We recall that in the steady-state approximation theory provides screens at finding solutions to Maxwell equations using a single limit consisting in the fact that the wavelength of entering the EMF shield should be much more basic geometric dimensions of the screen used. From (1) it follows that at $E_0/E_i=H_0/H_i=10^3$ screen attenuation of 60 dB numerically. This attenuation of external PEMI through the use of a metal screen corresponding geometric and electrical parameters is sufficient for reliable operation in the standard mode of virtually any of the protected equipment from the above mentioned contact technology. To enhance the screen effect (increase in (1) the numerical values of the ratios E_0/E_i and H_0/H_i) when electromagnetic and magnetostatic shielding protected the vehicle as additional screening tools in the areas of screens irregularities (for example, covers, hatches, vents, etc.) are applied electrically conductive sealing gaskets, conductive waveguide attachment, honeycomb grille, electrically conductive, thin conductive mesh and other screen elements [4, 15, 24].

Note that to create a screen, the attenuation of the field coming from outside electromagnetic interference, can be used metal building with protected devices including steel reinforcement of its concrete elements, equipotential conductors and grounding system [3]. In practice, you must strive to create around the screen

protected devices with a maximum value with respect to (1) screen attenuation A_e . To this end, all metal engineering communications (e.g. pipes, ventilation ducts, the shell of cable products, etc.) entering a building with protected equipment, fittings, metal box doors and windows of the building part of the building should be repeatedly galvanically (electrically) connected to each other, the metallic screen and grounding circuit [3].

4. Grounding devices utilization for the equipment protection against PEMI. The use of GD is one of the most common methods of equipment protection from the influence of their work interference (the induced) of voltages and currents, caused by exposure to these external PEMI and secure environment equipment service [3, 15, 25]. Therefore, in modern conditions the equipment GD considered by us, especially for electric power facilities, must comply with the requirements in the field of EMC and electrical safety of people [26]. These requirements are intended to perform application tasks and equipment protect their staff from PEMI, mainly arising, in particular, due to switching on power in electric networks of power frequency (50/60) Hz, and the impact of the lightning surge currents [27]. GD usually comprises a grounding conductor is rigidly connected to the grounding part of the device (e.g., with a metal screen housing of the equipment) and grounding made of a recessed metal which is in contact with the ground. Components of GD designed to drain into the land of the induced electromagnetic interference in a metal case, screen equipment charges and potentials, reduce stress touching the metal chassis-screen device and step voltage near the protected device (e.g., control cabinet in the territory of the electric power facilities as a substation) to safe levels [3, 15, 25-27]. Currently, GD for electric power objects (EPO) in many of the world countries is normalized, mainly for the grounding resistance values (from fractions to tens of Ω), building on the GD (from hundreds of V to tens of kV) and touch voltage (tens to hundreds V) [27, 28]. The numerical values of these standardized parameters depend strongly on the structural GD performance, the electrical parameters of the soil in which the memory of the grounding and electrical parameters of the protected object (e.g. power object to such parameters include a valid value short-circuit current, the response time of relay protection, voltage class, etc.) [28-30]. Long-term practice of operation of various electrical and power equipment as a part of industrial energy systems shows that the quality and performance of the character it depends essentially on EME GD and respect for him EMC requirements [3]. As a useful technical information on the GD in the power sector, we note that in [31] was introduced long held practically tested at power in Ukraine method of electromagnetic diagnostics (EMD), the state of their GD. When the EMD GD is running at under voltage electricity equipment control of structural memory execution is carried out, as a rule, by an induction method [26, 31].

According to [3, 15, 27] in solving problems of electrical safety personnel and EMC are three types of grounding used for equipment: the first type – *grounding of lightning protection* intended to divert into

the ground pulse current of lightning is usually characterized for its impulse components for up to 500 μs normalized amplitude up to 200 kA and long lasting components to 1000 ms averaged amplitude of 200 A [8, 13, 14]; the second type – *protective grounding* used to ensure the safety of the operating personnel of equipment by galvanic connection of the metal parts of electrical equipment which in normal operating conditions, have practically zero potential, and in the emergency mode of operation may be under stress, to the contour of the ground; the third type – *working grounding*, designed to create a reference equipotential level in electrical circuits and equipment systems, providing the required conditions for the normal mode of operation. In practice, while ensuring effective protection of EPO from the harmful effect of external PEMI applied the concept of the band to protect their equipment and therefore a holistic approach in the use of memory, providing for the installation in different zones of the protected EPO and equipment simultaneously the three types of grounding [3, 15, 26, 27].

5. ATP of main overvoltages at equipment protection against PEMI. According to [3, 18] and the requirements of GOST R 54149-2010 [32] on the quality of electricity in the air dangerous paths (cable) transmission lines, communication lines and control, «suitable» to the equipment EPO from lightning and switching in electricity may occur lightning impulse with an amplitude U_m up to 10 kV at the entrance to the building with protectable equipment (and with amplitude U_m up to 6 kV in the internal wiring of the building with equipment) and switching to the amplitude of U_m up to 4.5 kV overvoltage (Fig. 1).

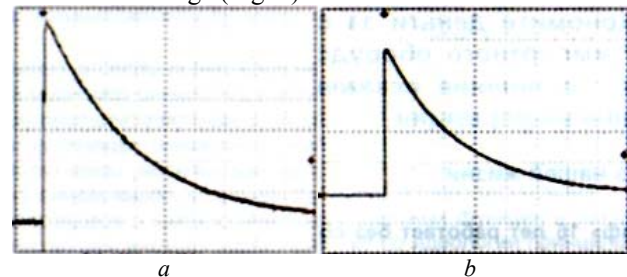


Fig. 1. Lighting (a) and switching (b) overvoltages of aperiodic form at the entrance to the building acting on the equipment (for a – 1/50 μs ; $U_m=10$ kV; the horizontal scale – 25 $\mu\text{s}/\text{cell}$; for b – 250/5000 μs ; $U_m=4.5$ kV; the horizontal scale – 2500 $\mu\text{s}/\text{cell}$) [18]

Network voltage «gaps» and «bursts» are possible. These «gaps» and «bursts» of the voltage in the equipment power supply network can be caused by emergency situations (open neutral when, instead of 220 V may appear voltage up to 380 V) and congestion in the electricity grid caused by connection (especially in winter), large the number of electric heaters. In the latter case, the equipment voltage power network instead of the required 220 V may continuously be in the range (160-180) V [18]. Fig. 2 shows the possible surge of the «gaps» and «bursts» in the power supply voltage.

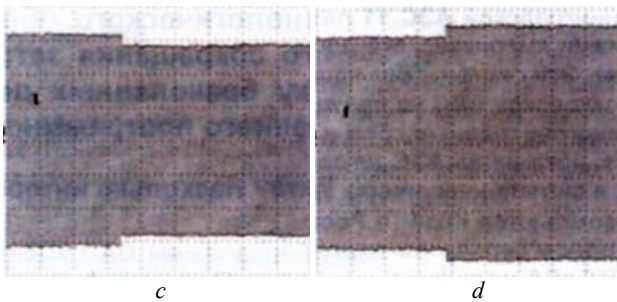


Fig. 2. Overvoltages in the supply network of protected devices caused by the «gap» (c) and the «burst» (d) for 10% of supply network voltage [18]

In addition, the dangerous paths of the above lines, «suitable» to the technical building with protected equipment, because of their exposure to the switching damped sinusoidal currents in EMP said electromagnetic nature may experience high «ringing wave» type surge frequency up to 0.1 MHz U_m amplitude up to 4 kV or at a frequency of 1 MHz at U_m up to 2 kV [18].

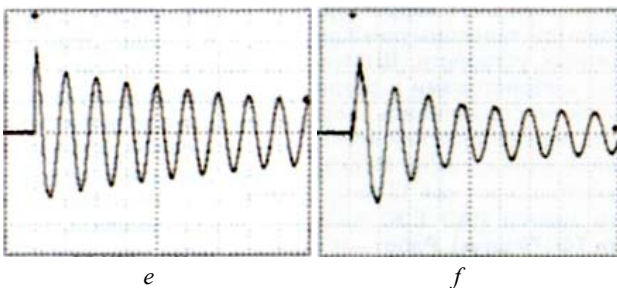


Fig. 3. Overvoltage of «ringing wave» type frequency up to 0.1 MHz with amplitude U_m up to 4 kV (e, the horizontal scale – 10 μ s/cell) and frequency of 1 MHz with amplitude U_m up to 2 kV (f, horizontal scale – 1 μ s/cell) in dangerous paths lines entering the building with protected equipment [18]

When choosing protection devices against interference with the equipment you must not forget about the possible surges in the electrical grid caused by short «bursts» feeding device voltage from 220 to 380 (Fig. 4,g), as well as the transient interference voltages aperiodic time form 5/50 ns with an amplitude U_m up to 2.5 kV (Fig. 4,h), «coming» on dangerous paths before us line to the entrance of the building with protected equipment [18]. Using the above data for the ATP major surge arising in «suitable» to the building with the equipment paths, consider further possible ways of their limitations.

We mention the fact that in 2012 at the Research and Designing Institute «Lightning» of the NTU «KPI» the generator of standard aperiodic switching voltage pulses of positive (negative) polarity temporary form 205/1900 μ s with amplitude of up to 2000 kW was created that meets the current requirements of today interstate [9] and is designed for field testing of full-scale power generation facilities to the electric strength of the outer (inner) insulation [33].

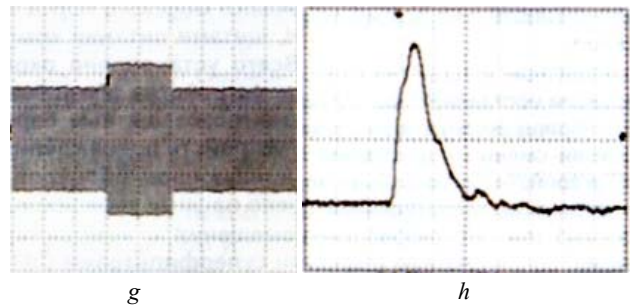


Fig. 4. Overvoltage in the mains protected and due to short-term «burst» are inside equipment building supply mains voltage from 220 to 380 V (g) and overvoltage in a dangerous path «suitable» to the entrance of the building with equipment caused by nanosecond pulse interference temporary form 5/50 ns (h, $U_m=2.5$ kV; the horizontal scale – 50 ns/cell) [18]

6. Some peculiarities of protection of low- and high-current equipment against PEMI. Disconnection of overvoltages (currents) of short-circuit and switching overvoltages (currents) in the industrial power supply low- and high-current devices or acting on their impulse currents (overvoltages) of lightning by electromechanical switches (EMS) it would probably be the simplest and most reliable protection of the equipment from the action on the they overvoltages from data PEMI. However, the work is especially low-voltage electronic circuits and related electronic and other electrical equipment at the indicated times and external PEMI by EMS operation in hundreds of ms is absolutely impossible. To implement the protection of such equipment their application of only EMS is not enough. In this case, to protect low- and high-current devices circuits by threatening them fast transient electromagnetic processes caused by emergency situations (e.g., short-circuit, switching, lightning strike and other factors), in the «appropriate» to them networks of power supply, cables, and the resulting they need such interference protection devices (IPD) which are able to disable (limit to safe levels) specified overvoltage (currents) for the dozens (hundreds) of nanoseconds. We will try to consider the following basic IPD suitable for the protection of the low- and high-current device circuits of the action of overvoltages caused by external PEMI of different nature.

7. Dischargers application for the equipment protection against PEMI. Most current IPD on the first (rough) restrictions stage affecting the protected devices overvoltaged contain two-electrode gas-filled high-voltage (less air) gaps [3, 15, 18, 34, 35]. Gas-filled surge arresters (Fig. 5) installed near the places of input power buses, potential equalization and grounding in the protected objects from the vehicle. Their task is to ensure the protection of the vehicle from the effects of the possible overvoltage by reducing them to a small level. Voltage their trip due to time-dependent characteristics of the ignition fuses is difficult to determine. They have sealed glass (ceramic) body filled with noble gas (argon or neon) [3, 35]. Metal electrodes in their discharge gap covered with a special thin layer of activator. They are capable of switching current pulses time 8/20 μ s with amplitude of up to 40 kA. In order to ensure the spread of small bit DC, these gaps are in a weak radioactive coating [3, 35].

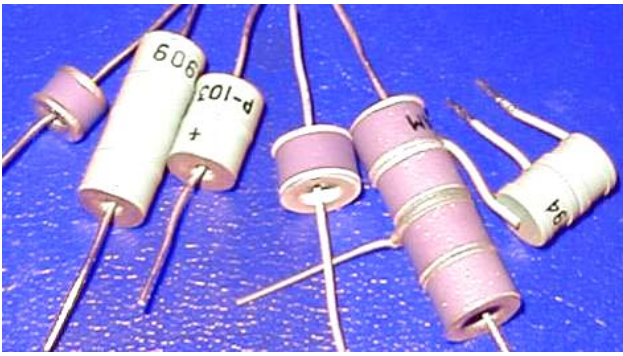


Fig. 5. External view of low-power gas-filled surge arresters (type P-103, and others) that can «skip» pulse currents 8/20 μ s with amplitude of up to 10 kA [35]

After the ignition of gas-filled voltage arrester between their first electrodes decreases to the glow discharge voltage (up to 100 V) and then with increasing switching current – to the electric arc voltage (to about (10-20) V) [3]. This type of arrester is triggered in the microsecond range (response time for their best designs up to microseconds). The AC voltage circuits they arc with accompanying shock itself unable to extinguish. In low-voltage networks DC arc like gas arrester extinguish independently [35].

Fig. 6 is an external view of the gas-filled surge arresters type the GDT, able to dissipate relatively high heat, «introduced by» in PEMI chain. Gas-filled dischargers GDT are used in telecommunications equipment, telephones and radio transmission equipment.



Fig. 6. External view of gas-filled dischargers GDT used in remote control and radioengineering [35]

It should be emphasized that own electric capacity of these gas-filled surge arresters is extremely small. So they cannot make a material misstatement of the useful electric signal. [35] Fig. 7 is an overall view of powerful lightning protection dischargers (RF) that can protect expensive electronic equipment from the direct effects of lightning current discharges [36].

Shown in Fig. 7 lightning protection dischargers are able to «pass» through itself and then sent to the standard grounding aperiodic current pulses 10/350 μ s lightning amplitude to (50-100) kA [36]. The main objective of these fuses when the vehicle protection PEMI is to limit the lightning surge to a residual level prescribed by it (from 1 to 2.5 kV) [35, 36]. Fig. 8 is an external view of foreign lightning protection dischargers with some of the best specifications [35].



Fig. 7. External view of powerful lightning protection dischargers used in the protection of electronic equipment against overvoltage caused by a direct blow to it of lightning (from left to right: P-77-1B and P-59 type) [36]



Fig. 8. The appearance of powerful lightning protection dischargers COMBTEC VV 335 and COMBTEC VS 335 type switching pulse currents 10/350 μ s lightning amplitude of up to 40 kA and limiting lighting overvoltages for electrical equipment to the level of 1 kV [35]

Fig. 9 presents a «line» of LV lighting protection dischargers (LPDL) developed by «EMSOTECH» Company (RF) [18, 37], designed to protect low-voltage bushings (220/380 V) in the building of low-voltage windings of transformers, autonomous energy sources (e.g., diesel-generators) and cable insulation from the effects of lightning and switching surges. These LPDL can reliably switch the lightning current pulses of a standard form of temporary 10/350 μ s with an amplitude I_m 25 to 100 kA [18, 37].



Fig. 9. External view of powerful LV lighting protection dischargers ПГЗН type (from left to right: ПГЗН-3/100-220 for $I_m=100$ kA; ПГЗН-3/50-220 for $I_m=50$ kA; ПГЗН-3/25-220 for $I_m=25$ kA; «EMSOTECH» Company, Kaluga, RF) [18, 37]

On the basis of these dischargers ПГЗН-3/100-220 (see Fig. 9) by specialists of the Russian «EMSOTECH» Company were created panels lightning protection, low-

voltage type ПГЗН (Fig. 10) which in 2010 found their practical implementation of the new system of lightning protection modern radio-complex of the RF to recognize space objects, the external view of which is shown in Fig. 11 [18].

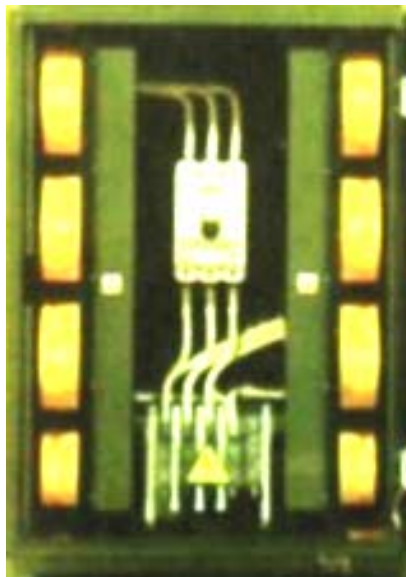


Fig. 10. General view of the panel low-voltage lightning protection redundant type ПГЗН-P-3/100-220 ($I_m=100$ kA; discharger type – ПГЗН-3/100-220; impulse breakdown voltage of each of eight dischargers – 4 kV; RF) [18, 37]



Fig. 11. General view of a unique radio-optical recognition complex of space objects (RF) equipped with a number of lightning protection panels type ПГЗН-P to protect against direct strokes of lightning in its elements [18, 37]

8. The use of overvoltage protective devices for the equipment protection against PEMI. Currently, non-linear overvoltage protective devices (OPD) are one of the most effective means of protection from various devices PEMI [38]. OPD (Fig. 12) is a high-voltage electrical apparatus designed to protect power grids of medium and high grade AC power frequency voltage and therefore we are considering switching from electrical and atmospheric (storm) surge. This unit can be called «*discharger without spark gaps*» [38]. Unlike traditional valve dischargers with spark gaps and carborundum resistors OPD does not contain spark gaps and consist only of the nonlinear resistors column («*pellets*») performed on the basis of zinc oxide and enclosed in a porcelain or polymer casing. The design of the OPD

allows their production in the form of one-column and multi-column devices.



Fig. 12. General view of widely used in power industry one-column OPD with polymer tires, providing reliable protection of their nonlinear resistors weatherproof [38]

The main element of the nonlinear resistors in OPD is a *varistor* performed usually in the form of «*tablets*» of zinc oxide (ZnO) with an outer sheath of glyptal enamel boosting its throughput current value [38]. Varistor material based on said oxide mixed with other metal oxides is a semiconducting structure consisting of a plurality of series-parallel connected *p-n* junctions [38]. This material, as compared with the resistor material in valve arresters has an increased capacity and highly linear current-voltage characteristic (CVC). It is because of this CVC varistors and, accordingly, the OPD can be energized for a long time, which provides a high level of protection of electric power equipment [38].

In normal operating mode, the current through the OPD is capacitive in nature and amounts to a few tenths of mA. If you have PEMI and therefore the impact on the non-linear resistors surge arrester their working material goes into a conducting state with low resistance, thereby limiting further growth overvoltage to a level safe for the protected electrical insulation and other equipment [38]. At the same time through the arrester can «*pass*» pulse currents with amplitudes of tens of kA. With the disappearance of the overvoltage OPD returns to its original non-conducting state. The values of operating voltages for OPD vary widely – from 3 to 750 kV [38-40]. The main places of installation of high-voltage arresters are open (closed) at the power distribution devices and approaches to buildings with equipment. Known in the world of manufacturers of such arresters are [38, 39]: «*Dervasil*» (SICAME Group, France); «*Siemens*» (Germany); «*ABB*» (Switzerland); «*SevZapProm*» (RF). In Ukraine, the forefront of manufacturing technology in the OPD 3-150 kV voltage class for the needs of the electric power company took ES «*Polymer*» (Artemovsk, Donetsk region) [40].

Fig. 13 is an external view of single- and multi-phase surge OPD designed to protect consumers of electricity, powered by electric networks with the frequency (50/60) Hz, surge, switching surge, differential surges and high frequency noise [41]. OPD in this case is established between the phase and earth or neutral conductor and earth. This necessarily requires a

grounding wire for the subsequent «reset» pulse of heat from PEIMI in grounding.

In actuality, the importance and the urgent need for greater use of OPD in the industrial power generation, high voltage (low voltage) electrical, remote control and electronics indicates that according to the American company «General Semiconductor» financial losses in the US industry of today only on the harmful effect on its development surge infrastructure (current) from the considered PEIMI up to 10 billion USD per year [42].



Fig. 13. A general view of one (left) and three-phase (right) OPD used in electric alternating voltage (current) of power frequency (50/60) Hz during input switching, main switchboards and equipment of apartment billboards residential buildings (manufacturer - «Schneider» Company, Germany) [41]

9. Varistors utilization for the equipment protection against PEIMI. As we know, the *varistor* is a semiconductor resistor whose resistance varies nonlinearly by an applied voltage thereto [38, 43]. Earlier in the Electrical and Electronics Engineering used varistors fabricated based on silicon carbide. Currently, commonly are used zinc oxide varistors for different values of power dissipation [3, 38]. The varistor has a symmetrical non-linear CVC. With increased acting voltage its resistance drops dramatically. Therefore, at a voltage pulse action on the varistor electric potential appearing on it may be limited. This physical property is used varistors when used in relation to the external electrical circuits protected equipment (Fig. 14) as a protective device against overvoltage limiting PEIMI. Varistors respond to their appearance on the pulse voltage for a nanosecond. Therefore, they have a short response time – (20-50) ns. While gas filled surge dischargers are activated in the microsecond time range ($\geq 1 \mu s$) [3, 18, 44].

Fig. 15 shows the combined interference waveform of current i and voltage u of a powerful varistor type Protec BR 150/320 (manufacturer – company «Iskra-protection»; Slovenia) tested the effects of «the incident» at him a standard impulse current of 10/350 μs of artificial lightning [3, 13].

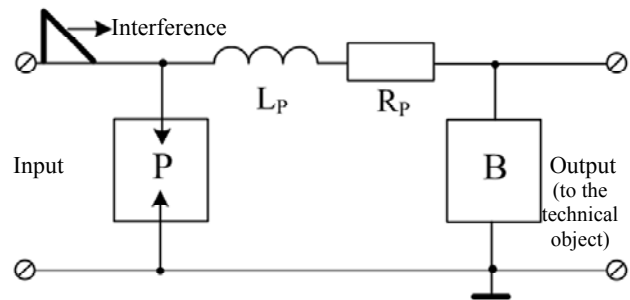


Fig. 14. IPD circuit with two voltage arresters against interference – discharger and varistor (P – high-voltage discharger; B – high-voltage varistor; R_p, L_p – active resistance and inductance of decoupling element in two-line electrical circuit of the IPD) [3]

For ease of processing of experimental data in Fig. 15 u voltage waveform interference on said varistor has been shifted to the right by one cell with respect to the waveform interference current flowing through it i . From the data in Fig. 15 it shows that the interfering current i across the varistor is almost linear decrease in its amplitude of about 21 kA [3]. Voltage u on the test through the varistor 400 μs after the interference amplitude of about 4 kV and accordingly the start of the overvoltage (current) assumes the value of about 1 kV. In was to remain almost unchanged duration of interference pulse current i u simulated lightning voltage across the varistor. However, some distortion in the shape of the voltage pulse interference u in Fig. 15 «made» wire connecting the varistor to our potential and grounded electrical conductors tested protective circuit. In this connection, the wire connection must be carried out in practice is extremely short in length [3]. A common disadvantage of varistors used in power networks with voltages 220/380 device to protect against overvoltage is relatively high residual voltage limitation (1 to 2.5 kV). In this regard, in their application required the second stage overvoltage limitation [3, 38].

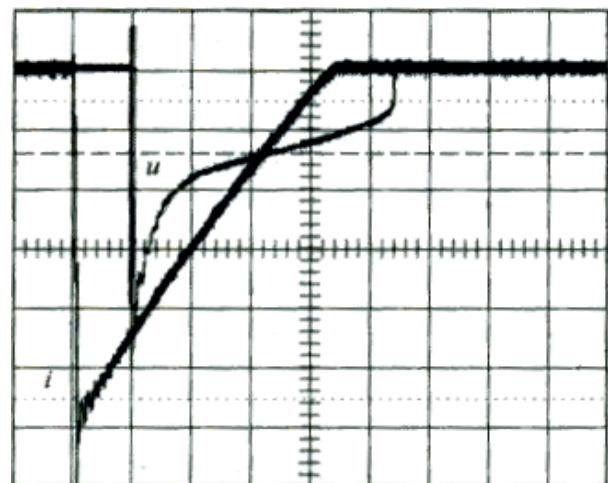


Fig. 15. Combined lightning current waveform interference i of aperiodic temporary form 10/350 μs affecting the varistor voltage and u interference the varistor (the vertical scale for the current – 3.7 kA/cell, the vertical scale for the voltage – 800 V/cell; the scale horizontal for time – 200 μs /cell) [3]

As shown in Fig. 14 protective circuit is necessary to coordinate the arrester varistor parameters P and B . This

coordination can be done through the use of elements of their isolation, as might be used resistors and inductance. The use of coils for decoupling dischargers and varistors is very limited [3]. Typically, such elements as are used wire junction equipment mains. According to the data of [3] between the overvoltage discharger P and powerful high-voltage varistor B the length of the network cables power supplied to the vehicle, should be about 10 m. The length of the wires of the network between the varistor B and protected the device should be at least 5 m [3].

One of the advantages to the gas-filled dischargers varistors is that they are not short-circuited when triggered circuit. Therefore, varistors elements as IPD are used in many power circuits of the device. A relatively large electrical capacitance varistor limits their use in high-frequency electrical circuits (in this case, due to such parasitic capacitance value of the additional attenuation and distortion of the desired signal can occur) [3, 38].

10. Limiting diodes utilization for equipment protection against PEMI. Most sensitive to the effects of surge voltages (currents) induced by EMP natural (artificial) origin, as well as caused by switching and atmospheric (lightning) processes at the «appropriate» to the building of a protectable equipment wires and cables, are the devices connected to them with integrated microcircuits (IMC) and semiconductors. It is known that the minimum energy, causing unrecoverable damage sensitive action PEMI semiconductor devices and IMC ranging from 10^{-2} to 10^{-7} J [7, 42]. In addition to the gas-filled dischargers and metal oxide varistor one of the main security features are also TVS (Transient Voltage Suppressor)-diodes [3, 42]. In the domestic literature they are called «suppressor» or «diodes for transients suppression». TVS-diodes are often confused with Zener diodes [42]. Note that the TVS-diodes have been specially developed for the first time in the United States to protect electronic equipment from various equipment influence on it powerful overvoltages. Silicon Zener diodes intended for voltage control and are not designed to work with large circuits pulsed electric loadings. Abroad TVS-diodes known under the following names: Transil, Insel, Transzorb, etc. We note that the response time for asymmetrical TVS-diode is on the order of 10^{-12} s, and for balanced - about $5 \cdot 10^{-9}$ s [42]. Pulse currents limit for them ranged from a few to hundreds of amperes and voltage limits - from a few to hundreds of volts [3, 42]. Another important characteristic of these diodes is a typical capacitance of $p-n$ junction, is up to 100 pF [42]. This allows the use of TVS-diodes for protection of communication lines with the current frequency to 100 MHz from surge, as well as many radio-frequency circuits, which include sensitive to transient electromagnetic processes of semiconductor devices and IMC. The principle of the TVS-diode which has a pronounced non-linear current-voltage characteristics is explained in Fig. 16. In normal operation of the protected circuit (electrical load) TVS-diode «invisible» and it does not affect its operation. In the event of over-voltage pulse to the TVS-diode, the amplitude of the voltage exceeds its avalanche breakdown, he «opened» and «misses» by itself

on the ground threatening the protected device electric current. At the same time he also carries out and limiting «coming» surge voltage to a safe level [3].

The principal feature of the TVS-diode of the gas-filled dischargers is that their breakdown voltage is below the voltage limit. For arresters same voltage electrical breakdown of the insulating gaps significantly higher discharge sustain voltage. Therefore, when using the TVS-diode protected circuit are not shunted after passing through their $p-n$ junctions powerful impulse noise current.

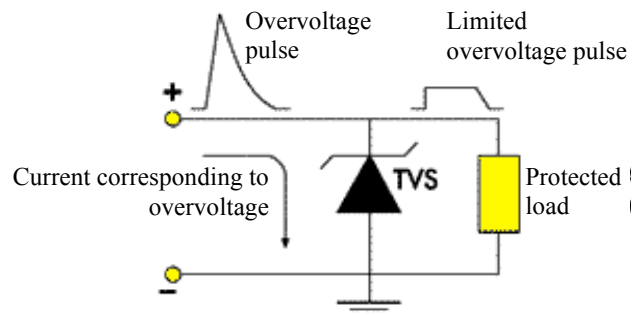


Fig. 16. The simplest electrical circuit explaining the physical principle of TVS-diode operation [42]

11. Utilization of combined IPD for the equipment protection against PEMI. In practice, the protection of many of the devices from the harmful effect they have found application PEMI multistage surge arresters that use both in the same IPD we have described above the gas-filled dischargers, varistors and metal oxide TVS-diodes. In such protective circuits used high performance of some elements and reduces the influence of other elements on the shortcomings of such circuits functioning of the process. Fig. 17 shows the vehicle three-stage protection circuit with overvoltages decoupling elements [3, 7].

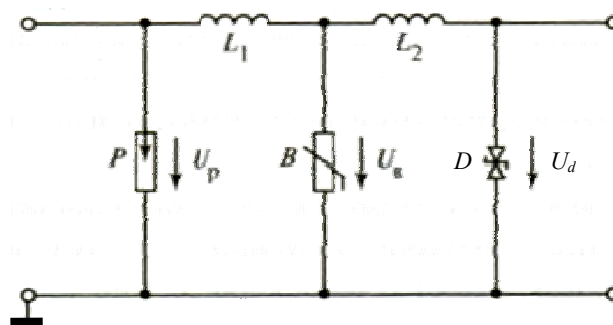


Fig. 17. Schematic diagram of the combined equipment protection with semiconductor devices and IMC from interfering overvoltage and overcurrent (P – gas-filled discharger; B – metal oxide varistor, D – counter included limiting TVS-diodes; L_1, L_2 – decoupling inductances) [3, 7, 15]

When the input to the protection circuit according to Fig. 17 pulse overvoltage or conductive interference TVS-diodes are activated first (*fine protection*) ensuring high speed IPD (up to nanoseconds) [3, 42]. These diodes are capable of passing pulse current interference $8/20 \mu s$ with amplitude of 0.6 kA at a voltage of its avalanche breakdown to 6 V [3, 42]. In this part of the current PEMI diverted to the ground, and at the entrance of the

protected equipment voltage U_{II} is limited in accordance with the CVC used TVS-diode (up to 10 V). Further increasing tension on isolated element L_2 triggers the varistor B , the discharging of the current interference is also on the ground and limiting interference voltage U_B to around 100 V [3]. Then increase the voltage on the decoupling inductances L_1 and L_2 triggers arrester P (coarse protection), in addition to discharging ground current interference. Due to the separation of thermal energy in the spark gap F and the low value of the remaining voltage on it (up to 20 V) facilitates the work of the varistor B . At the same time, a varistor in a certain extent, protect the gap from P electrothermal effect on its working elements PEMI current and possible destruction. The limiting voltage U_p at the discharger P is about 1 kV. Thus, the combined IPD (see Fig. 17) can be realized a significant decrease in overvoltage caused by external PEMI. At the time, this conclusion was confirmed experimentally by the author [45]: three-tier application under consideration device protection scheme PEMI lightning origin enabled through the use of 1,5KE6,8A type TVS-diode ($U_{\text{II}} \approx 6.8$ V), MOV type FNR07K820 ($U_B \approx 135$ V) and the gas-filled spark discharger type LSA140 ($U_p \approx 1.1$ kV) to reliably protect from direct (indirect) impacts RS-485 communication interface lightning line for providing information interaction in a complex EME electronic computing means radio engineering complex, designed and developed in Ukraine.

12. Filters utilization for the equipment protection against PEMI. In the field of EMC and equipment protection from interference, most problems arise from penetration PEMI the protected electrical equipment through the communication circuit, and power management. Therefore, protection of the vehicle power supply networks in the world paid much attention. Fig. 18 is a general view of the German line filter (LF) type FMW2-41-B/1, intended for the protection of industrial power supply circuits in the workplace and at home against pulse PEMI [46]. Schematic diagram of the SF is shown on top of its metal casing monitor. According to Fig. 18 electrical parameters of the LF are: input capacitance – 15 nF; inductances – 0.8 mH; output capacities – 2.2 nF.



Fig. 18. External view of the line filter for protection against pulse PEMI (current – 6 A; voltage – 250 V; frequency – 50/60 Hz; manufacturer – «Schurter» Company, Germany) [46]

Fig. 19 is a external view of another modification of the German LF used in suppressing PEMI coming by power network wires [3].



Fig. 19. External view of the line filter for the PEMI suppression B84115-E-B30 type (current – 6 A; voltage – 250 V; frequency – 50/60 Hz; manufacturer – «Epcos» Company, Germany) [46]

Typically, LF are a low pass filters (LPF) installed in the power supply circuits of most electronic devices. Fig. 20 is an external view of the inner «filling» EMI-filter used for the protection of automation equipment from the effects of high-frequency PEMI [47].



Fig. 20. External view of the EMI-filter (with open plastic cover of the insulating housing LPF) for protection against impulse interference of automation and control devices (current – 10 A, voltage – 260V, frequency – 50/60 Hz) [47]

Fig. 21 shows a circuit diagram of a interference protection EMI-filter used for suppressing PEMI in automation and control circuits [47].

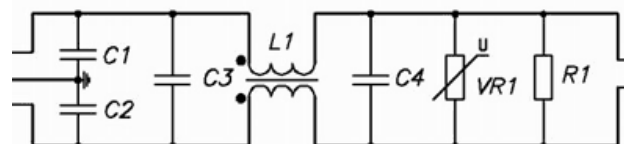


Fig. 21. A circuit diagram of the EMI-filter to for the protection against pulse interference of automation and control circuits

13. Correctors, compensators and relays-voltage circuit breakers utilization for the equipment protection against PEMI. In cases where the mains voltage supply of computer equipment and information (CEI) is reduced to a level of 200 V or less, or increased to a level of 240 V or more, which leads to malfunction

CEI, in order to protect the equipment from external PEMI commonly used voltage correctors (VC). Fig. 22 shows the external views of IPD KH type developed by «EMSOTECH» Company (Kaluga, RF) [18].

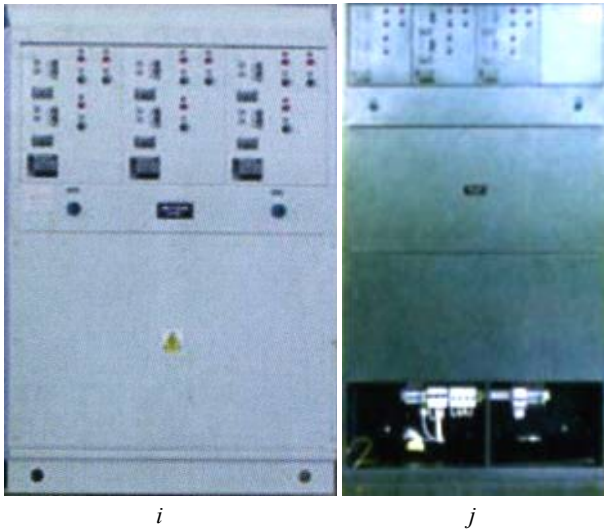


Fig. 22. External views of voltage correctors type KH-T-63-Б (*i*, power – 63 kW; load current – 95 A) and type KH-T-40-C (*j*, power – 40 kW; load current – 60 A) [18]

To protect the supply of higher harmonics and unloading neutral in three-phase networks CEI power compensators applied voltage distortion (CVD). Fig. 23,*k* is a external view of one type of such compensators type КИИ-25-Д (power – 25 kW, the load current – 40 A) [18]. To compensate for the «failures» of the voltage in the power network using triggered after 200 ms compensators of «failures» voltage (CFV) in CEI supply network caused by the influence of her external PEMI [18]. Fig. 23,*l* is an external view of one type of such compensators type КИИ-Т-40-Б (power – 40 kW, the load current – 60 A) [18].

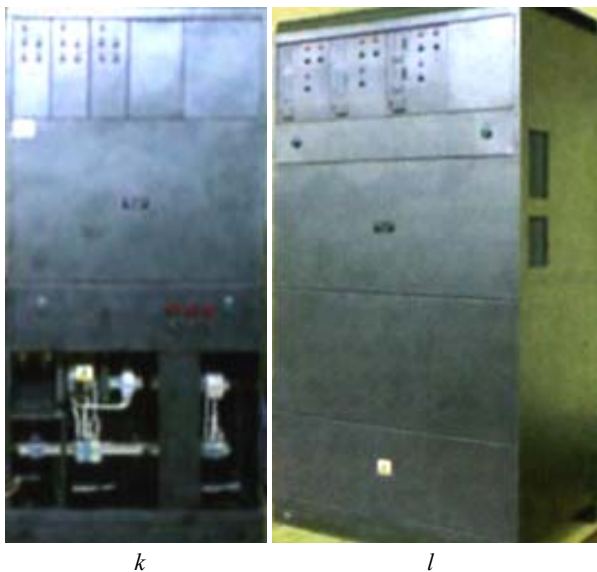


Fig. 23. General views of the power compensator applied voltage distortion type КИИ-25-Д (*k*, power – 25 kW; load current – 40 A) and compensator of «failures» voltage type КИИ-Т-40-Б (*l*, power – 40 kW; load current – 60 A) [18]

Specified in this section IPD (VC, CVD and CFV) effectively protect modern CEI, avionics and electrotechnological equipment, which are critical to a change in power supply voltage to the (20-40) % of the nominal level.

Fig. 24 is a general view of the voltage relay VOLT CONTROL RN-104 type (40 A) produced in Ukraine and intended for disconnection from the network of household power supply (industrial) electronics up to 9 kW to the desired delay in unacceptable voltage fluctuations in its electricity network with automatic insertion after restoring network settings [48].



Fig. 24. External view of the domestic voltage relay type VOLT CONTROL PH-104 (current – up to 40 A; voltage – (160-280) V; delay time – (5-900) s; Ukraine) [48]

14. Electromagnetic isolation of external circuit utilization for the equipment protection against PEMI.

One of effective methods of reducing the influence of external PEMI on the functioning of the equipment inside the building is the external electromagnetic isolation of electrical circuits, «suitable» to the protected building with device or «exhaust» of it [3, 15, 19]. The main methods of electromagnetic isolation of external electrical circuits of considered equipment concerns [3, 15, 19]: application of decoupling inductances are often implemented at the expense of the electrical parameters of «suitable» to the device protected power supply wires; the use of an isolation transformer, installed in the gaps of electrical circuits and grounding circuits; installation in the gap the pair of phase and neutral conductors of the longitudinal choke; use bifilar choke with ferrite rings; application in the chain breaks optoelectronic circuits (e.g., optocouplers, optocoupler diode, transistor optocouplers, optical fiber communication lines, etc.).

15. Resistive circuits utilization for the equipment protection against PEMI. Currently, in the protection of powerful high-voltage capacitor bank energy content in hundreds kJ of fault currents and micro-millisecond duration and amplitude of up to hundreds of kA, capable

of causing destruction explosion-punched high-current electrical discharge capacitors with metal and insulating housings have been used new resistive circuits [49, 50]. Fig. 25 is a general view of a fragment of a powerful high-voltage capacitive energy storage (CES) single-module performance developed by the Research and Designing Institute «Lightning» of the NTU «KPI» and intended to form in laboratory conditions on a low-resistance and low-inductance electrical load major components of pulse current artificial lightning with standardized ATP [49] and which was used to protect the resistive circuit capacitors from its fault currents on the basis of the type of resistors TBO-60-24 Ω .



Fig. 25. General view of a fragment of a powerful high-voltage CES single module performance at a rated voltage of ± 50 kV and rated stores electric energy 420 kJ with its parallel-connected capacitors type ИК-50-3 in the amount of 112 pieces. and rigidly mounted on their findings of high-volume constant high voltage protective graphite-ceramic resistors TBO type-60-24 Ω [49]

The above protection scheme based on the use of the composition of high voltage graphite-ceramic fixed resistors type TBO-60 with value of resistance from 24 to 100 Ω installed directly on the high-voltage output of individual capacitors. In [20, 21] were brought engineering and technical advice on the construction of such protection schemes and approximate ratio calculated by the choice of the protective resistors depending on the developer used a high-voltage pulse technique of constructing principle (single or multi-module version) powerful electrical capacitor banks.

Conclusion. The solution of the global problem of EMC and protection against the harmful effect of PEMI of natural and artificial nature of radioelectronic, electrical and power equipment requires for the successful achievement of the above objectives more active and widespread use on general industrial and domestic levels of effective IPD in various designs.

REFERENCES

1. Khabiger E. *Elektromagnitnaia sovместimost'. Osnovy ee obespecheniia v tekhnike* [Electromagnetic compatibility.

- Fundamentals of its maintenance technique]. Moscow, Energoatomizdat Publ., 1995. 304 p. (Rus).
2. Dyakov A.F., Maksimov B.K., Borisov R.K. *Elektromagnitnaya sovместimost' v elektroenergetike i elektrotekhnike* [Electromagnetic compatibility in power engineering and electrical engineering]. Moscow, Energoatomizdat Publ., 2003. 768 p. (Rus).
3. Dyakov A.F., Kuzhekin I.P., Maksimov B.K., Temnikov A.G. *Elektromagnitnaya sovместimost' i molniezashchita v elektroenergetike* [Electromagnetic compatibility and lightning protection in the power]. Moscow, MEI Publishing House, 2009. 455 p. (Rus).
4. Ricketts L.U., Bridges J.E., Mayletta J. *Elektromagnitnij impul's i metody zashchity* [Electromagnetic pulse and methods of protection]. Moscow, Atomizdat Publ., 1979. 328 p. (Rus).
5. Kravchenko V.I., Bolotov E.A., Letunova N.I. *Radioelektronnye sredstva i moshchnye elektromagnitnye pomехи* [Radioelectronic means and powerful electromagnetic hindrances]. Moscow, Radio and Communications Publ., 1987. 256 p. (Rus).
6. Myrova L.O., Chepizhenko A.Z. *Obespechenie stojkosti apparatury svyazi k ionizyruyushchim i elektromagnitnym izlucheniyam* [Ensuring stability of communications equipment to the ionizing and electromagnetic of radiations]. Moscow, Radio and Communications Publ., 1988. 296 p. (Rus).
7. Kravchenko V.I. *Hrozozashchita radioelektronnykh sredstv* [Lightning protection of radioelectronic facilities]. Moscow, Radio and Communications Publ., 1991. 264 p. (Rus).
8. Baranov M.I. *Izbrannye voprosy elektrofiziki. Tom 2, Kn. 2: Teoriia elektrofizicheskikh effektov i zadach* [Selected topics of Electrophysics. Vol.2, Book 2. A theory of electrophysical effects and tasks]. Kharkiv, NTU «KhPI» Publ., 2010. 407 p. (Rus).
9. *GOST 1516.2-97. Elektrooborudovanie i elektroustanovki peremennogo toka na napriazhenie 3 kV i vyshe. Obshchie metody ispytaniy elektricheskoi prochnosti izoliatsii* [GOST 1516.2-97. Electrical equipment and electrical options of alternating current voltage 3 kV and above. Common test methods for dielectric strength]. Minsk, Publishing house of standards, 1998. 31 p. (Rus).
10. *GOST 30585-98. Stoikost' k vozdeistviu grozovykh razriadov. Tekhnicheskie trebovaniia i metody ispytaniy* [GOST 30585-98. Resistance to lightning. Technical requirements and test methods]. Kiev, State Standard of Ukraine Publ., 1998. 27 p. (Rus).
11. *GOST R 50746-2000. Sovместimost' tekhnicheskikh sredstv elektromagnitnaia. Tekhnicheskie sredstva dlia atomnykh stantsii. Trebovaniia i metody ispytaniy* [GOST R 50746-2000. Compatibility of technical equipment. Technical equipment for nuclear power plants. Requirements and test methods]. Moscow, Publishing House of Standards, 2001. 42 p. (Rus).
12. IEC 61000-4-32. Part 4-32. Testing and measurement techniques-High-altitude electromagnetic pulse (HEMP) simulator compendium. Geneva, IEC Publ., 2002. 108 p.
13. IEC 62305-1: 2010 «Protection against lightning. Part 1: General principles». Geneva, IEC Publ., 2010. 56 p.
14. *GOST R MEK 62305-1-2010. Menedzhment riska. Zashchita ot molnii. Chast' 1: Obshhie principy* [GOST R IEC 62305-1-2010. Risk management. Protection from lightning. Part 1: General principles]. Moscow, Standartinform Publ., 2011, 46 p. (Rus).
15. Brzhezitskiy V.A., Isakova A.V., Rudakov V.V. *Tekhnika i elektrofizyka vysokikh napruh* [Technics and Electrophysics of High Voltages]. Kharkov, Tornado Publ., 2005. 930 p. (Ukr).

16. Kozlov D.A., Kuzhekin I.P., Hribar J. Testing objects for resistance to lightning currents. *Technologies of electromagnetic compatibility*, 2004, no.2(9), pp. 35-39. (Rus).
17. DSTU 2793-94. *Sumisnist tekhnichnykh zasobiv elektromahnitna. Stiikist do potuzhnykh elektromahnitnykh zavod. Zahalni polozhennia* [DSTU 2793-94. Electromagnetic compatibility of hardware. Stability to the powerful electromagnetic hindrances. General principles]. Kiev, State Standard of Ukraine Publ., 1994. 24 p. (Ukr).
18. Suhorukov S.A. *Pomehozashhitnye ustrojstva ZAO «EMSOTEH»* [Hindrane protective devices of CCA «EMSOTEH»]. Kaluga, 2014. 72 p. (Rus).
19. Kravchenko V.I. *Weapon on non-traditional physical principles: Electromagnetic weapon*. Kharkov, NTMT Publ., 2009. 266 p. (Rus).
20. Baranov M.I. Key indicators thermo protection in high-voltage capacitors charge-discharge circuit powerful capacitive energy storage of emergency overcurrent. *Bulletin of NTU «KhPI»*, 2014, no.50(1092), pp.20-27. (Rus).
21. Baranov M.I., Rudakov S.V. Development of new charts of capacitance-resistance defense of high-voltage capacitors of powerful capacity stores of energy from emergency currents. *Electrical engineering & electromechanics*, 2015, no.6, pp. 47-52. (Rus). doi: 10.20998/2074-272x.2015.6.08.
22. Shapiro D.N. *Osnovy teorii elektromahnitnogo ekranirovaniya* [Basic theory of electromagnetic screening]. Leningrad, Energy Publ., 1975. 112 p. (Rus).
23. Apollonsky S.M. *Raschet elektromagnitnykh ekraniruyushchih obolochek* [Calculation of electromagnetic shielding of shells]. Leningrad, Energoizdat Publ., 1982. 144 p. (Rus).
24. Vance E.F. *Vliyanie elektromagnitnykh polej na ekranirovannye kabeli* [The impact of electromagnetic fields on the shielded cables]. Moscow, Radio and Communications Publ., 1982. 120 p. (Rus).
25. Ryabkova E.Y. *Zazemleniya v ustanovkah vysokogo napryazheniya* [Grounding installations high voltage]. Moscow, Energy Publ., 1978. 224 p. (Rus).
26. SOU 31.2-21677681-19:2009. *Viprobuvannya ta kontrol' prystroyiv zazemleniya elektroustanovok. Tipova instruktsiya*. [SOU 31.2-21677681-19:2009. Test and control devices, electrical grounding. Standard instruction]. Kyiv, Minenergovugillya Ukrainy Publ., 2010. 54 p. (Ukr).
27. *Pravila ulashtuvannya elektroustanovok. Rozdil 1. Zagal'ni pravila. Glava 1.7. Zazemlennya i zakhisni zakhodi vid urazhennya elektrichnim strumom* [Rules of the device electroinstallations. Chapter 1. General rules. Grounding and protective measures against electric shock]. Kyiv, Minenergovugillya Ukrainy Publ., 2011. 72 p. (Ukr).
28. Koliushko G.M., Koliushko D.G., Rudenko S.S. On the problem of increasing computation accuracy for rated parameters of active electrical installation ground grids. *Electrical engineering & electromechanics*, 2014, no.4, pp. 65-70. (Rus). doi: 10.20998/2074-272x.2014.4.13.
29. Kostruba S.I. *Izmerenie elektricheskikh parametrov zemli i zazemlyayushchih ustrojstv* [Measurement of electrical parameters of the earth and grounding device]. Moscow, Energoatomizdat Publ., 1983. 168 p. (Rus).
30. Burgsdorf V.V., Jacobs A.I. *Zazemlyayushchie ustrojstva elektroustanovok* [Earthing devices of electric options]. Moscow, Energoatomizdat Publ., 1987. 400 p. (Rus).
31. Borisov R.K., Koliushko G.M., Grimud G.I. Technique to study the ground grids of electric power facilities. *Energy and Electrification*, 2000, no.4, pp. 29-32. (Rus).
32. GOST R 54149-2010. *Normy kachestva elektricheskoi energii v sistemakh elektroshchitnogo obshchego naznacheniia* [GOST R 54149-2010. Norms of quality of electric energy in power systems for general purposes]. Moscow, Standartinform Publ., 2010. 52 p. (Rus).
33. Baranov M.I., Koliushko G.M., Kravchenko V.I. A switching aperiodic superhigh-voltage pulse generator for testing the electric strength of insulation of technical objects. *Instruments and Experimental Technique*, 2013, vol.56, no.6, pp. 653-658. doi: 10.1134/s0020441213050126.
34. IEC 62305-4: 2010 «Protection against lightning.– Part 4: Electrical and electronic systems within structures». Geneva, IEC Publ., 2010. 59 p.
35. Available at: <http://www.schrack-technik.ru/shop/grozozashchitnye-razrjadniki-razrjadniki-dlja-zashchity-ot-perenapryazhenija-i-zazemlenie.html> (accessed 21 May 2015). (Rus).
36. Available at: <http://www.plasmalabs.ru/files/products/sverhmoshchnie.pdf> (accessed 10 October 2015). (Rus).
37. Available at: <http://newet.ru/catalog/pomekhozashchitnoe-oborudovanie-ems-otekh> (accessed 21 February 2014). (Rus).
38. Available at: <http://electricalschool.info/main/elsnabg/220-primeneniye-ogranichitelej.html> (accessed 28 September 2014). (Rus).
39. Dem'yanenko K.B., Titkov V.V. Comparison of the main technical characteristics of OPN in porcelain and polymer insulation of LLC «SEVZAPPROM». *ELEKTRO. Electrical engineering, power industry, electrical industry*, 2007, no.2, pp. 31-33. (Rus).
40. Shumilov Yu.N., Shumilov M.Yu., Taran V.N., Ganpanturova S.Iu., Kovtun A.N., Tel'manova E.N., Nebogataia V.V., Zaderikhin A.A., Lenev D.N. Non-linear terminators of overvoltage 3-150 kV in polymer corps. *Energetic and electrification*, 2010, no.9, pp. 26-30. (Rus).
41. Available at: <http://electric-talk.ru/ogranichiteli-perenapryazhenij-zashchita-ot-molnii> (accessed 23 July 2015). (Rus).
42. Available at: http://www.compitech.ru/html/cgi/arhiv/01_01/stat-32.htm (accessed 10 April 2015). (Rus).
43. *Bol'shoj illjustrirovannyj slovar' inostrannykh slov* [Large illustrated dictionary of foreign words]. Moscow, Russkie slovari Publ., 2004. 957 p. (Rus).
44. Komel'kov V.S. *Tehnika bol'shih impul'snykh tokov i magnitnykh polej*. [Technique large pulsed currents and magnetic fields]. Moscow, Atomizdat Publ., 1970. 472 p. (Rus).
45. Baranov M.I. *Izbrannye voprosy elektrofiziki. Tom 3: Teorija i praktika elektrofizicheskikh zadach* [Selected topics of Electrophysics. Vol. 3: Theory and practice of electrophysics tasks]. Kharkiv, Tochka Publ., 2014. 400 p. (Rus).
46. Available at: <http://www.musidora.ru/dimFiltrs.htm> (accessed 21 May 2015). (Rus).
47. Available at: <http://www.symmetron.ru/suppliers/infineon/files/pdf/infineon/INF13.pdf> (accessed 10 April 2014). (Rus).
48. Available at: <http://bt.rozetka.com.ua/3502659/c3502659/?gclid=CPeh-OidlckCFebhcgoddGgA1A> (accessed 12 July 2016). (Rus).

49. Baranov M.I., Koliushko G.M., Kravchenko V.I., Nedzel'skii O.S., Dnyshchenko V.N. A Current Generator of the Artificial Lightning for Full-Scale Tests of Engineering Objects. *Pribory i tehnika eksperimenta – Instruments and Experimental Technique*, 2008, no.3, pp. 401-405. doi: **10.1134/s0020441208030123**.

50. Baranov M.I., Koliushko G.M., Kravchenko V.I., Rudakov S.V. A generator of aperiodic current pulses of artificial lightning with a rationed temporal form of 10 μ s/350 μ s with an amplitude of $\pm(100-200)$ kA. *Instruments and Experimental Technique*, 2015, vol.58, no.6, pp. 745-750. doi: **10.1134/s0020441215060032**.

M.I. Baranov, Doctor of Technical Science, Chief Researcher, Scientific-&-Research Planning-&-Design Institute «Molniya» National Technical University «Kharkiv Polytechnic Institute», 47, Shevchenko Str., Kharkiv, 61013, Ukraine, phone +38 057 7076841, e-mail: eft@kpi.kharkov.ua

Received 25.11.2015

How to cite this article:

Baranov M.I. An anthology of the distinguished achievements in science and technique. Part 33: Electromagnetic compatibility and protection from action of powerful electromagnetic interference of radioelectronic, electrical engineering and electric power equipment. *Electrical engineering & electromechanics*, 2016, no.4, pp. 3-15. doi: 10.20998/2074-272X.2016.4.01.

Yu.M. Vaskovskiy, A.M. Melnyk, O.I. Tytko

ELECTROMAGNETIC VIBRATION DISTURBING FORCES AT THE ECCENTRICITY OF ROTOR OF TURBOGENERATOR

Electromagnetic vibration disturbing forces in different variants of the rotor displacement from an axis of the stator bore is carried out. Investigation for TG type TGV-200-2 by finite element method in COMSOL Multiphysics is carried out. The field mathematical model of static and dynamic eccentricity is described. The amplitude vibration disturbing forces are greatest, when a static eccentricity direction coincides with an axis of the stator winding phase is shown. The diagnostic features static and dynamic eccentricities are formulated. The most value of forces in the point with minimal air gap is shown. The diagnostic features static and dynamic eccentricities and the method of diagnostic eccentricity are formulated. Diagnostic feature of static eccentricity is to change the amplitude Maxwell stress tensor is established. The dynamic eccentricity diagnostic features are appearance in the spectrum of vibration disturbing forces rotating and multiple harmonics. References 8, tables 3, figures 6,

Key words: turbogenerator, field mathematical model, electromagnetic vibration disturbing forces, Maxwell stress tensor, eccentricity, damage of rotor, diagnostic feature.

В статье исследовано электромагнитные вибровозмущающие силы турбогенератора при наличии дефекта ротора. Исследования выполнены для турбогенератора типа ТГВ-200-2 методом конечных элементов в программном обеспечении COMSOL Multiphysics. Описано полевую математическую модель статического и динамического эксцентриситета, которая позволяет смоделировать сигналы датчика вибраций как функции реального времени. Выполнено серию расчетов электромагнитных сил при различных вариантах смещения ротора с оси расточки статора. Показано, что при возникновении эксцентриситета наблюдается существенное увеличение вибровозмущающих сил и наибольшее значение сил будет в точке с минимальным воздушным промежутком. Введено новые диагностические параметры и предложено методику диагностирования эксцентриситета. На основе проведенного математического моделирования установлено, что диагностическим признаком статического эксцентриситета является изменение амплитуды тензора магнитного тяжения, а признаком динамического эксцентриситета – наличие в спектре вибровозмущающих сил оборотной и кратных ей гармоник. Библи. 8, табл. 3, рис. 6

Ключевые слова: турбогенератор, полевая математическая модель, электромагнитные вибровозмущающие силы, тензор магнитного тяжения, эксцентриситет, дефект ротора, диагностический признак.

Introduction. Recently the problem of timely monitoring and diagnostics and eliminate injuries powerful electric machines is particularly important due to the aging fleet of existing machines and the increasing number of cases of an emergency stop with significant economic losses. In particular this applies powerful synchronous turbogenerators (TG), which are widely used in thermal and nuclear power plants. Particular attention is paid to TG rotor which is complex and node design.

In recent years in Ukraine and abroad, studies of the physical processes that occur in the presence of synchronous generator rotor their defects [1-8]. By defects rotor may also include uneven of air gap (AG) between the stator and rotor (eccentricity). This failure can occur as a result of manufacturing defects, and in the operation of TG. When the rotor eccentricity refers displacement axis rotor stator bore axis [4]. There are: a) static eccentricity (SE) in which the AG configuration for rotation of the rotor remains unchanged, i.e. the minimum and maximum period do not change their position; b) dynamic eccentricity (DE), in which the minimum and maximum of AG rotates with the rotation of the rotor.

TG rotor eccentricity appearance leads to a distortion of the magnetic field in AG, the occurrence of electromagnetic forces sided magnetic attraction, of additional higher harmonics of the field, increase local overheating. In the array of rotor turbine flow eddy currents that lead to significant heat damage and structural elements of the rotor (grooving wedges bandage rings).

The eccentricity of the rotor may be the installation of the rotor TG or during its operation (as a result of wear

of bearings, offset supports, flex shaft, etc.). Significant identify the nature and magnitude of the eccentricity of the rotor in the synchronous generator without the withdrawal of the mode of operation is a relevant and complex engineering task of solving the effectiveness of which depends on the amount of electricity generated, durability, efficiency and safety of TG.

There are many methods for detecting and diagnosing damage of electric machines, the main ones are the methods of mechanical, vibration, electromagnetic diagnostic method for the analysis phase current range and others [1-3, 6]. The feasibility of selecting one of these methods for diagnosing rotor eccentricity of the TG due to their reliability and sensitivity of diagnostic parameters, the complexity of technical implementation, the cost of hardware and methodological support and other factors. The comparative analysis of these methods has shown that the solution SE and DE of the TG appropriate to use the method of vibration diagnosis, due to the simplicity of implementation and high reliability of the identification of defects. To determine the diagnostic features is necessary to study electromagnetic forces that change the appearance of the SE or DE.

The goal of the work is to study methods of mathematical modeling of electromagnetic vibration disturbing forces under static and dynamic eccentricity of the TG and to determine diagnostic features for diagnosing these types of defect. The modeling is performed using the finite element method implemented in a software environment *COMSOL Multiphysics*. Diagnosis is sug-

gested to conduct on the basis of spectral analysis of functions of tensor magnetic stress tensor using fast Fourier transform (FFT).

Problem definition. Mathematical model involves solving equations of the electromagnetic field in the core of the TG and definition vibration disturbing forces in the selected stator point where conventional vibration sensor is placed. Given the considerable axial length of the core of the TG compared to the long pole graduations, just consider the field in two-dimensional approach in cross section. We shall consider quasi-static processes, suggesting that all field functions change in time for the harmonic law. In general, the basic equations of the electromagnetic field is relatively complex amplitude of the magnetic vector potential, which has only one spatial (axial) component \vec{A}_z , in the stator coordinate system is as follows:

$$\vec{A}_z - j\omega\mu\gamma\vec{A}_z + \mu\gamma\omega_R(R \times \text{rot}\vec{A}_z) = -\mu\vec{J}_{ext}, \quad (1)$$

where \vec{J}_{ext} is the density of external currents (in our case, this is the density of current in the stator slots, which is set to correspond to the stator windings circuit); ω is the angular frequency of changes over time of the magnetic vector potential; ω_R is the angular frequency of the rotor rotation; γ is the electrical conductivity; R is the radius-vector of an arbitrary point of the rotor. The angular frequency changes over time magnetic potential and angular rotor speed depends on the choice of coordinate, which implemented the solution. For synchronous machines without eddy currents in the stator and rotor cores equation (1) takes the following form:

$$\Delta\vec{A}_z = -\mu\vec{J}_{ext}. \quad (2)$$

Field sources are external currents densities of three phases of the stator winding:

$$\begin{aligned} \vec{J}_{Aext} &= I_m u_n / S_n, \\ \vec{J}_{Bext} &= I_m u_n [\cos(-2\pi/3) - j\sin(-2\pi/3)] / S_n, \\ \vec{J}_{Cext} &= I_m u_n [\cos(-4\pi/3) - j\sin(-4\pi/3)] / S_n, \end{aligned} \quad (3)$$

where I_m is the amplitude of the current in the phase of the stator winding; u_n is the number of series-connected conductors in the stator slot; S_n is the sectional area of the stator slot.

Equation (2) is complemented by homogeneous boundary conditions of the first kind in the line of the outer surface of the stator yoke which limits the calculated area:

$$\vec{A}_z \Big|_G = 0. \quad (4)$$

The value of μ at each point calculation area where the ferromagnetic materials present is determined by the corresponding magnetization curves. The components of magnetic induction in the Cartesian coordinate system defined by relations:

$$\vec{B}_x = \partial\vec{A}_z / \partial y, \quad \vec{B}_y = \partial\vec{A}_z / \partial x, \quad (5)$$

Vibration disturbing forces density is proportional to the magnetic stress tensor that has the physical dimension of the pressure (N/m²). Modules of normal and tangential components of magnetic stress tensor are expressed as:

$$T_n = \left| \frac{1}{2\mu} (\vec{B}_n^2 - \vec{B}_\tau^2) \right|, \quad T_\tau = \left| \frac{1}{\mu} (\vec{B}_n^2 \cdot \vec{B}_\tau^2) \right|, \quad (6)$$

respectively normal (directed along the vector normal to the surface at a given point) and tangential (directed along the tangent to the surface at a given point) projection of magnetic induction. Normal and tangential components of the magnetic induction determined through induction projection vector in Cartesian coordinates by the expression:

$$\begin{aligned} \vec{B}_n &= \vec{B}_y \cos\alpha + \vec{B}_x \sin\alpha = (y\vec{B}_y + x\vec{B}_x) / R_\delta, \\ \vec{B}_\tau &= \vec{B}_x \cos\alpha - \vec{B}_y \sin\alpha = (y\vec{B}_x - x\vec{B}_y) / R_\delta, \end{aligned} \quad (7)$$

where x, y are the projections of the radius-vector on the axis of the coordinate system; R_δ is the radius of the bore of the stator. Further deals radial vibration occurring by the action of the normal component of the magnetic stress tensor.

To take into account changes over time of the tensor model involves changing the configuration time calculation area while moving the rotor relative to the stator. Moving of the rotor are simulated by changes of coordinates x, y of points of the rotor. Changes $\Delta x, \Delta y$ of rotor coordinates by a time Δt are given by the following formulas:

$$\begin{cases} \Delta x = \cos[\omega_R \cdot (t + \Delta t)] \cdot x - \sin[\omega_R \cdot (t + \Delta t)] \cdot y - x; \\ \Delta y = \sin[\omega_R \cdot (t + \Delta t)] \cdot x + \cos[\omega_R \cdot (t + \Delta t)] \cdot y - y. \end{cases} \quad (8)$$

The time interval T on which analyzed signal analysis is carried out corresponds to one period is one complete revolution of the rotor – for bipolar TG $T = (0 \dots 0.02)$ s. Number of calculation steps is 200, meaning that one time step is 10^{-4} s. During one step back rotor relative to the stator a third of the rotor division that meets the conditions of accuracy.

A model of static and dynamic eccentricity. Relative value of the eccentricity is determined by the formula:

$$\varepsilon = \frac{\delta_{\max} - \delta_{\min}}{\delta_{\max} + \delta_{\min}}, \quad (9)$$

where $\delta_{\max}, \delta_{\min}$ are the maximal and minimal values of AG, respectively. In this paper the static and dynamic rotor eccentricity are considered at shifting its axis relative to the axis of the stator bore by two coordinates X (horizontal eccentricity) and Y (vertical).

To simulate the eccentricity using the above-mentioned field mathematical model that takes into account the rotation of the rotor at the time. Fig. 1 shows the displacement of the rotor axis stator static (*a*) and dynamic (*b*) eccentricity. In this model, SE simulated displacement axis of the rotor relative to the stator geometrical axis by the amount ΔR which generally is decomposed into bias coordinates of the center of the rotor on the Y axis on the value of $\Delta Y = \Delta R \cdot \sin\alpha$ (Fig. 1,*a*), and the displacement coordinates on the X axis equals $\Delta X = \Delta R \cdot \cos\alpha$.

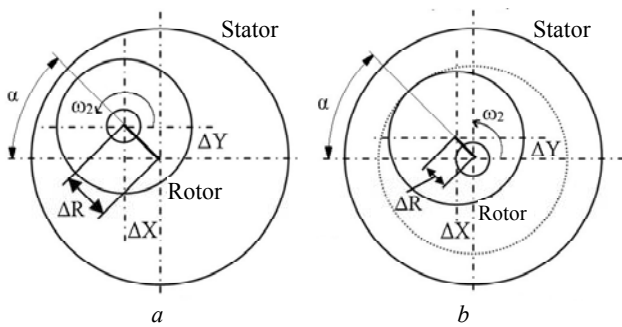


Fig. 1. Models of static (a) and dynamic (b) eccentricity

Calculated area includes two sub-areas: fixed, which includes a stator and a moving containing a rotor. The border between the two subregions is in the middle of AG, and with uneven refers to sub-areas of the stator. DE is modeled by geometric displacement of axis of the rotor relative to the axis of rotation on the value ΔR . This move all points of the rotating subregion by the coordinates X and Y are the same and the equation of motion will match the expression (8). Note that at DE to the calculated rotating subregion rotor not only, but also uneven AG are included.

Mathematical model (1-8) can simulate the signals of conventional vibration sensors (vibration acceleration sensors) as a function of time. To this end, points 1, 2, 3 of conventional location of sensors (Fig. 2) by the expression (7) is calculated normal component of magnetic stress tensor (MST) as the value of the acceleration is proportional to value of the magnetic disturbing force.

Results of investigations. Investigations are conducted by the example of the TG type TGV-200-2. Based on the above described mathematical model further investigated magnetic disturbing forces arising due to normal component tensor magnetic tension (ceteris paribus technical condition of the stator). As you know, one sensor setting is not sufficient to determine whether the SE because of vibration investigated crowns on teeth in the stator bore three points 1, 2, 3. Fig. 2 shows a picture of the distribution of the magnetic vector potential and magnetic flux density at time $t = 0.02$ s in the active zone of the TG.

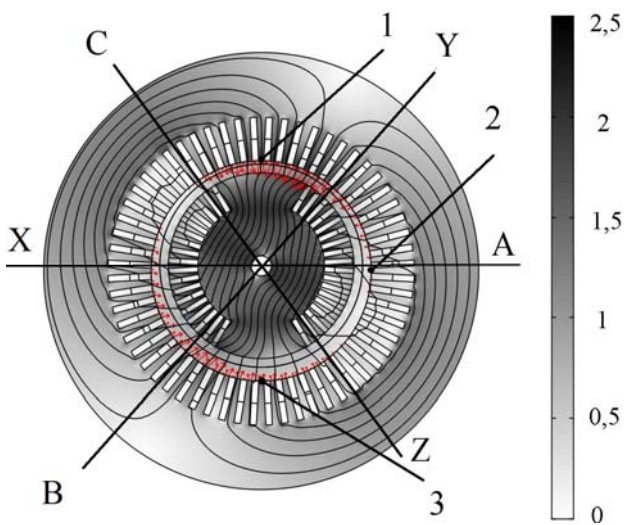


Fig. 2. Distribution of the magnetic vector potential and magnetic flux density with calculated points

Modeling was performed for nominal operation mode of the generator with good condition (no SE and DE) and when defective (presence of eccentricity). SE was simulated by displacement of the rotor along Y coordinates with the angle $\alpha = 90^\circ$. Fig. 3 and Fig. 4, respectively, in these three points on the crowns of teeth of the stator depicted settlement functions of the magnetic stress tensor over time in the presence of SE and DE (for $\varepsilon = 0.25$ when the rotor displacement along the axis of symmetry phase A). Figures shows that the signals of the 1st and 2nd sensors shifted between a time phase that meets their spatial shift of 90° along the stator bore. The numbers on the charts correspond to the designation of calculated points.

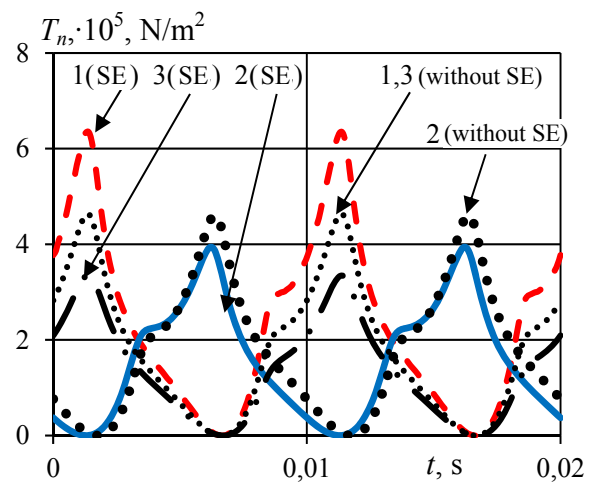


Fig. 3. MST functions at calculated points at presence of SE

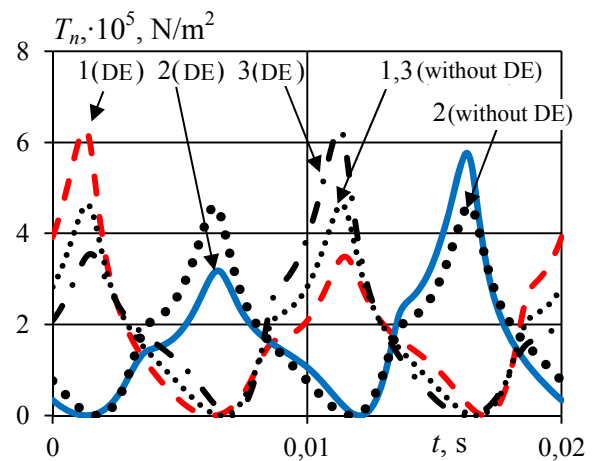


Fig. 4. MST functions at calculated points at presence of DE

From the results of spectral analysis for different values of SE ($\varepsilon=0.1$, $\varepsilon=0.2$ and $\varepsilon=0.25$) we can see increasing amplitude harmonic 100 Hz respectively of 10, 15 and 30%. Comparison of MST when SE shows that when $\Delta R = 25$ mm ($\varepsilon=0.25$) in point 3 of the largest AG amplitude of MST decreased 1.4 times and at point 1 –increased 1.37 times. This effect is clearly seen from the graphs at the DE when the rotor rotates value of AG is constantly changing, and MST function is asymmetric and obviously that will have additional spectrum harmonic multiples rotating frequency.

In view of the above, an effective method of analysis of the time functions of electromagnetic vibration disturbing forces is determination of their spectral composition using fast Fourier transform. Fig. 5 shows the amplitude of MST at SE depending on the value of ε for different variants displacement of the rotor relative to the stator winding phase zones. Note that different variants of displacement of the rotor axis of rotation were conducted at a fixed position axis phase zone A which coincides with the modeling of a horizontal axis. MST amplitudes are shown in three points of location of sensors (points 1-3). The results of mathematical modeling showed that if SE when $\Delta R = 25$ mm ($\varepsilon=0.25$) amplitude of the fundamental harmonic electromagnetic forces increased by 32 %. Also present spectrum vibration disturbing forces components that create vibrations at frequencies of 200, 300, 400 Hz are respectively 15, 18 and 12 % relative to the fundamental harmonic.

Thus, the most dangerous is eccentricity when the eccentricity direction coincides with the axis of the stator phase. So, Fig. 5,a shows that even at $\varepsilon = 0.1$ amplitude of vibration disturbing forces increases by 13 %.

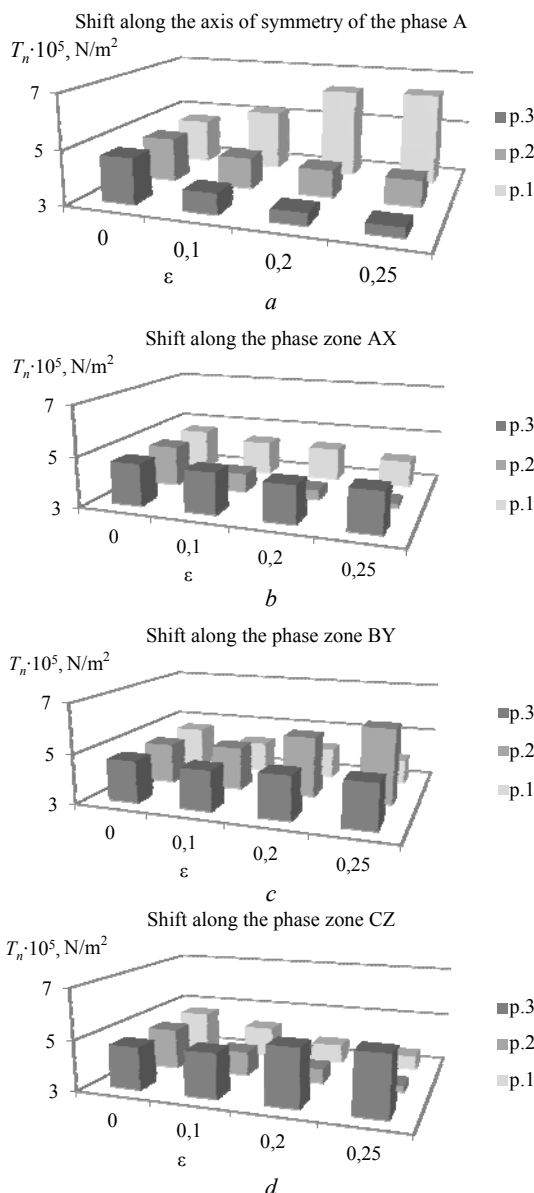


Fig. 5. Amplitudes of magnetic stress tensor vs eccentricity factor

Figure 6 for the DE case shows amplitude spectra of MST for 50 Hz (a), 150 Hz (b) and 250 Hz (c).

From Fig. 6,a,b one can see that the amplitude of each harmonic of the rotation frequency of 50 Hz and aliquot to it 150 Hz are 12 % (at $\varepsilon=0.1$), 25 % (at $\varepsilon=0.2$) and 30 % (at $\varepsilon=0.25$) of the basic harmonic 100 Hz. These results can be the basis for the formulation of appropriate diagnostic features and determining the presence of a defect.

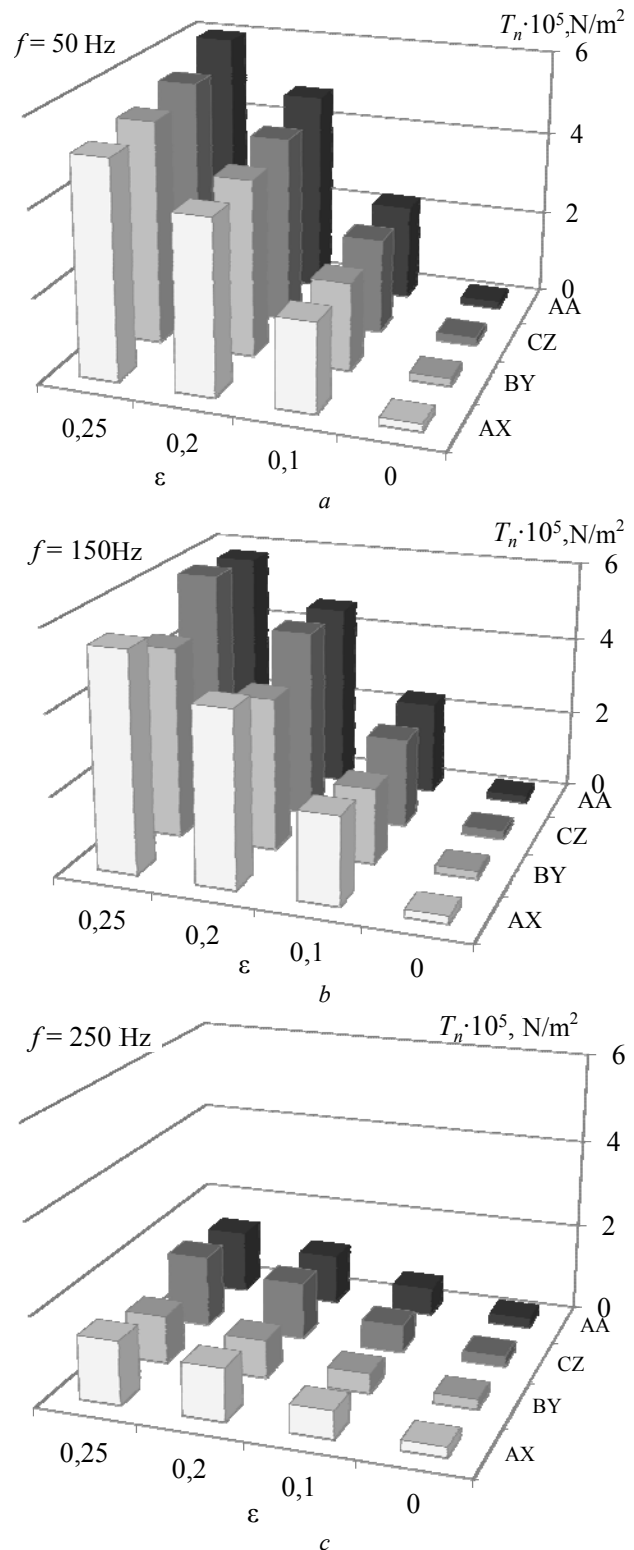


Fig. 6. Amplitudes of magnetic stress tensor spectrum frequencies vs value of eccentricity

Important technical assessment of the state of the generator with the appearance of damage provides analysis of changes in total harmonic vibration of all, characterized by RMS. Change factor of RMS of the MST spectrum k_{rms_T} describes ratio of RMS of the MST spectrum of the damaged TG to RMS of the MST spectrum of the un hurt TG and is calculated as follows:

$$k_{rms_T} = \sqrt{\frac{\sum_{i=1}^N |T_{i_fault}|^2}{\sum_{i=1}^N |T_{i_no_fault}|^2}}, \quad (10)$$

where N is number of accounted harmonics in spectrum; i is the number of harmonics; T_{i_fault} , $T_{i_no_fault}$ are the amplitudes of the i -th harmonics of MST in spectra of vibration sensor signal regarding damaged and un hurt TG.

Table 1 shows the range of RMS of MST spectrum calculated in point 1. Legends AX, BY and CZ correspond to the rotor displacement along the axis of the corresponding phase zone, marking AA meets at the location of the sensor in the area at minimum AG at the rotor displacement along the axis of symmetry of the phase A of the stator winding. Table 1 shows that the overall level of vibrations of electromagnetic origin at the SE is the largest when the direction of eccentricity coincides with the axis of the stator winding phase (in this case with a vertical axis). Electromagnetic vibrations under other phases at SE (AX, BY, CZ) decrease.

Table 1

Ration of the RMS change of MST spectrum at eccentricity

	E	AA	AX	BY	CZ
SE	0.1	1.111	0.912	0.904	0.93
	0.2	1.326	0.954	0.899	0.838
	0.25	1.329	0.967	0.851	0.8
DE	0.1	1.015	1.012	1.01	1.01
	0.2	1.079	1.038	1.02	1.074
	0.25	1.123	1.065	1.035	1.112

Therefore, to determine the maximum vibration sensor must be installed opposite phase stator winding axis. When installing the wrong sensor measurement results will indicate the reduction of vibrations that will not re-

veal the presence of SE. At DE total level of vibration is independent of the direction of eccentricity. However, despite the fact that the vibrations of electromagnetic origin is less than the SE, you need to take into account the fact that there are vibrations of mechanical origin associated with fluctuations in the center of mass of the rotor. Therefore, the total vibrations can be more than the vibrations at the SE.

Generalize the results of mathematical modeling by introducing diagnostic parameters at different values of AG and direction of displacement of the rotor relative to the stator winding phase zones. Table 2 shows the diagnostic feature k_{δ} which allows to diagnose the occurrence of SE based on measurement of the amplitudes of sensor signals.

$$k_{\delta} = T_{fault} / T_{no_fault}. \quad (11)$$

Table 3 shows the value of diagnostic feature k_e characterizing the ratio of the difference of the amplitudes of MST in the first and second points (k_{e12}) and the first and third points (k_{e13}) according to the amplitude of NTM in the first point at different values of the coefficient of eccentricity.

$$k_{e12} = \frac{T_{\tau1} - T_{\tau12}}{T_{\tau1}}; \quad k_{e13} = \frac{T_{\tau1} - T_{\tau13}}{T_{\tau1}}. \quad (12)$$

The obtained diagnostic parameters are given in Table 2 and 3. The results allow to formulate a reasonable method of diagnosing eccentricity. To determine the SE we must mount at least two sensors, for example, the top and bottom of the vertical axis, as the most likely direction of displacement of the rotor along the vertical axis. A comparison of the signals of two sensors will help diagnose the occurrence of eccentricity. To diagnose DE it is enough to mount one sensor vibration because with this type of defect of AG at one point is not permanent. After measuring the sensor signal is decomposed in Fourier series and if there are harmonics of the signal multiple rotating frequency, it can be argued the presence of DE.

Table 2

Diagnostic feature k_{δ}

Phase zone of the stator winding relatively that the rotor displacement was modeled	AG between stator and rotor, δ , mm						
	75	80	90	100	110	120	125
AA	1.371	1.356	1.126	1	0.802	0.74	0.716
AX	0.873	0.933	0.94	1	0.992	0.958	0.982
BY	0.857	0.906	0.911	1	0.984	1.01	1.021
CZ	0.764	0.806	0.91	1	1.016	1.125	1.145

Table 3

Diagnostic features k_{e12} and k_{e13}

Phase zone of the stator winding relatively that the rotor displacement was modeled	k_{e12}	k_{e13}	k_{e12}	k_{e13}	k_{e12}	k_{e13}
	$\varepsilon=0.1$		$\varepsilon=0.2$		$\varepsilon=0.25$	
AA	0.207	0.281	0.365	0.452	0.379	0.473
AX	0.140	-0.065	0.219	-0.037	0.215	-0.136
BY	-0.119	-0.091	-0.291	-0.125	-0.516	-0.202
CZ	0.063	-0.128	0.045	-0.410	0.084	-0.514

Conclusions.

1. In the event of static eccentricity in the zone of minimum air gap a significant increase of vibration disturbing forces is observed, whose analysis can diagnose damage to the rotor. It is shown that the coincidence of

the direction of the static eccentricity of the geometrical axis of one of the phases of the stator winding, increased vibration is maximized. This fact is expedient to consider when phase stator winding arrangement relative to the horizontal axis turbine generators in the manufacturing

process, taking into account the most likely direction of occurrence of static eccentricity caused, for example, gravity, and so on.

2. In the event of dynamic vibrations of electromagnetic origin eccentricity is less than the static eccentricity, but the mechanical vibration component associated with fluctuations in the center of mass of the rotor, makes a significant contribution to the overall level of vibration. Diagnostic features k_{δ} , k_{e12} , k_{e13} are introduced on which can be built a system and method of diagnosing eccentricity.

3. A diagnostic feature of static eccentricity is changing of amplitude of vibration disturbing forces in the zone of minimum air gap. The spectrum of harmonic of 100 Hz at static eccentricity within $\varepsilon=0.1$; 0.2 and 0.25 in the zone of minimum air gap increases respectively by 10, 15 and 30 %. Diagnostic features of dynamic eccentricity are the appearance in the spectrum of vibration disturbing forces of rotating and multiple harmonics.

REFERENCES

1. Vaskovskyi Yu.M., Tytko O.I., Melnyk A.M. Diagnosis of damage to the excitation winding powerful turbogenerator based on the analysis of electromagnetic forces. *Works of the Institute of Electrodynamics of the National Academy of Sciences of Ukraine*, 2013, no.36, pp. 40-46. (Ukr).
2. Vaskovskyi Yu.M., Tsyvinskyi S.S., Tytko O.I. Electromagnetic processes in the damper winding of hydro generator with eccentricity of air gap. *Tekhnichna elektrodynamika*, 2015, no.1, pp. 65-71. (Ukr).
3. Haidenko Yu.A., Vishnevskiy T.S. Electromagnetic method of diagnostic of static eccentricity of synchronous generator. *Hydropower Ukraine*, 2011, no.2, pp. 52-57. (Rus).

How to cite this article:

Vaskovskyi Yu.M., A Melnyk.M., Tytko O.I. Electromagnetic vibration disturbing forces at the eccentricity of rotor of turbogenerator. *Electrical engineering & electromechanics*, 2016, no.4, pp. 16-21. doi: 10.20998/2074-272X.2016.4.02.

4. Levytskyi A.S., Fedorenko H.M. Characterization of air gap fault in hydrogenerators to data by sensors located on stator. *Hydropower Ukraine*, 2008, no.1, pp. 30-33. (Ukr).
5. Kuchynskiy K.A. Analysis of temperature field of rotor of turbogenerator capacity 300 mW at asymmetry of cooling of grooving zone. *Tekhnichna elektrodynamika*, 2013, no.4, pp. 59-66. (Rus).
6. Milykh V.I., Polyakova N.V Comparative analysis of the variable magnetic field on the surface of the rotor of turbogenerators with different numbers of stator teeth in the load condition. *Tekhnichna elektrodynamika*, 2014, no.2, pp. 29-36. (Rus).
7. Sedky M.M. Diagnosis of static, dynamic and mixed eccentricity in line start permanent magnet synchronous motor by using FEM. *International journal of electrical, robotics, electronics and communications engineering*, 2014, vol.8, no.1, pp. 29-34.
8. Yonggang Li, Guowei Zhou, Shuting Wan, Heming Li. Analysis of unbalanced magnetic pull on turbo-generator rotor under air-gap eccentric fault and rotor short circuit fault. *International journal of advancements in computing technology*, 2013, vol.5, no.4, pp. 523-530. doi: 10.4156/ijact.vol5.issue4.62.

Received 16.03.2016

Yu.M. Vaskovskyi¹, Doctor of Technical Science, Professor,
A.M. Melnyk², Postgraduate Student,
O.I. Tytko², Corresponding member of NAS of Ukraine, Professor,
¹National Technical University of Ukraine
«Kyiv Polytechnic Institute»,
37, Prospect Peremohy, Kyiv-56, 03056, Ukraine.
e-mail: vun157@gmail.com
²The Institute of Electrodynamics of NAS of Ukraine,
56, Prospekt Peremogy, Kiev-57, 03680, Ukraine.
e-mail: ied10@ukr.net

M.G. Pantelyat, I. Doležel

FINITE ELEMENT TECHNIQUE FOR SOLUTION OF THERMO-CONTACT PROBLEMS AND ITS APPLICATION IN NUMERICAL ANALYSIS OF DEVICES WORKING WITH INDUCTION HEATING

Purpose. To develop an effective approach for the numerical solution of transient thermo-contact problems and present a typical example of its utilization regarding devices working on the principle of thermoelasticity produced by induction heating and specific technological processes intended for assembly and disassembly of systems containing shrink fits. *Methodology.* A finite element technique for solution of 2D multiphysics (electromagnetic, thermal and structural) problems is developed, taking into account temperature dependences of material properties and continuous variations of the contact surfaces. Modeling of the contact interaction between two parts is based on the concept of a special contact finite element having no thickness. The functional for the temperature problem is supplemented with components corresponding to the thermal conductivity of this contact layer. The heat generated due to mutual sliding of both parts can also be taken into account, but the heat capacity (specific heat) of the contact layer is neglected. Using a special 1D 4-node finite elements a system of equations for the description of the thermo-contact problem is obtained. *Originality.* Relatively simple analytical formulae for calculation of the contact thermal resistances occurring in specific parts of electrical machines are known. The paper offers an alternative approach for the numerical solution of transient thermo-contact problems based on the concept of a special 1D contact finite element having no thickness. *Results.* The presented technique is applied for the computer simulation of assembly and disassembly of a shrink fit using induction heating. *Conclusions regarding the choice of technological modes are made. Comparative computations for drills made from hard alloy and alloyed tool steel are carried out.* References 8, figures 6.

Key words: induction heating, thermoelasticity, multiphysics problems, numerical analysis, finite element method.

Описана методика решения методом конечных элементов мультифизических (электромагнитных, тепловых и механических) задач с учетом зависимостей свойств материалов от температуры и изменения контактных поверхностей. Предложенный подход использован для численного анализа устройств, функционирующих на базе явления термоупругости в процессе индукционного нагрева и оригинальных технологических процессов, предназначенных для сборки и разборки конструкций с напряженными посадками. Применено разработанной методики проиллюстрировано на конкретном примере. Приведен анализ полученных результатов. Библ. 8, рис. 6.

Ключевые слова: индукционный нагрев, термоупругость, мультифизические задачи, численный анализ, метод конечных элементов.

Introduction. Investigation of behavior of numerous electrical devices in different operation regimes often requires considering relevant multiphysics phenomena of electromagnetic, thermal and structural origins. In many cases, multiphysics analysis of such devices must also include the influence of thin insulation layers and contact thermal resistances for obtaining more realistic results. Thin layers occur, for example, in the form of various bandages [1], contact resistances (of thermal origin) play a significant role in different shrink fits [2] and devices for a number of industrial purposes [3].

Relatively simple analytical formulae for calculation of the contact thermal resistances occurring in specific parts of electrical machines are presented in [1]. These can directly be used as material parameters during the solution of the temperature problem.

The paper offers an alternative approach for the numerical solution of transient thermo-contact problems. Currently the proposed technique is used for solving such problems in 2D Cartesian and axisymmetric systems. A similar technique for solving 3D problems is being developed nowadays. The aim of the paper is to describe this technique in detail and present a typical example of its utilization.

Formulation of technical problem. Many modern industrial technologies are based on the principle of induction heating. The paper, however, will focus on its application in production of shrink fits for specific purposes. Typical is, for example, setting the disks on shafts, fixing high-speed machine tools, or connecting pipes by

fixing sleeves, which always represent connecting of two metal parts with an interference whose value is decisive for the transferrable mechanical force or torque.

The process of manufacturing shrink fits starts with induction heating of one of the parts, which leads to increase of its dimensions. Then it is connected with another part and the whole system is cooled. The shrink fit is obtained after cooling. A typical example of fixing a drilling tool in the chuck is depicted in Fig. 1.

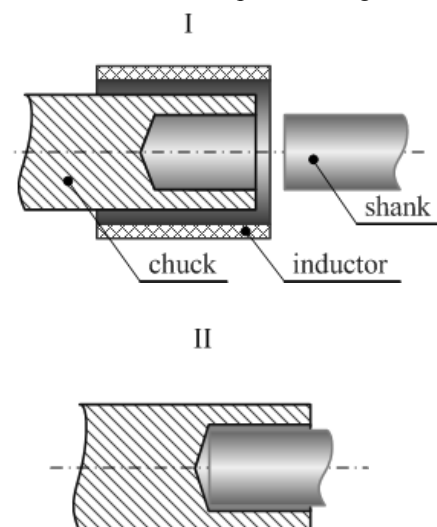


Fig. 1. Arrangement of drilling machine:
I – heating of chuck and inserting of shank into it
II – cooling of system and fixing of shank in chuck

© M.G. Pantelyat, I. Doležel

From the physical viewpoint, the process represents a strongly nonlinear and nonstationary multiphysics problem characterized by mutual interaction of magnetic field, temperature field and field of thermoelastic displacements (and corresponding strains and stresses). Another aspect to be involved in the model is the contact problem that plays an important role when quantifying transfer of heat between both connected parts.

The numerical solution of the model should provide a sufficiently accurate idea about the whole process and mainly the steady-state parameters of the system under investigation.

Continuous mathematical model. The mathematical model of the process consists of three partial differential equations (PDEs) describing three involved physical fields and relations describing the contact problem.

Magnetic field. Distribution of magnetic field in the system may be described using several formulations [4]. When using, for example, the magnetic vector potential \mathbf{A} , the above field obeys the equation

$$\operatorname{curl}\left(\frac{1}{\mu}\operatorname{curl}\mathbf{A}\right)+\gamma\frac{\partial\mathbf{A}}{\partial t}=\mathbf{J}_{\text{ext}}, \quad (1)$$

where μ is the magnetic permeability, γ stands for the electric conductivity and \mathbf{J}_{ext} represents the current density applied to the inductor. The boundary condition along a sufficiently distant artificial boundary is of the Dirichlet type and reads $\mathbf{A}=\mathbf{0}$.

The eddy currents produced by time-variable magnetic field in electrically conductive bodies (whose density is given by the second term on the left-hand side in (1)) give rise to the volumetric Joule losses w_J (the influence of magnetization losses being neglected)

$$w_J=\gamma\left|\frac{\partial\mathbf{A}}{\partial t}\right|^2, \quad (2)$$

whose magnitude decreases roughly exponentially with the distance from the surface of the heated body.

In fact, the complete solution of (1) is practically unfeasible due to relatively long time of the heating process. That is why the model was simplified by considering the magnetic field harmonic. Now (1) can be rewritten in terms of the phasor $\underline{\mathbf{A}}$ of the magnetic vector potential \mathbf{A} in the form

$$\operatorname{curl}(\operatorname{curl}\underline{\mathbf{A}})+j\cdot\omega\gamma\mu\underline{\mathbf{A}}=\mu\underline{\mathbf{J}}_{\text{ext}}, \quad (3)$$

where $j=\sqrt{-1}$ and ω denotes the angular frequency.

The computations must be now, however, carried out iteratively, and at every step the permeability μ in any element containing ferromagnetic material has to be adjusted to the real value of the local magnetic flux density.

Temperature field. The temperature field T is described by the equation [5]

$$\operatorname{div}(\lambda\operatorname{grad}T)=\rho c_p\frac{\partial T}{\partial t}-w_J, \quad (4)$$

where λ is the thermal conductivity, ρ denotes the mass density and c_p stands for the specific heat at a constant pressure.

The boundary condition on the surface of system is given by the formula

$$-\lambda\frac{\partial T}{\partial n}=\alpha_{\text{gen}}(T-T_{\text{ext}}), \quad (5)$$

where n denotes the outward normal, α_{gen} is a coefficient generally quantifying both convection and radiation and T_{ext} stands for the temperature of sufficiently distant environment.

Thermoelastic problem. Mechanical status of structural parts of the considered devices is described by the following system of three-dimensional tensor equations [6]

$$\begin{aligned} \sigma_{ij,i}+f_j &= 0, \\ \varepsilon_{ij} &= \frac{1}{2}(u_{i,j}+u_{j,i}), \\ \sigma_{ij} &= \frac{E}{1+\nu}\left(\varepsilon_{ij}+\frac{\nu}{1-2\nu}\delta_{ij}e\right), \end{aligned} \quad (6)$$

where σ_{ij} is the tensor of mechanical stresses, ε_{ij} is the tensor of mechanical strains, \mathbf{u} is the vector of mechanical displacements, \mathbf{f} is the vector of the external volumetric forces, E is the temperature-dependent modulus of elasticity of the material, ν is the temperature-dependent Poisson ratio of the material, δ_{ij} is the Kronecker delta, and $e=\varepsilon_{kk}(k=i,j)$.

The first part of (6) is the system of equilibrium equations describing the correlation between the mechanical stress tensor

$$\sigma_{ij}=\begin{pmatrix} \sigma_{11}\sigma_{21}\sigma_{31} \\ \sigma_{12}\sigma_{22}\sigma_{32} \\ \sigma_{13}\sigma_{23}\sigma_{33} \end{pmatrix} \quad (7)$$

and given volumetric forces components f_i .

The second part of (6) is the system of cinematic equations representing the correlation between the strain tensor

$$\varepsilon_{ij}=\begin{pmatrix} \varepsilon_{11}\varepsilon_{21}\varepsilon_{31} \\ \varepsilon_{12}\varepsilon_{22}\varepsilon_{32} \\ \varepsilon_{13}\varepsilon_{23}\varepsilon_{33} \end{pmatrix} \quad (8)$$

and components u_i of the mechanical displacement vector.

The third part of (6) is the constitutive equations presenting the correlation between the mechanical stress tensor σ_{ij} and strain tensor ε_{ij} .

In the system of equations (6) the following tensor and vector operations are used

$$\sigma_{ij,i}=\frac{\partial\sigma_{ij}}{\partial x_i}, \quad u_{i,j}=\frac{\partial u_i}{\partial x_j}, \quad u_{j,i}=\frac{\partial u_j}{\partial x_i}, \quad (9)$$

where $i=1,2,3$ and $j=1,2,3$ are the indices of the coordinate axes.

In the axisymmetric case, the mechanical deformed state of the device is described by the system of equations [6, 7]

$$\begin{aligned} \frac{\partial\sigma_{rr}}{\partial r}+\frac{\partial\tau_{rz}}{\partial z}-\frac{\sigma_{rr}-\sigma_{\theta\theta}}{r}+f_r &= 0; \\ \frac{\partial\tau_{rz}}{\partial r}+\frac{\partial\sigma_{zz}}{\partial z}+\frac{\tau_{rz}}{r}+f_z &= 0; \\ \varepsilon_{rr} &= \frac{\partial u_r}{\partial r}; \quad \varepsilon_{zz} = \frac{\partial u_z}{\partial z}; \\ \gamma_{rz} &= \frac{\partial u_r}{\partial z}+\frac{\partial u_z}{\partial r}; \quad \varepsilon_{\theta\theta} = \frac{u_r}{r}, \end{aligned} \quad (10)$$

where σ_{rr} , σ_{zz} , $\sigma_{\theta\theta}$, τ_{rz} are the radial, axial, circumferential and shear mechanical stresses, respectively, ε_{rr} , ε_{zz} , $\varepsilon_{\theta\theta}$, γ_{rz}

are the radial, axial, azimuthal and tangential mechanical strains, respectively, u_r and u_z are the radial and axial mechanical displacements, and f_r, f_z are the given radial and axial forces, respectively.

In order to simulate the mechanical state of the structure under consideration, elastic, plastic and thermal deformations are generally considered. Therefore, the strain tensor ε_{ij} is presented as a sum of the elastic ε_{ij}^e , plastic ε_{ij}^p and thermal ε_{ij}^T components [7], thus

$$\varepsilon_{ij} = \varepsilon_{ij}^e + \varepsilon_{ij}^p + \varepsilon_{ij}^T. \quad (11)$$

The elastic strains are described in the following way [6]

$$\varepsilon_{ij}^e = \frac{1}{E} \left[(1 + \nu) \sigma_{ij} - \delta_{ij} \nu \sigma_{kk} \right] \quad (12)$$

where $k = i, j$.

The thermal strains are represented in the form

$$\varepsilon_{ij}^T = \alpha \Delta T \delta_{ij}, \quad (13)$$

where α is the temperature-dependent coefficient of the temperature expansion of the material, and ΔT is the difference of temperatures.

Irreversible and, therefore, unacceptable plastic deformations described by tensor ε_{ij}^p are not considered in this paper.

Final remark. Many material parameters are significantly dependent on temperature. Mentioned can be, for example, electric conductivity, magnetic permeability, thermal conductivity, specific heat, coefficient of linear expansion, etc. All these dependences (as far as they are known) are included in the computations.

Numerical solution. Magnetic field is solved in a classic way using second-order finite element method. The discretization mesh must cover not only the system, but also its relatively large neighborhood. It is calculated independently and takes into account only temperature variations of the electric conductivity γ and magnetic permeability μ . The mesh remains the same in the course of the calculations, the geometric changes due to thermoelastic dilatation are neglected.

Solution of the temperature field is carried out by an algorithm based on the generalized Crank–Nicolson method that respects the temperature variations of parameters λ and ρc_p .

The solution of the thermoelastic problem by the finite element method uses at every time step a linearized Lagrange variational equation for increments [7] in the form

$$\begin{aligned} & \iint_{S_0} \left(\Delta \sigma^{ij} \delta \Delta e_{ij} + \sigma^{ij} \delta \Delta \eta_{ij} - \Delta F^i \delta \Delta u_i \right) r \cdot dS - \int_{l_0} \Delta P^i \delta \Delta u_i r \cdot dl + \\ & + \iint_{S_0} \left(\sigma^{ij} \delta \Delta e_{ij} - F^i \delta \Delta u_i \right) r \cdot dS - \int_{l_0} P^i \delta \Delta u_i r \cdot dl = 0; \\ & \iint_{S_0} \left(\Delta \sigma^{ij} \delta \Delta e_{ij} + \sigma^{ij} \delta \Delta \eta_{ij} - \Delta F^i \delta \Delta u_i \right) r dS - \int_{L_0} \Delta P^i \delta \Delta u_i r dL + \\ & \iint_{S_0} \left(\sigma^{ij} \delta \Delta e_{ij} - F^i \delta \Delta u_i \right) r dS - \int_{L_0} P^i \delta \Delta u_i r dL, \quad (14) \end{aligned}$$

where S_0 and L_0 are the surface and boundary of the meridian cross-section of the structure, σ^{ij} and $\Delta \sigma^{ij}$ denote the components of the stress tensor and their increments,

Δe_{ij} and $\Delta \eta_{ij}$ stand for the increments of the linear and nonlinear parts of the strain tensor, Δu_{ij} are the increments of components of the displacement vector, f^i and Δf^i are the components of the volume loads (for example gravitational) and their increments in one time step and, finally, P^i and ΔP^i denote the components of the surface load and their increments.

Unfortunately, in the devices under consideration, from time to time it is necessary to take into account the exchange of heat inside the gap between individual structural parts of the device. This exchange is realized through the contact zone that varies in time and that must be determined in the course of solution of the thermoelastic problem. There are several possibilities to take into account the dependence of the contact thermal conductivity K_n on the contact pressure p_c .

In many cases it is enough to use only two values of K_n . For $p_c \geq 0$ (absence of the contact) we put

$$K_n(T, p_c) = K_n^+, \quad \text{for } p_c < 0 \quad (\text{presence of the contact})$$

$$K_n(T, p_c) = K_n^-.$$

Here, K_n^+ is a relatively small value (or even zero) describing the heat conductivity of the contact layer through the ambient environment, while $K_n^- \approx \lambda / h$, where λ is the thermal conductivity of the layer, and h denotes its roughness.

For more accurate computations it is recommended to use more complicated empirical formulae such as that given in [8].

Even when the mechanical problem is considered to be linear (without plastic deformations), searching of the unknown contact domain (or domains) between both parts in each step is realized by means of an iterative process.

Contact problem. Modeling of the contact interaction between two parts is based on the concept of a special contact finite element having no thickness. The functional for the temperature problem is supplemented with components corresponding to the thermal conductivity of this contact layer. The heat generated due to mutual sliding of both parts can also be taken into account, but the heat capacity (specific heat) of the contact layer is neglected. Using a special 1D 4-node finite elements we obtain a system of equations for the description of the thermo-contact problem.

The functional of the temperature problem for the contact layer can be written in the form [7]

$$\begin{aligned} I = & \frac{1}{2} \int_{L_k} \left[K_n(S_\mu, \sigma_n) (T_2 - T_1)^2 + Q(S_\mu, \sigma_n, \nu) T_1 + Q(S_\mu, \sigma_n, \nu) T_2 \right] r_0 d\tau - \\ & - \int_{L_{q1}} q_1(S_\mu, \sigma_n) T_1 r_0 d\tau - \int_{L_{q2}} q_2(S_\mu, \sigma_n) T_2 r_0 d\tau + \\ & + \int_{L_{a1}} \alpha_1(S_\mu, \sigma_n) [T_1 - T_\infty(S_\mu, \sigma_n)] T_1 r_0 d\tau + \\ & + \int_{L_{a2}} \alpha_2(S_\mu, \sigma_n) [T_2 - T_\infty(S_\mu, \sigma_n)] T_2 r_0 d\tau, \quad (15) \end{aligned}$$

where $K_n(S_\mu, \sigma_n)$ is the contact thermal conductivity (not the contact thermal resistance), which can be estimated as a ratio «thermal conductivity of material of the layer» / «thickness of the layer», S_μ are the subdomains («macro-elements») made of different materials, σ_n is the

normal contact pressure, T_1, T_2 are the surface temperatures of contacting parts (bodies), $Q(S_\mu, \sigma_n, \nu_r)$ denotes the internal heat source arising due to relative sliding of surfaces at the given friction, ν_r stands for the relative velocity of sliding contacting surfaces, q_1, q_2 are the heat fluxes into the contacting bodies, respectively, $T_\infty, \alpha_1, \alpha_2$ denote the temperature of the medium and heat transfer coefficients for the first and second bodies, respectively and r_0 is the distance from the contact point to the z -axis (for the axisymmetric problem) or the thickness of the subdomain (for the planar problem).

The internal heat sources due to mutual sliding of both parts are calculated as follows

$$Q = \sigma_n \nu_r f_f, \quad (16)$$

where f_f is the coefficient of friction between both surfaces.

These sources can be distributed between both contacting parts (bodies) by using the corresponding velocities ν_{r1} and ν_{r2} of sliding for both surfaces

$$Q_1 = \sigma_n \nu_{r1} f_f, \quad Q_2 = \sigma_n \nu_{r2} f_f \quad (17)$$

to take into account boundary conditions of the 2nd kind for both surfaces at the contact point.

Taking (17) into account, the variation of the functional (15) can be written in the form

$$\begin{aligned} \delta I = & \int_{L_k} [K_n(S_\mu, \sigma_n)(T_2 - T_1)(\delta T_2 - \delta T_1)] r_0 d\tau - \\ & - \int_{L_{q1}} q_1(S_\mu, \sigma_n) \delta T_1 r_0 d\tau + \\ & + \int_{L_{\alpha_1}} \alpha_1(S_\mu, \sigma_n) [T_1 - T_\infty(S_\mu, \sigma_n)] \delta T_1 r_0 d\tau + \\ & + \int_{L_k} \sigma_n \nu_{r1} f_f \delta T_1 r_0 d\tau - \\ & - \int_{L_{q2}} q_2(S_\mu, \sigma_n) \delta T_2 r_0 d\tau + \\ & + \int_{L_{\alpha_2}} \alpha_2(S_\mu, \sigma_n) [T_2 - T_\infty(S_\mu, \sigma_n)] \delta T_2 r_0 d\tau + \\ & + \int_{L_k} \sigma_n \nu_{r2} f_f \delta T_2 r_0 d\tau = 0 \end{aligned} \quad (18)$$

The temperature distribution in the 1D 4-node finite element can be represented in the form

$$\begin{aligned} T_1(\tau) &= T_{i1} \varphi_i(\tau) + T_{j1} \varphi_j(\tau); \\ T_2(\tau) &= T_{i2} \varphi_i(\tau) + T_{j2} \varphi_j(\tau), \end{aligned} \quad (19)$$

where $T_{i1}, T_{i2}, T_{j1}, T_{j2}$ are the nodal temperatures on the contact surfaces of both bodies, respectively, and $\varphi_i(\tau), \varphi_j(\tau)$ are the coordinate functions

$$\varphi_i(-\tau) = \frac{\tau_j - \tau}{\tau_j - \tau_i}; \quad \varphi_j(\tau) = \frac{\tau - \tau_i}{\tau_j - \tau_i}. \quad (20)$$

Substituting (19) into (20) and collecting terms at the same variations, we can obtain a system of equations for the thermo-contact element as follows

$$\begin{aligned} A_{i,i} T_i + A_{i,i+1} T_{i+1} + A_{i,j} T_j + A_{i,j+1} T_{j+1} &= b_i; \\ A_{i+1,j} T_i + A_{i+1,i+1} T_{i+1} + A_{i+1,j} T_j + A_{i+1,j+1} T_{j+1} &= b_{i+1}; \\ A_{j,i} T_i + A_{j,i+1} T_{i+1} + A_{j,j} T_j + A_{j,j+1} T_{j+1} &= b_j; \\ A_{j+1,i} T_i + A_{j+1,i+1} T_{i+1} + A_{j+1,j} T_j + A_{j+1,j+1} T_{j+1} &= b_{j+1}; \end{aligned} \quad (21)$$

where

$$\begin{aligned} A_{k,k} &= \int_{L_k} K_n(S_\mu, \sigma_n) \varphi_k^2(\tau) r_0(\tau) d\tau + \\ & \int_{L_{\alpha_1}} \alpha_1(S_\mu, \sigma_n) \varphi_k^2(\tau) r_0(\tau) d\tau; \\ A_{k,k+1} &= A_{k+1,k} = - \int_{L_k} K_n(S_\mu, \sigma_n) \varphi_k^2(\tau) r_0(\tau) d\tau; \\ A_{k+1,k+1} &= \int_{L_k} K_n(S_\mu, \sigma_n) \varphi_k^2(\tau) r_0(\tau) d\tau + \\ & + \int_{L_{\alpha_2}} \alpha_2(S_\mu, \sigma_n) \varphi_k^2(\tau) r_0(\tau) d\tau; \\ A_{i,j} &= A_{j,i} = - \int_{L_k} K_n(S_\mu, \sigma_n) \varphi_i(\tau) \varphi_j(\tau) r_0(\tau) d\tau + \\ & + \int_{L_{\alpha_1}} \alpha_1(S_\mu, \sigma_n) \varphi_i(\tau) \varphi_j(\tau) r_0(\tau) d\tau; \\ A_{i+1,j+1} &= A_{j+1,i+1} = - \int_{L_k} K_n(S_\mu, \sigma_n) \varphi_i(\tau) \varphi_j(\tau) r_0(\tau) d\tau + \\ & + \int_{L_{\alpha_2}} \alpha_2(S_\mu, \sigma_n) \varphi_i(\tau) \varphi_j(\tau) r_0(\tau) d\tau; \\ A_{i,j+1} &= A_{j+1,i} = A_{i+1,j} = A_{j,i+1} = \\ & = - \int_{L_k} K_n(S_\mu, \sigma_n) \varphi_i(\tau) \varphi_j(\tau) r_0(\tau) d\tau; \\ b_k &= \int_{L_{\alpha_1}} \alpha_1(S_\mu, \sigma_n) T_\infty(S_\mu, \sigma_n) \varphi_k(\tau) r_0(\tau) d\tau + \\ & + \int_{L_{q1}} q_1(S_\mu, \sigma_n) \varphi_k(\tau) r_0(\tau) d\tau + \int_{L_k} \sigma_n(\tau) \nu_{r1} f_f \varphi_k(\tau) r_0(\tau) d\tau; \\ b_{k+1} &= \int_{L_{\alpha_2}} \alpha_2(S_\mu, \sigma_n) T_\infty(S_\mu, \sigma_n) \varphi_k(\tau) r_0(\tau) d\tau + \\ & \int_{L_{q2}} q_2(S_\mu, \sigma_n) \varphi_k(\tau) r_0(\tau) d\tau + \\ & + \int_{L_k} \sigma_n(\tau) \nu_{r2} f_f \varphi_k(\tau) r_0(\tau) d\tau; \end{aligned} \quad (22)$$

where $k = i, j$;

After discretizing the model consisting of (15) – (22), it remains to cope with the displacements and mechanical strains and stresses along particular sliding surfaces (see Figs. 2 and 3).

At the points of the interpenetration of contact surfaces in the normal direction with condition

$$u_n^1 - u_n^2 - \delta_n < 0; \quad (23)$$

where u_n^1, u_n^2 are the displacements of the contact surfaces and δ_n is the width of the gap in the direction of the normal, we introduce sufficiently high contact stiffness C_n

in the normal direction in order to prevent the surfaces from penetrating each other. Should friction be taken into account, we further introduce an analogous tangential stiffness C_τ .

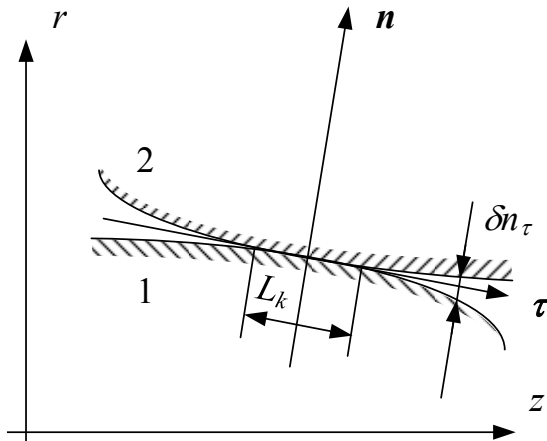


Fig. 2. Contact length L_k and gap δ_n between contacting bodies 1 and 2

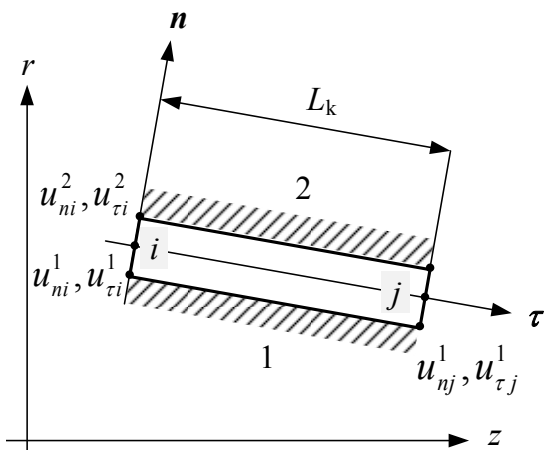


Fig. 3. Nodal displacements of the contact surfaces

The stresses in the contact layer are now given by the formulae

$$\sigma_n = C_n(u_n^1 - u_n^2 - \delta_n); \quad \sigma_\tau = C_\tau(u_\tau^1 - u_\tau^2 - \delta_\tau). \quad (24)$$

As far as the condition $\sigma_n f_f < |\sigma_\tau|$ of slipping is satisfied, the tangential stresses are expressed as

$$\sigma_\tau = \sigma_n f_f \text{sign}(u_\tau^1 - u_\tau^2 - \delta_\tau), \quad (25)$$

where u_n^1, u_τ^1 are the shifts of both surfaces and δ_τ is their difference at the beginning of the contact. In the zone of slipping the tangential stiffness is equal to zero and the functional is supplemented with the work of the friction forces on the corresponding shifts.

Illustrative example. A typical example is solved concerning the problem of assembly and disassembly of high-speed machine tools. The basic axisymmetric arrangement of the system is depicted in Fig. 4, together with the principal dimensions. The interference between the two connected parts is 0.01 mm.

During the process of assembly the chuck spindle has to be heated by the inductor until the internal diameter of the bore exceeds the diameter of the shank. The drill shank is then put into the bore and the system is cooled until we obtain a shrink fit.

On the other hand, the process of disassembly is characterized by fast heating of the system that causes different displacements in the chuck (that are relatively high) and in the drill shank (much lower). In a short time the pressed joint is released and the shank can be drawn out of the hole.

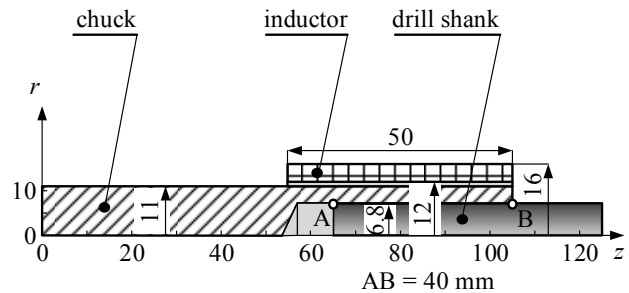


Fig. 4. Basic disposition of investigated system (dimensions in mm)

The chuck is made from steel. Comparative computations for drills made from hard alloy and alloyed tool steel are carried out, the inductor remaining the same.

The principal data of the problem follow (at the room temperature $T = 20^\circ\text{C}$):

- steel chuck: electric conductivity $\gamma_{20} = 3.2 \cdot 10^6 \text{ S/m}$, thermal conductivity $\lambda_{20} = 47 \text{ W/mK}$, heat capacity $\rho c_{p20} = 4 \cdot 10^6 \text{ J/m}^3\text{K}$, coefficient of linear thermal expansion $\alpha_{T20} = 2 \cdot 10^{-5} / \text{K}$, modulus of elasticity $E_{20} = 2 \cdot 10^{11} \text{ Pa}$, Poisson ratio $\nu = 0.3$.

- Hard alloy: electric conductivity $\gamma_{20} = 2.8 \cdot 10^6 \text{ S/m}$, thermal conductivity $\lambda_{20} = 85 \text{ W/mK}$, heat capacity $\rho c_{p20} = 2 \cdot 10^6 \text{ J/m}^3\text{K}$, coefficient of linear thermal expansion $\alpha_{T20} = 0.5 \cdot 10^{-5} / \text{K}$, modulus of elasticity $E_{20} = 5.3 \cdot 10^{11} \text{ Pa}$, Poisson ratio $\nu = 0.25$.

- Alloyed tool steel: electric conductivity $\gamma_{20} = 2.5 \cdot 10^6 \text{ S/m}$, thermal conductivity $\lambda_{20} = 37 \text{ W/mK}$, heat capacity $\rho c_{p20} = 3.2 \cdot 10^6 \text{ J/m}^3\text{K}$, coefficient of linear thermal expansion $\alpha_{T20} = 1.1 \cdot 10^{-5} / \text{K}$, modulus of elasticity $E_{20} = 1.9 \cdot 10^{11} \text{ Pa}$, Poisson ratio $\nu = 0.3$.

- Field current density $J_{\text{ext}} = 28.275 \text{ A/m}^2, f = 1 \text{ kHz}$.

- Cooling by forced air: $\alpha = 200 \text{ W/m}^2\text{K}$.

The contact mechanical problem is the main part of numerical analysis. Fig. 5 and 6 represent the calculated distributions of temperature and contact pressure at various time instants of the assembly and disassembly processes for drills made from hard alloy and alloyed tool steel. The maps were performed for the cross section $z = 85 \text{ mm}$. Some preliminary results can be found in [2]. The most important conclusions follow:

- Regarding assembly for both of materials (hard alloy or alloyed tool steel) of the drill: the chuck has to be heated during 3.5 s. Maximal temperature in it is 228°C , maximal difference through the thickness is 86°C .

- Regarding disassembly:

- Drill made of hard alloy: complete disassembly of the joint takes place in about 4 s after switching on the inductor. Maximum temperature in the chuck is 231°C (external edge of its face), in the drill is 85°C .

- Drill made of alloyed tool steel: duration of treatment is about 4.25 s.

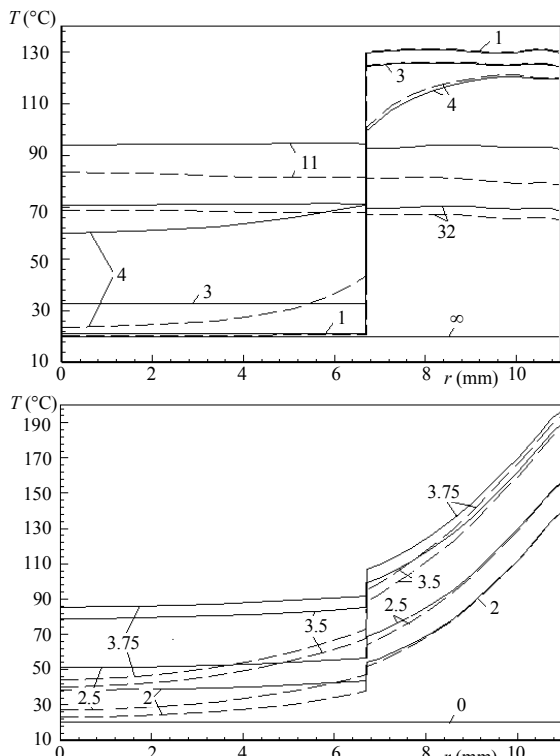


Fig. 5. Temperature distribution along joint radius ($z = 85$ mm) at various time levels (in s):
 up – assembly, bottom – disassembly.
 — drill made of hard alloy,
 - - - drill made of alloyed tool steel

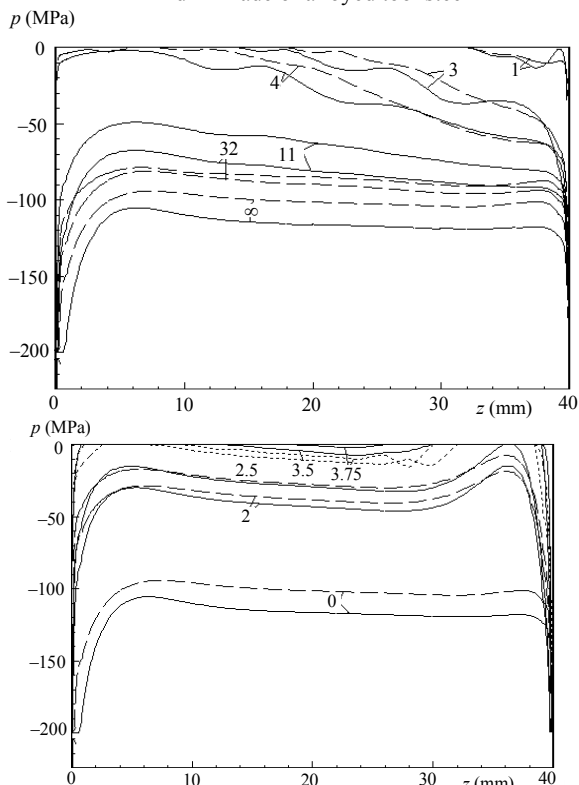


Fig. 6. Contact pressure distribution at various time levels (in s):
 up – assembly, bottom – disassembly
 — drill made of hard alloy, - - - drill made of alloyed tool steel

How to cite this article:

Pantelyat M.G., Doležel I. Finite element technique for solution of thermo-contact problems and its application in numerical analysis of devices working with induction heating. *Electrical engineering & electromechanics*, 2016, no.4, pp. 22-27. doi: 10.20998/2074-272X.2016.4.03.

Conclusions. A 2D finite element technique for solution of multiphysics (electromagnetic, thermal and structural) problems taking into account contact interaction between structural parts is proposed. The contact problem solution is based on a concept of a special 1D contact finite element (layer) having no thickness. The presented technique is applied for the computer simulation of assembly of a shrink fit.

REFERENCES

1. Driesen J., Belmans R.J.M., Hameyer K. Finite-element modeling of thermal contact resistances and insulation layers in electrical machines. *IEEE Transactions on Industry Applications*, 2001, vol.37, no.1, pp. 15-20. doi: 10.1109/28.903121.
2. Shulzhenko N.G., Gontarowsky P.P., Matyukhin Yu.I., Pantelyat M.G., Doležel I., Ulrych B., Beneš K. Computer modeling of induction heating-based assembly and disassembly of shrink fits. *Acta Technica CSAV*, 2004, vol.49, no.2, pp. 169-183.
3. Doležel I., Karban P., Ulrych B., Pantelyat M.G., Matyukhin Yu.I., Gontarowsky P.P., Shulzhenko N.G. Limit operation regimes of actuators working on principle of thermoelasticity. *IEEE Transactions on Magnetics*, 2008, vol.44, no.6, pp. 810-813. doi: 10.1109/tmag.2007.916226.
4. Chari M.V.K., Salon S.J. *Numerical Methods in Electromagnetism*. Academic Press, New York, 2000. ISBN 978-0126157604.
5. Holman J.P. *Heat Transfer, 10th edition*. McGraw-Hill, New York, 2002. ISBN 978-0073529363.
6. Timoshenko S., Goodier J.N. *Theory of Elasticity, 3rd Edition*. McGraw Hill, New York, 1970. ISBN 978-0070701229.
7. Podgorny A.N., Gontarowsky P.P., Kirkatsch B.N., Matyukhin Yu.I., Khavin G.L. *Zadachi kontaktного vzaimodeistviia elementov konstruksii* [Tasks of contact interaction in construction elements]. Kiev, Naukova Dumka Publ., 1989. ISBN 5-12-000891-7. (Rus).
8. Schlykov Yu.P., Ganin E.A., Carevskij S.N. *Kontaktnoe termicheskoe soprotivlenie* [Contact thermal resistance]. Moscow, Energiya Publ., 1977. (Rus).

Received 15.03.2016

M.G. Pantelyat¹, Candidate of Physics and Mathematics, Associate Professor,
 Ivo Doležel², Professor,

¹National Technical University «Kharkiv Polytechnic Institute», 21, Kyrpychova Str., Kharkiv, 61002, Ukraine, e-mail: m150462@yahoo.com

²Czech Academy of Sciences, Institute of Thermomechanics, 5, Dolejškova, 182 00 Praha 8, Czech Republic, e-mail: dolezel@fel.cvut.cz

V.V. Shevchenko

INFLUENCE OF MANUFACTURING QUALITY OF LAMINATED CORE ON A TURBOGENERATOR EXPLOITATION TERM

The problem of calculating the flexural deformation of the laminated core of the stator turbogenerator is examined. The evaluation of the effect of gluing the core sheets on its bending stiffness based on the compliance of the insulating cover sheet of active steel. An impact of pressing effort on the relative movement of the package of sheets is determined. An effect of wear of the insulating layer between sheets of laminated core on its reliability is determined. Conclusions are drawn on how to determine the possibility of extending the life of turbogenerators on the basis of the data obtained. References 8, table 1, figures 5.

Key words: laminated core, flexural deformation, stator of turbogenerator, flexural stiffness, insulation coating, pressing, time of exploitation.

Рассмотрен расчет изгибной деформации шихтованного сердечника статора турбогенератора. Выполнена оценка влияния склейки листов сердечника на его изгибную жесткость с учетом податливости изоляционного покрытия листов активной стали, значения усилия прессовки пакета на относительное перемещение листов. Определено влияние износа изоляционного слоя между листами шихтованного сердечника на его надежность. Сделаны выводы, как на основании полученных данных установить возможность продления срока эксплуатации турбогенераторов. Библ. 8, табл. 1, рис. 5.

Ключевые слова: шихтованный сердечник, изгибная деформация, статор турбогенератора, изгибная жесткость, изоляционное покрытие, прессовка, время эксплуатации

Introduction. The economic condition of the country makes it impossible to perform the timely replacement of electrical equipment, which has worked on the technical specification operational time of the plant unit. Therefore, the period of its work can be extended only by means of modernization and/or partial replacement of major components. Modernization of turbogenerators (TG) is provided with the increase power in the installed overall dimensions, sometimes performed with replacement of refrigerant. Therefore, in the construction to be upgraded it is necessary to consider the accumulated experience of manufacturing and operation, to exclude all of the factors that lead to the destruction of the assembly machines and units, especially, a stator core, for reliability. Its destructions are the most frequent cause of crashes.

TG reliability and durability are reduced due to a complex laminated core structure, vibration, electromagnetic continuous variables, thermal and mechanical loads. Due to the frequent destruction of the cores the researchers are looking for new design solutions for increasing operational reliability TG. The new design is based on the use of new materials and new techniques in the production of technology, on the knowledge of data exploitation and modern trends of development of the theory of the creation of turbogenerators [1-3].

The aim of the article is to determine the effect of TG stator core assembly technology to its reliability and the definition of the possibility extending the service life (impact gluing the core sheets on its bending stiffness, impact of pressing forces on the relative movement of the package sheet and wear of the insulating layer between sheets of the laminated core).

The main text of the article. The design quality of the laminated stator core determines its bending stiffness and consequently affects the value of the radial vibration and reliability. The works of many authors are devoted to these issues, [4-8], which also show the results of the research physical and mechanical properties of the insulating cover sheet steel. Also, the temperature coefficients of the materials that are used, static and dynamic loads; the

presence, size, shape of ventilation ducts between packets impact on it.

Consider the impact on the operational status of the core circuit stacking the stacked sheets and the quality of insulation coatings under the action of forces that cause the flexural deformation and the relative movement of the stacked sheets. Let us allocate part of the laminated core package, where several floors (joints) fall. We represent this part as a straight girder, which is made of rectangular thick electrical steel sheets with a thickness h and isolated coatings δ , Fig. 1.

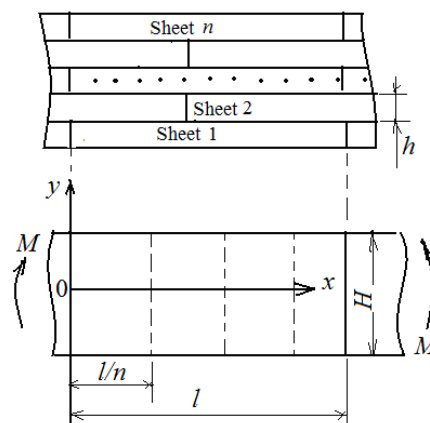


Fig. 1. Laminated veneer lumber: h – thickness of the sheets constituting the laminated board (package of the stacked plates); M – moment of bending forces; H – width of the beam; l – length of the considered area (wave height); n – number the joints, got in area under consideration

We believe in the calculations that the tension in all the sheets is identical. We obtain under the law of pairing shear stresses, that tangential stresses in the cross section are shear stresses, which arise in the longitudinal sections. It is suffice to consider the deformation of the strip in n layers, when the sheets are stacked to overlap by $1/n$ part of their length, because in the other layers of pattern the same will happen.

© V.V. Shevchenko

Use Zhuravsky formula for further calculations, which allows you to determine the tangential stresses in bending. These stresses arise from the external force P in the points of girder cross section, which are at a distance l from the neutral axis x , Fig. 2. In the beam appear normal and tangent stresses, which are directed from the edge to the edge of the law paired relationship.

We calculate the shear stresses that occur. Spend two verticals through the beam cross section at a distance dx from one another. Let us note a horizontal section at a distance $(h/2-y)$ of the neutral layer. That is, we select the element with the size: $dx, (h/2-y), b$.

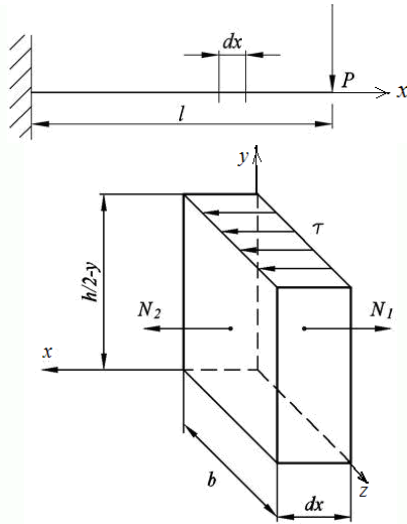


Fig. 2. Model actions of on a girder of the external force F , which is located at a distance l from the neutral axis x

We lay off on the axis x all the forces that act on the system for drawing up the balance equations. The action of elementary tangential force $dT=N_2-N_1$, which is equal to the element $(b \cdot dx)$, is equal to $dT=\tau \cdot b \cdot dx$, is balanced by the difference of normal forces (N_2-N_1) . Normal stresses that act on the infinitely small side area dF , disposed at the neutral axis y can be calculated:

$$\sigma = \frac{M \cdot y}{J_x}$$

The force dN_1 that acts on the area element is equal to:

$$dN_1 = \frac{M \cdot y}{J_z} \cdot dF$$

On the whole side face of area F the aggregate force of N_1 will operate:

$$N_1 = \int_F dN_1 = \int_F \frac{M \cdot y}{J_z} \cdot dF = \frac{M}{J_z} \cdot \int_F y \cdot dF = \frac{M \cdot S_z}{J_z}$$

where S_z – distribution of the tangential stresses a relatively the neutral axis z ; J_z – axial moment inertia of the regarded section.

Similarly, the force that acts on the next side face of the selected element N_2 :

$$N_2 = \frac{(M + dM) \cdot S_z}{J_z}$$

where $N_2 - N_1 = dT = \frac{dM \cdot S_z}{J_z} = \tau \cdot b \cdot dx$.

We write down the value of tangential stress τ :

$$\tau = \frac{dM \cdot S_z}{dx \cdot J_z \cdot b} = \frac{Q \cdot S_z}{J_z \cdot b}, \quad (1)$$

where Q – transverse elemental force of the bending moment that acts on the length of the fixed element ($Q = dM/dx$).

The tangential stresses that arise in the material above the neutral layer is directly proportional to the transverse force, to the static moments square section under consideration, and is inversely proportional to the axial moment of inertia and its width. Then the distribution of tangential stresses over the cross section will be:

$$S_z = F \cdot y_0 = b \cdot \left(\frac{h}{2} - y \right) \cdot \left(y + \frac{h-y}{2} \right) =$$

$$= \frac{b}{2} \cdot \left(\frac{h}{2} - y \right) \cdot \left(\frac{h}{2} + y \right) = \frac{b}{2} \cdot \left[\left(\frac{h}{2} \right)^2 - y^2 \right]$$

Substitute the S_z in the formula (1). Define a tangential stress in a selected element based on the fact that the axial moment of inertia for the rectangular cross section is

$$J_z = \frac{b \cdot h^3}{12} :$$

$$\tau = \frac{\frac{b}{2} \cdot \left[\left(\frac{h}{2} \right)^2 - y^2 \right] \cdot Q}{\frac{b \cdot h^3}{12} \cdot b} = \frac{6 \cdot Q}{b \cdot h^3} \cdot \left(\frac{h^2}{4} - y^2 \right)$$

The tangential stresses on the central axis with $y = 0$ will be a half time more than average values in the sections, Fig. 3.

$$\tau_{\max} = \frac{6 \cdot Q}{b \cdot h^3} \cdot \frac{h^2}{4} = \frac{3}{2} \cdot \frac{Q}{b \cdot h} = \frac{3}{2} \cdot \frac{Q}{F} = \frac{3}{2} \cdot \tau_{\text{mid}}$$

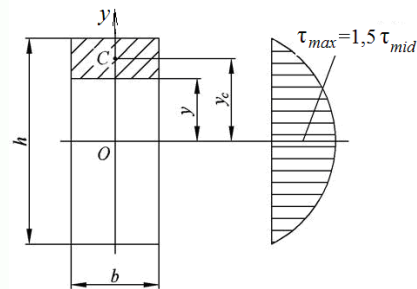


Fig. 3. The distribution of tangential stresses

The tangential stresses are the maximum value in the neutral layer; the normal stresses are equal to zero. So the tangential stresses are on the surface of the beam, only normal. It is believed that the transverse carved by area are level and are rotated by the action of the bending moments. But the tangential stresses distort the form of the deformation. Elements of the material between the two cross sections warp the proportion to the magnitude of these stresses. These distortions effect a little on the value of longitudinal deformation of the elements that make up the beam. This allows the use of a formula for the normal stresses:

$$\sigma_{\max} = \frac{M_{\text{use}}^{\max}}{W_z} \leq [\sigma]$$

From beams of rectangular cross-section (Fig. 4,a) an element of length dz is cut out (Fig. 4,b).

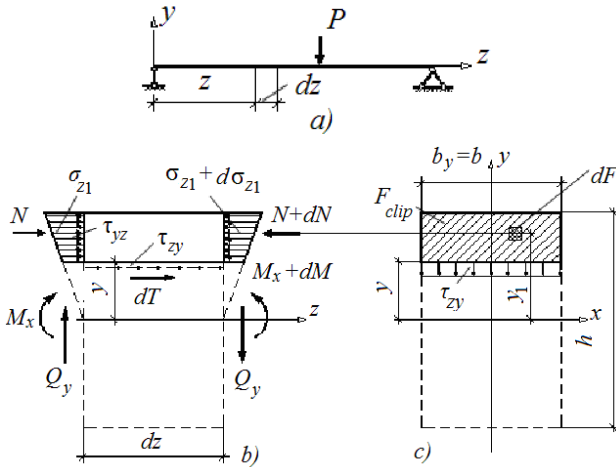


Fig. 4. The scheme of calculating tangential stresses in bending beam

Consider the balance of the top of the beams section, where stresses arise due to the difference of bending moments. In order this portion of the beam is in equilibrium ($\Sigma Z=0$), in a longitudinal section of the beam there must be the tangential force dT .

The equilibrium equation of the girder:

$$\Sigma Z = \int_{F_{clip}} \sigma_{z1} \cdot dF - \int_{F_{clip}} (\sigma_{z1} + d\sigma_{z1}) \cdot dF + dT = 0.$$

Here

$$dT = \int_{F_{clip}} d\sigma_{z1} \cdot dF = \int_{F_{clip}} \frac{dM_x}{I_x} \cdot y_1 \cdot dF = \frac{dM_x}{I_x} \cdot S_x^{clip},$$

where the integration is performed only over the severed part of the cross sectional area of F_{clip} beams (the shaded area in Fig. 4,c); S_x^{clip} – static moment of inertia of cross sectional area dF of about the neutral axis x :

$$S_x^{clip} = \int_{F_{clip}} y_1 \cdot dF.$$

Assume that the tangential stress (τ_{yz}), which arises in longitudinal section beams, distributed uniformly over its width (b_y). Then:

$$dT = \tau_{yz} \cdot b_y \cdot dz.$$

Considering that $\tau_{yz} = \tau_{zy}$, the tangential stress (τ_{zy}) in the points in the cross section beams at a distance y from the neutral axis x , can be calculated:

$$\tau_{yz} = \frac{dM_x}{dz} \cdot \frac{S_x^{clip}}{I_x \cdot b_y}, \text{ where } \frac{dM_x}{dz} = Q_y, \tau_{zy} = \frac{Q_y \cdot S_x^{clip}}{I_x \cdot b_y}.$$

Longitudinal strain and stress have a major importance in the flexural deformation in a solid and glued laminated tool bar, as shown in [8]. We can assume that the tangential stress and normal stresses from deformation along the other axes are missing: $\sigma_y = \sigma_z = \tau_{xy} = \tau_{xz} = \tau_{yz} = 0$.

We believe that the core layers operate only shear and that the longitudinal displacement of points r_i ($i = 1, 2, \dots$ where n – number of the layer) on each sheet of thickness are the same. We obtain from the equilibrium conditions for the laminated section [7]:

$$\left. \begin{aligned} E \cdot h \cdot \frac{\partial^2 R_1}{\partial x^2} &= \frac{G}{\delta} \cdot (2R_1 - R_2 - R_n); \\ E \cdot h \cdot \frac{\partial^2 R_2}{\partial x^2} &= \frac{G}{\delta} \cdot (2R_2 - R_1 - R_3); \\ &\dots \\ E \cdot h \cdot \frac{\partial^2 R_i}{\partial x^2} &= \frac{G}{\delta} \cdot (2R_i - R_{i-1} - R_{i+1}); \\ &\dots \\ E \cdot h \cdot \frac{\partial^2 R_n}{\partial x^2} &= \frac{G}{\delta} \cdot (2R_n - R_{n-1} - R_1), \end{aligned} \right\} \quad (2)$$

where E – effective elastic modulus for the electrical steel sheet in the longitudinal direction (Unge modulus), $E = 2 \cdot 10^5$ MPa; G – the shear modulus in the stacked structure (in the «glued layer»), $G = 79,3 \cdot 10^3$ MPa.

We shall seek solution of the system of equations (2) as the dependence:

$$R_i = A_i(y) \cdot e^{\lambda x}, \quad (3)$$

where $A_i(y)$ – the amplitude of the movement of the stacked structure along the axis y ; λ – a constant which depends on the material (first Lamé parameter).

For a particular material λ expressed by Unge modulus E and Poisson's ratio ν :

$$\lambda = \frac{\nu \cdot E}{(1 + \nu) \cdot (1 - 2\nu)}.$$

After a few solution transformations the following can be represented:

$$R_i = A_{i0} + B_{i0} \cdot x + \sum_{k=1}^{n-1} (A_{ik} \cdot e^{\lambda_k \cdot x} + B_{ik} \cdot e^{-\lambda_k \cdot x}), \quad (4)$$

where $A_{ik}(y)$ and $B_{ik}(y)$ – the function-coordinates of points along the y axis y in a quantity $2n^2$.

The expressions for A_{ik} and B_{ik} present with the use of the coefficient B_0 :

$$A_{ik} = B_0 \cdot a_k; \quad B_{ik} = B_0 \cdot b_k, \quad (5)$$

where a_k and b_k – the numerical coefficients.

The solution of system (4) can finally be written:

$$R_i = A_0(y) + B_0(y) \cdot x + B_0(y) \cdot \sum_{k=1}^{n-1} a_{ik} \cdot (a_k \cdot e^{\lambda_k \cdot x} + b_k \cdot e^{-\lambda_k \cdot x}). \quad (6)$$

The average cross-section of each sheet is not corrected due to the symmetry of the tensions distribution. Therefore, we can write for the case of even n :

$$R_{n/2}(0, y) = 0; \quad R_{(n/2)+1}(l/n, y) = \alpha \cdot y. \quad (7)$$

The function $B_0(y)$ is a linear function of the coordinates y according to the equation (10). The dependence of the $B_0(y)$ expressed in terms of stress, rather than through the angular movement.

It can be concluded from the relation (6), which in laminated beams, as in the continuous beams, tensions adjustment section is distributed linearly. Then the function $B_0(y)$ can be represented:

$$B_0(y) = C \cdot y, \quad (8)$$

where C – the coefficient of proportionality.

We determine its meaning, assuming that the bending moment along the length of the beam is constant:

$$2E \cdot h \cdot \sum_{i=1}^n \int_0^{H/2} \frac{\partial R_i}{\partial x} \cdot y \cdot dy =$$

$$= 2E \cdot h \cdot \int_0^{H/2} n \cdot C \cdot y^2 \cdot dy = \frac{h \cdot n \cdot H^2}{6} \cdot \sigma_0, \quad (9)$$

where σ_0 – the maximum value of the bending stress in the continuous bar in the same section as laminated beams, and the same value of the bending moment. Then:

$$C = \frac{2\sigma_0}{E \cdot H}. \quad (10)$$

The shear stresses in the insulating layer will be the greatest in the corners of the steel sheets, [8]:

$$\tau'_{\max} = -\frac{G}{\delta} \cdot [R_1(0) - R_n(0)]$$

$$\tau''_{\max} = -\frac{G}{\delta} \cdot [R_1(0) - R_2(0)] \quad (11)$$

If we assume that the relative displacement along the x axis for the two points of outer surface of located at a distance l from one another for a continuous beam at $y = H/2$ is:

$$\Delta R_0 = \frac{\sigma_0 \cdot l}{E}, \quad (12)$$

then laminated to the bar is the offset that can be presented subject to the availability of the axial displacement of the joints of two successive sheets in a layer (the first three summands), and the presence of the relative displacement of the edges of the sheet (last summand):

$$\Delta R = 2R_1\left(0, \frac{H}{2}\right) - R_2\left(0, \frac{H}{2}\right) - R_n\left(0, \frac{H}{2}\right) +$$

$$+ \sum_{i=1}^n \int_0^{l/n} \frac{\partial R_i(x, \frac{H}{2})}{\partial x} \cdot dx. \quad (13)$$

From equations (5), (6), (12) it follows that:

$$\sum_{i=1}^n A_{ik} = 0, \quad \sum_{i=1}^n B_{ik} = 0. \quad (14)$$

Then on the grounds of (9) and (13):

$$\sum_{i=1}^n \int_0^{l/n} \frac{\partial R_i(x, \frac{H}{2})}{\partial x} \cdot dx = \int_0^{l/n} \frac{n \cdot \sigma_0}{E} \cdot dx = \frac{\sigma_0 \cdot l}{E}. \quad (15)$$

The ratio of $\Delta R/\Delta R_0$ characterizes increase flexural laminated steel bar compliance compared with a solid rod in the same cross-sectional. Consider the three schemes laying steel sheets lapped by 1/2, 1/3 and 1/4 of the sheet (respectively, $n = 2, 3, 4$). Finally, we get:

$$1) n = 2, \quad \frac{\Delta R}{\Delta R_0} = 1 + \frac{4}{\lambda \cdot l}, \quad \lambda = \sqrt{\frac{4G}{E \cdot h \cdot \delta}},$$

$$\left| \tau'_{\max} \right| = \left| \tau''_{\max} \right| = \frac{2G \cdot \sigma_0}{\lambda \cdot E \cdot \delta},$$

$$2) n = 3, \quad \frac{\Delta R}{\Delta R_0} = 1 + \frac{3}{\lambda \cdot l}, \quad \lambda = \sqrt{\frac{3G}{E \cdot h \cdot \delta}},$$

$$\left| \tau'_{\max} \right| = \left| \tau''_{\max} \right| = \frac{3G \cdot \sigma_0}{\lambda \cdot E \cdot \delta}, \quad (16)$$

$$3) n = 4, \quad \frac{\Delta R}{\Delta R_0} = 1 + \frac{8}{l \cdot (\lambda_1 + 2\lambda_2)},$$

$$\lambda_1 = \sqrt{\frac{4G}{E \cdot h \cdot \delta}}, \quad \lambda_2 = \sqrt{\frac{2G}{E \cdot h \cdot \delta}},$$

$$\left| \tau'_{\max} \right| = \frac{6G \cdot \sigma_0}{E \cdot \delta \cdot (\lambda_1 + 2\lambda_2)}, \quad \left| \tau''_{\max} \right| = \frac{2G \cdot \sigma_0}{E \cdot \delta \cdot (\lambda_1 + 2\lambda_2)}.$$

Thus, the relative pliability laminated timber ($\Delta R/\Delta R_0$) are determined by the longitudinal length and the thickness of sheet, method of laying, the strength characteristics of steel and the thickness of the insulating layer. The pliability decreases with an increasing length of the sheet. This dependence to the insulation layer is not present. And maximum tangential stress is proportional to the maximum bending stress in the steel.

If laminated core packets are not glued and are pressed only by uniform pressure p_0 , the bending deformations cause the slip of sheet steel in the area of junctions (Fig. 5).

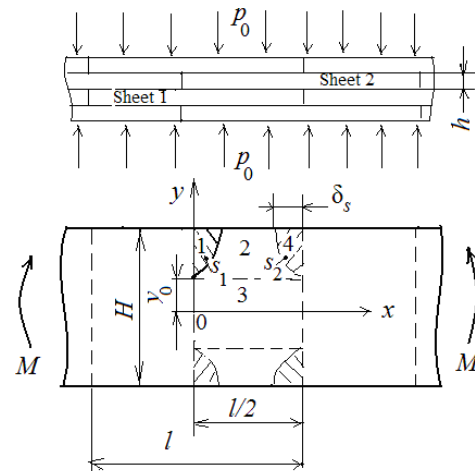


Fig. 5. The bar that is laminated and pressed

Sliding is present in zones 1 and 4 (in zones 2 and 3, sliding is not) when sheets are stacked with overlapping on the 1/2 of sheet:

- in zones 1 and 4:

$$\frac{\partial^2 R_1}{\partial x^2} = -\frac{2f \cdot p_0}{E \cdot h}, \quad \frac{\partial^2 R_2}{\partial x^2} = \frac{2f \cdot p_0}{E \cdot h}, \quad (17)$$

- in zones 2 and 3:

$$\frac{\partial^2 R_1}{\partial x^2} = \frac{2G}{E \cdot h \cdot \delta} \cdot (R_1 - R_2), \quad \frac{\partial^2 R_2}{\partial x^2} = -\frac{2G}{E \cdot h \cdot \delta} \cdot (R_1 - R_2), \quad (18)$$

where f – coefficient friction of sliding steel on steel.

Consider a turbogenerator TGV-225-2. Let us substitute in the formula (17) such values as $E=2 \cdot 10^5$ MPa, $\delta=0,3$ mm, $h=0,5$ mm, $l = 40$ mm, $G=79,3 \cdot 10^2$ MPa. The number of layers selected for calculation is equal to $n=2,3,4$. The calculation results are shown in Table 1.

Table 1

The maximum bending stress in the laminated core

n	H , mm	$\Delta R/\Delta R_0$	T_{\max} , kH/m ²
2	1.0	1.027	900
3	1.5	1.024	800
4	2.0	1.023	400

The solution of equations (17) and (18) shown later (the first index – the number of the sheet, the second – the number of the zone where bending occurs):

$$\begin{cases}
R_{11} = -\frac{f \cdot p}{E \cdot h} \cdot x^2 + C_1 \cdot x + C_2; \\
R_{14} = -\frac{f \cdot p}{E \cdot h} \cdot x^2 + C_1' \cdot x + C_2'; \\
R_{21} = \frac{f \cdot p}{E \cdot h} \cdot x^2 + D_1 \cdot x + D_2; \\
R_{24} = \frac{f \cdot p}{E \cdot h} \cdot x^2 + D_1' \cdot x + D_2'; \\
R_{12} = A_0 + B_0 \cdot x + A_1 \cdot \varepsilon^{\lambda x} + B_1 \cdot \varepsilon^{-\lambda x}; \\
R_{22} = A_0 + B_0 \cdot x - A_1 \cdot \varepsilon^{\lambda x} - B_1 \cdot \varepsilon^{-\lambda x}; \\
R_{13} = A_0' + B_0' \cdot x + A_1' \cdot \varepsilon^{\lambda x}; \\
R_{23} = A_0' + B_0' \cdot x + A_1' \cdot \varepsilon^{\lambda x} + B_1' \cdot \varepsilon^{-\lambda x}; \\
\lambda = \sqrt{\frac{4G}{E \cdot h \cdot \delta}},
\end{cases} \quad (19)$$

where ε – the elastic deformation of the sample, which causes a voltage (it equals the ratio of change of the sample size after deformation to its initial size).

Most commonly the relationship between stress and deformation is linear (Hooke's law): $\sigma = \varepsilon \cdot E$.

The values of the coefficients of equations (19) can be obtained from the condition that the deformation is symmetrical, using the boundary conditions (20) and the conditions at the zones boundaries of sliding (21):

$$\begin{cases}
\frac{\partial R_{23}}{\partial x} \Big|_{x=0} = \frac{\partial R_{21}}{\partial x} \Big|_{x=0} = 0; \\
\frac{\partial R_{14}}{\partial x} \Big|_{x=\frac{l}{2}} = \frac{\partial R_{13}}{\partial x} \Big|_{x=\frac{l}{2}} = 0; \\
R_{11} \Big|_{s1} = R_{12} \Big|_{s2}; \quad R_{12} \Big|_{s2} = R_{14} \Big|_{s2}; \\
R_{21} \Big|_{s1} = R_{22} \Big|_{s1}; \quad R_{22} \Big|_{s2} = R_{24} \Big|_{s2}; \\
\frac{\partial R_{11}}{\partial x} \Big|_{s1} = \frac{\partial R_{12}}{\partial x} \Big|_{s1}; \quad \frac{\partial R_{12}}{\partial x} \Big|_{s2} = \frac{\partial R_{14}}{\partial x} \Big|_{s2}; \\
\frac{\partial R_{21}}{\partial x} \Big|_{s1} = \frac{\partial R_{22}}{\partial x} \Big|_{s1}; \quad \frac{\partial R_{22}}{\partial x} \Big|_{s2} = \frac{\partial R_{24}}{\partial x} \Big|_{s2}; \\
-\frac{G}{\delta} \cdot (R_{11} - R_{21}) \Big|_{s1} = f \cdot p; \\
-\frac{G}{\delta} \cdot (R_{14} - R_{24}) \Big|_{s2} = f \cdot p.
\end{cases} \quad (20)$$

where α – angular deformation (rotation angle of a bar cross-sections at a height y from the middle cross section), degrees:

$$\begin{aligned}
\alpha \cdot y &= \frac{f \cdot p_0}{E \cdot h} \cdot (l + 2x_1) \cdot x_1 - \\
& - \frac{f \cdot p_0 \cdot \delta \cdot \lambda \cdot \left(\varepsilon^{\lambda x_1} - \varepsilon^{\frac{\lambda \cdot l}{2}} \cdot \varepsilon^{-\lambda x_1} \right)}{2G \cdot \left(\varepsilon^{\lambda x_1} + \varepsilon^{\frac{\lambda \cdot l}{2}} \cdot \varepsilon^{-\lambda x_1} \right)} \cdot \left(\frac{l}{2} + 2x_1 \right) + \\
& + \frac{f \cdot p_0 \cdot \delta}{G} \approx \frac{f \cdot p_0}{E \cdot h} \cdot (l + 2x_1) \cdot x_1 + \\
& + \frac{f \cdot p_0 \cdot \delta}{G} \cdot \left(1 + \frac{\lambda \cdot l}{4} + \lambda \cdot x_1 \right); \\
x_2 &= \frac{l}{2} - x_1.
\end{aligned} \quad (22)$$

From the side of the equation (22), which is indicated by (\approx), we will find:

$$x_1 = -\frac{\lambda \cdot l + 4}{4\lambda} + \sqrt{\frac{\lambda^2 \cdot l^2 - 16}{16\lambda^2} + \frac{2G}{f \cdot p_0 \cdot \delta \cdot \pi^2}} \cdot \alpha \cdot y. \quad (23)$$

From here the maximum width the zone of sliding α is determined depending on the pressing pressure p_0 and the amount of the angular deformation bend of laminated element for a specific material, whose parameters are given values of E, G, f and dimensions of the steel sheets (H, h, δ):

$$\begin{aligned}
b_s &= x_1 \cdot \left(\frac{H}{2} \right) = -\frac{\lambda \cdot l}{4\lambda} + \\
& + \frac{1}{\lambda} \cdot \sqrt{\frac{\lambda^2 \cdot l^2 - 16}{16\lambda^2} + \frac{G \cdot H}{f \cdot p_0 \cdot \delta}} \cdot \alpha.
\end{aligned} \quad (24)$$

Let us substitute into the equation (23) the value of $x_1 = 0$ to obtain the coordinates of the lower point of the zone of sliding y_0 (Fig. 2):

$$y_0 = \frac{f \cdot p_0 \cdot \delta}{\alpha \cdot G} \cdot \left(1 + \frac{\lambda \cdot l}{4} \right). \quad (25)$$

If $y_0 \geq h/2$, that the sliding of sheet is virtually absent, and angular deformation α can be determined in this case as:

$$\alpha = \alpha_n = \frac{2f \cdot p_0 \cdot \delta}{G \cdot H} \cdot \left(1 + \frac{\lambda \cdot l}{4} \right), \quad (26)$$

where α_n – angular deformation (rotation angle of the n -th plate in a section of the rod at the height y from the middle cross section), degrees.

We introduce auxiliary coefficients:

$$a = \frac{2G \cdot H}{f \cdot p_0 \cdot \delta \cdot \lambda^2}, \quad b = \frac{\lambda^2 \cdot l^2}{16\lambda^2}.$$

The total bending moment $M(\alpha)$ for the two sections of adjacent sheets does not depend on the position of the point of consideration (does not depend on the coordinate x).

Moment depends only on the angular deformations α :

$$\begin{aligned}
M(\alpha) &= 2h \cdot E \cdot \int_0^{H/2} \left(\frac{\partial R_1}{\partial x} + \frac{\partial R_2}{\partial x} \right) \cdot y \cdot dy = \\
& = 4h \cdot E \cdot \left(\int_0^{y_2} B_0' \cdot y \cdot dy + \int_{y_0}^{H/2} B_0 \cdot y \cdot dy \right) = \\
& = \frac{8h \cdot E \cdot \lambda}{3(4 + \lambda \cdot l)} \cdot \alpha \cdot y_0^5 - f \cdot l \cdot \left(\frac{H^2}{4} - y_0^2 \right) + \\
& + \frac{16f \cdot p_0}{15\alpha^2} (3a \cdot y - 2b) \cdot \sqrt{(b + a \cdot y)^3} \Big|_{y_0}^{H/2}.
\end{aligned} \quad (27)$$

For continuous a bar of the same dimensions:

$$M_0 = \frac{E \cdot h \cdot H^3}{3l} \cdot \alpha_0. \quad (28)$$

If necessary to consider only the α and the angular deformation of the system there is no relative sliding, the bending moment in the angular area of deformations can be calculated:

$$M(\alpha) = \frac{E \cdot h \cdot \lambda \cdot H^3}{3(4 + \lambda \cdot l)} \cdot \alpha. \quad (29)$$

The relative increase in the flexural suppleness laminated element can be calculated as the ratio of $M(\alpha)$ to

M_0 (based on the presence of the insulation between the sheets and the possible the relative sliding of the sheets):

$$\frac{\alpha}{\alpha_0} = \frac{E \cdot h \cdot H^3 \cdot \alpha}{3l \cdot M(\alpha)}. \quad (30)$$

If in (30) substitute the value of $M(\alpha)$ from (29), the relative change in the flexural compliance laminated element can be represented by:

$$\frac{\alpha}{\alpha_0} = 1 + \frac{4}{\lambda \cdot l}.$$

Therefore, the relative change in the flexural compliance laminated element does not depend on α .

Conclusions:

1. The results of the calculation of the flexural deformation of the laminated core of turbogenerator based on the compliance of the insulating cover sheet active steel are obtained. These calculations allow making a conclusion that the flexural rigidity of the core in the glued cores of turbogenerators decreases slightly, no more than 3 %. Therefore the modulus of elasticity of glued laminated of the core is reduced by no more than 3 % compared to module of monolithic steel. In the not-bonded cores in which interconnection is provided only the pressing of sheets, stiffness decreases with increasing the flexural deformation.

2. The selection of the compaction pressure of the laminated core should be carried out based on the possible slip of sheets when vibration occurs, also taking into account knowledge of strength the adhesive layer and safe limits of relative sliding. Correctly selected compression effort reduces the relative sliding of the sheets in the package:

- the relative sliding of the laminated core sheets exists on the width not more than 2 mm ($b_s < 2$ mm) in the joint area when pressure of pressing is $p_0 \geq 1$ MPa and a amplitude of radial oscillations of vibration that do not exceed $A \leq 20$ mkm. The effect of relative sliding sheet decreases a little the bending stiffness of the core in this case, not more than 1 %:

- the relative sliding of the core sheets is practically absent in this range of vibrations and with compacting pressure $p_0 \geq 1,5$ MPa. Accordingly, weakening the pression in the core leads to an increase of vibration, to a reduce of the bending rigidity, to a reduce of the bending rigidity, to an increase of the relative sliding sheets (up to 10 mm), to an abrasion of insulating coating of sheet active steel, to the connection of adjacent sheets, to increased losses in the steel, to heat until the «fire in the steel». Gluing laminated core sheets reduces the impact of this phenomenon.

3. Due to the presence the struts of radial ventilation the uneven pressure distribution arises after pressing, which can be neglected. This can be done, because this unevenness may be compensated in the glued packages with the help of binder materials, a shift steel sheets in packs without gluing only in a narrow region near the joints sheets sufficiently wide range of pressures. Ventilation spacers which establish beside the joints of sheets support the local increase of the pressure and decrease the

slip zone. If the spacers are installed far away from the joints of sheets, they reduce the bending stiffness of the core and they extend the relative sliding zone.

4. Wear insulating layer between sheets of laminated core can be neglected, because:

- during the exploitation the pressure pressing cores decreases, which reduces the intensity of wear of the insulating layer;

- in areas where an insulating layer is erased, the products of wear are not removed but accumulated, and continue to perform the insulation function;

- during an operating process, the lacquer polymerization process that isolates, is continuing, which increases gluing of active steel sheets, increases the bending stiffness, reduces the vibration.

5. As a result it can be concluded that the period of exploitation of turbogenerators may be not less than 50 years, and not 20-25 years as previously thought, [4, 5]. This conclusion can be fundamental in determining possibility of extending the time of exploitation of the turbogenerators.

REFERENCES

1. Shevchenko V.V. Methods of quantitative assessment of technical condition electrical equipment to determine the need for its rehabilitation or replacement. *Collected materials of the Int. sci.-pract. conf. «Modern trends in the MRO. Diagnostics of equipment of mining and metallurgical and energy complexes (PBMCs)»*, 10-12 September 2015, pp. 39-42. (Rus).
2. Vasilev V.S., Johansen V.I. Experience and projects construction of deep modernization of powerful turbogenerators stator in the conditions of power. *Electrical Appliances 2003: Abstracts of the conference*. St. Petersburg, Electrosila, 2003. pp. 9-12. (Rus).
3. Shevchenko V.V., Minko A.N. Modernization of constructions domestic turbogenerators taking into account the requirements to maintain their competitiveness. *Bulletin of NTU «KhPI»*, 2014, no.38(1081), pp. 146-155. (Rus).
4. Warsawskiy G.Y. Influence segments and laminating the stator iron on the magnetic vibration of electrical machines AC. *St. Petersburg: Collected Electrosila*, 1989, no.37, pp. 42-45. (Rus).
5. Vaskovskiy Yu.N., Shumilov Yu.A., Shtogrin A.V. Analysis of vibration-exciting axial forces in a powerful turbo-generator stator core. *Electrical engineering & electromechanics*, 2009, no.2, pp. 21-26. (Rus). doi: 10.20998/2074-272x.2009.2.04.
6. Geller P.L., Burak A.M., Sinayuk S.L. Indicators of active stator turbogenerator packages strength steel, which are glued. *Dynamics and strength of powerful turbo- and hydrogenerators. – Collected USRIE*, 1987, pp. 9-14. (Rus).
7. Johansen V.I. The effect on the rigidity of the stator core turbogenerator pasting active steel. *Leningrad: Collection «Methods for calculating the turbo- and hydrogenerators»*, 1975, no.95, p. 103. (Rus).
8. Johansen V.I., Storozhev V.D. Calculation of the mechanical characteristics of the bonded electrical steel packages. *Leningrad: Collection Electrosila*, 1976, no.31, pp. 102-105. (Rus).

Received 25.04.2016

V.V. Shevchenko, Candidate of Technical Science, Associate Professor,

National Technical University «Kharkiv Polytechnic Institute», 21, Kyrpychova Str., Kharkiv, 61002, Ukraine.
phone +380 50 407845, e-mail: zurbagan_@mail.ru

How to cite this article:

Shevchenko V.V. Influence of manufacturing quality of laminated core on a turbogenerator exploitation term. *Electrical engineering & electromechanics*, 2016, no.4, pp. 28-33. doi: 10.20998/2074-272X.2016.4.04.

V.V. Budashko

INCREASING CONTROL'S EFFICIENCY FOR THE SHIP'S TWO-MASS ELECTRIC DRIVE

Purpose. For shipboard lifting and transporting machinery (LTM) with AC thyristor electric drives (ED) the problem of minimizing sway through the formation of the special law to change the principle of ED control over the lifting process is solved. *Methodology.* This goal was achieved through the following objectives: analysis of current studies on the reduction of the negative effects of load fluctuations, fixed on the suspension with variable parameters; determining the criteria to optimize the movement of the lifting mechanism and transfer control laws under which the load fluctuations are reduced; develop the methodology and experimental study of the main characteristics of the mobile model ED lifting mechanism with its load suspended from the perspective of both the parameterization of the control system (CS) as well as elements of ED. For realization of tasks in research methods of mathematical modeling of dynamic processes on the computer, structural methods of control theory, experimental studies in the laboratory setting have been used. *Results.* Based on analysis of current research can be concluded that the stability of the ED of LTM to the disturbing points provided coincidence zero electric coordinates and speed deviation diametric plane of the vessel from the vertical position. Criteria for optimizing CS used by the ED LTM mathematical description of its dynamics differential equations to the estimated coefficients derived from the functions of state variables. The experimental dependence of dynamic equations of motion of an object under the influence of disturbing forces in the coordinate plane allowed to parameterize characteristic equation to the form, providing the solution to sustainability since the motor shaft of LTM. The functional circuit of CS eliminates the aperiodic components in the control in compliance with the criteria of sustainability and quality of transients by applying all-range regulator coordinate characteristics of forcing overcoming the dead zone and increase electric resistance as the dynamic object. *Practical value.* Completion of the complex research may find practical application in the ED of ship's LTM, which will improve their performance, decrease between the operating and maintenance simple. References 15, figures 9.

Key words: ship's two-mass electric drive, control system, load sway, mathematical modeling, improvement, adaptability, stabilization.

На основании теоретических и практических исследований двухмассового электропривода судовой грузовой системы рефрижераторного судна, в работе решена научно-техническая проблема усовершенствования системы управления электроприводом, находящегося под разновекторными возмущениями. Результатом выполненных исследований является объединение уравнений, описывающих перемещение груза механизмом подъема рамки держателя паллет, в систему дифференциальных уравнений с коэффициентами, зависящими от колебаний судна. В теоретической части синтезировано математическую модель электромеханической системы механизма подъема, что позволило исследовать способы минимизации углов раскачивания рамки держателя паллет и временных интервалов, необходимых для стабилизации перемещения груза двухмассовым электроприводом механизма подъема, что дало возможность косвенно имплементировать сигнал, связанный со стохастической природой момента колебания судна, на координатную плоскость электропривода подъема. Также усовершенствован и исследован способ параметрической оптимизации математической модели электромеханической системы в функции угла раскачивания груза. На основании определения структуры и алгоритмов работы повышена эффективность системы управления двухмассовым электроприводом механизма подъема с точки зрения уменьшения времени стабилизации перемещаемого груза. Библ. 15, рис. 9.

Ключевые слова: судовой двухмассовый электропривод, система управления, раскачивание груза, математическое моделирование, усовершенствование, адаптивность, стабилизация.

Introduction. There are a number of ship's lifting and transporting mechanisms (LTM) on which thyristor electric AC or DC drives are set: powerful overhead cranes, conveyors, high-performance column cranes. For such mechanisms tasks to minimize load sway can be effectively addressed through the formation of special laws for motor control, as the control system (CS) is built by a flexible technology. Currently, there are a number of solutions that reduce mechanical vibrations of the load [1]. These solutions are intended to limit accelerations in the transient and obtain a smooth change of the controlled parameter. These solutions include the use of master of intensity, utilization of filters on regulators outputs, the introduction of feedback by derivative controlled parameters, change of regulators gear ratios, regulation of starting and braking time [2]. When using the mentioned methods, significantly limit of load sway is achieved by significantly increasing the time of transients of load moving which reduces the performance of mechanisms. There is a need for the development of such control systems for LTM electric drives the use of which will most

effectively limit load sway at high performance of the electric drive and the possibility of flexible mechanisms control using regression methods [3].

Investigations are carried out as a part of the research state budget work «Concepts, technologies and ways of improvement of ship power systems (SPS) of combined propulsive complexes (CPC)» of the National University «Odessa Maritime Academy» (state registration number 0114U000340).

Problem definition. For ship's LTM a special operating mode is such in which there is need for change a control principle during the load lifting process that connected primarily with permanent effects of environment on automatic control object (ACO). Moreover, when ACO is meant a subsystem formed for the following conditions: CS allows purposefully to change the controlled variables at some regular intervals; targeted adjustment of controlled variables is assessed by measuring in real time. Accident-free flow of various technological, industrial and transport processes can be achieved only when certain

© V.V. Budashko

essential for these processes physical quantities are changed in some way. Task of respect the position is to provide practical change of the controlled value according to specified action when subjected to perturbation on the control process. In general, any automatic control system (ACS) can be build from two functionally complete sub-systems: ACO and a unit of automatic control (UAC) interconnected in accordance with the control principle.

ACS performing anti-sway functions are divided into two main groups: with closed and disconnected control circuits [4]. The first ones are based on the feedback signal from the current load, angular deviation, the position of the electric drive elements and its speed measured by additional sensors. Systems with open circuit are using the warning of the fact of the controlled parameter out the limit and their operation principle is based on the attempt to eliminate the error before it occurs.

At present there are different approaches to mitigate the release of load that moves from the steady state. In [5] they apply an intellectual approach to the input of the signal generated to prevent the sway, the so-called compensation method with derivative proportional the controlled parameter. The same control principle using a neural controller based on the principle of compensation of the uncertainty was proposed in [6]. Control based on an observer was developed and tested in a real bridge crane [7]. In [8], at the investigation of two-dimensional model of the gantry crane with a PD *fuzzy*-controller they used detention of the feedback signal with compensation of the generated input signal of the error.

The aim of the paper is improvement of efficiency of the control process of ship's lifting and transporting mechanism electric drive as an electromechanical object, the most dependent on the position of the ship's plane to reduce the duration of operational downtimes.

To achieve the mentioned goal, in the work it is necessary to solve the following problems:

- to analyze current investigations on reducing the negative effects of load sways mounted on hanger with variable parameters;
- to define criteria of optimization of control laws of motion for mechanisms to lift and move in which the load sways are reduced;
- to develop a technique of experiment and investigate the basic characteristics of a moving model of the electric drive of the lifting mechanism with hanging on it the load from point of view of parameterization of both the ACS and UAC elements;
- on the basis of investigations to offer a functional circuit of the ACS for movement of lifting and transporting mechanism working in synergy, and show the positive aspects of the application of the CS followed by the prospect of their integration into any technological process associated with ship handling and operational modes changes.

The object of investigations is control processes for two-mass electric drive of the ship's handling systems.

The subject of investigation is structural circuits and transformation of automatic controls of ship's load lifting AC electric drives.

Methods of investigations. For realization of tasks in research we will use methods mathematical modeling of dynamic processes on the computer, structural methods of automatic control theory, experimental investigations in a laboratory setup.

At this stage should be noted that the destabilization of the LTM movement depends primarily on the mismatch of control processes inside the ACS with other technological process on the ship as the object influenced by the environment. And if we consider SPS of CPC at the dynamic positioning (*DP*) mode, to do not take into account destabilizing factors is the right way to unresolved problems of load sway in general [9, 10].

Analyzing, for example, stability by Lyapunov, it is first need to pay attention to spatial equations describing the CS considering disturbing environmental factors affecting the CPC. That is, we can state necessity to improve Lyapunov methods because stability definition for a dynamic system, which is the ACS excluding the impact on it of the CPC behavior does not make sense [11].

There are many criteria for ACS stability but for CPC in general and in particular for the SPS as controlled objects a nonlinear transient structure that imposes restrictions on the application of these criteria for the time invariant nonlinear ACS for ship's characterized is characterized. Therefore, while the second Lyapunov method, on the other hand, infringes on versatility, and it is a prerequisite to analyze stability of nonlinear dynamic ACS, accurate solutions of its application is nothing to wait because they may be out of reach, and obtaining a successful result can be a daunting task, even – unfulfilled [12].

The next is the fact that for stationary linearized ACS inherent a problem of optimizing the gear ratios of regulators while respecting all electric performance of all electric drive as a part of the SPS of CPC. This is achieved by successive iterative reduction of gear ratios by the Lyapunov method typically using differential equations written in matrix form of linear inequalities to ensure the performance of electric drive [13]. Numerical examples show that the method is effective at identifying ACS controllers with too reduced gear factors that satisfy typical limitation of the performance, and as the main method, it can be extended to handle nonlinear ACS and controllers [14].

Fig. 1 shows a fragment of a handling systems of an upgraded refrigerated ship designed to guarantee parallel to the main on the upper deck technological process of pallet loading.

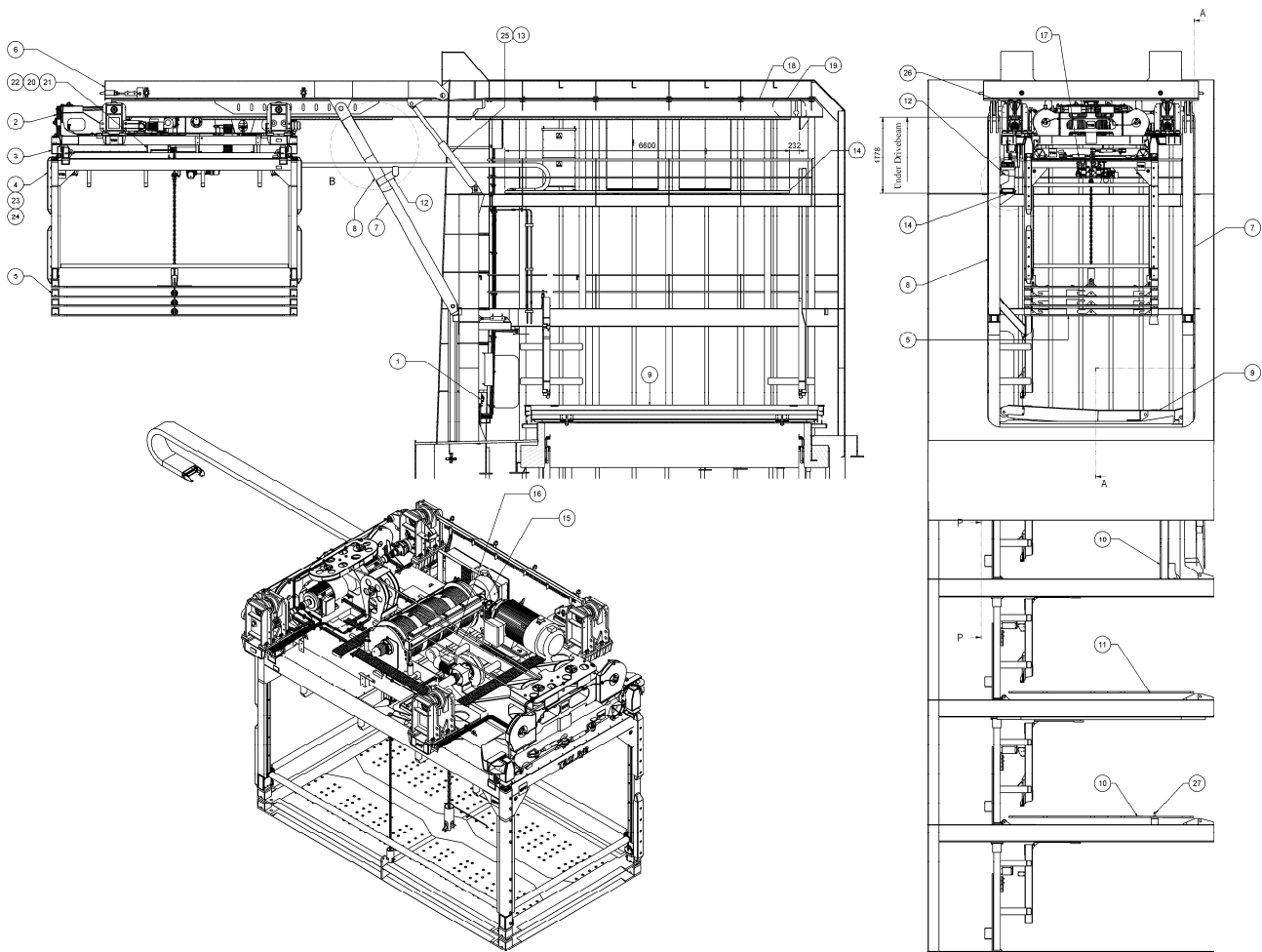


Fig. 1. A pallet handling system of a refrigerator ship: 1 – hydraulic installation; 2 – mounted metal trolley structure; 3 – mounted metal dispatcher structure; 4 – cage; 5 – additional low plate; 6-8 – side doors; 9 - manhole cover of the upper deck; 10 – manhole cover of the 2nd/4th deck; 11 – manhole cover of the 3rd deck; 12 – cable of the support network of left-hand assembly; 13 – cylinder bracket on the deck; 14 – tray for cable chain; 15, 16 – cable; 17 – hitch; 18, 19 – left and right trolley drives, respectively; 20 – power cable; 21 – cable fastening bracket; 22 – cable clamps; 23 – extra-heavy connector; 24 – cable input; 25 – hydraulic cylinder; 26 – anvil for sensor; 27 – axle; 28 – plate for blocking the internal trolley position; 29-31 – washer of the drive attachment Drivebeam; 32 washer; 33 – hexagonal self-locking nut; 34 – cylinder block head screw

The movement of loaded pallets is characterized by transient modes that depend on the behavior of the ship, so to describe it control laws for the lifting mechanism with smoothly variable acceleration were used. Identification of the ACS of the LTM for the pallet as stationary is possible with the assumption that the mass of the pallet is constant furthering its movement, so requirements are imposed to total time of the cargo operation.

The actual load oscillation is a very complex process that for practical calculations can be replaced by harmonic vibrational motion. The rate of vertical movement of the load is large enough. It should be borne in mind that the ship has the oscillatory motion with frequency usually lower than the frequency of oscillation of cargo. As a result, the speed of movement of the cable will be equal to the algebraic sum of the rates of movement of cargo and

cable fastening points.

Solving the first and the second problems based on the equations of motion of a rigid body a system of equations for the determination of the relative vertical movement of the suspended frame of the pallet holder of the refrigerator ship's LTM (Fig. 2) was composed. Since such a parameter as ship's weight is decisive in the transient CPC and SPS in particular, the parameters of the loading electric drive can be neglected. In this regard account of ship's oscillations, change of the SPS and CPC parameters is generally carried out based on the use of so-called *DMI*-model models of ships depending on tonnage, disturbing factors and gear factors of regulators for all modes taking into account the ship transition to another operating mode.

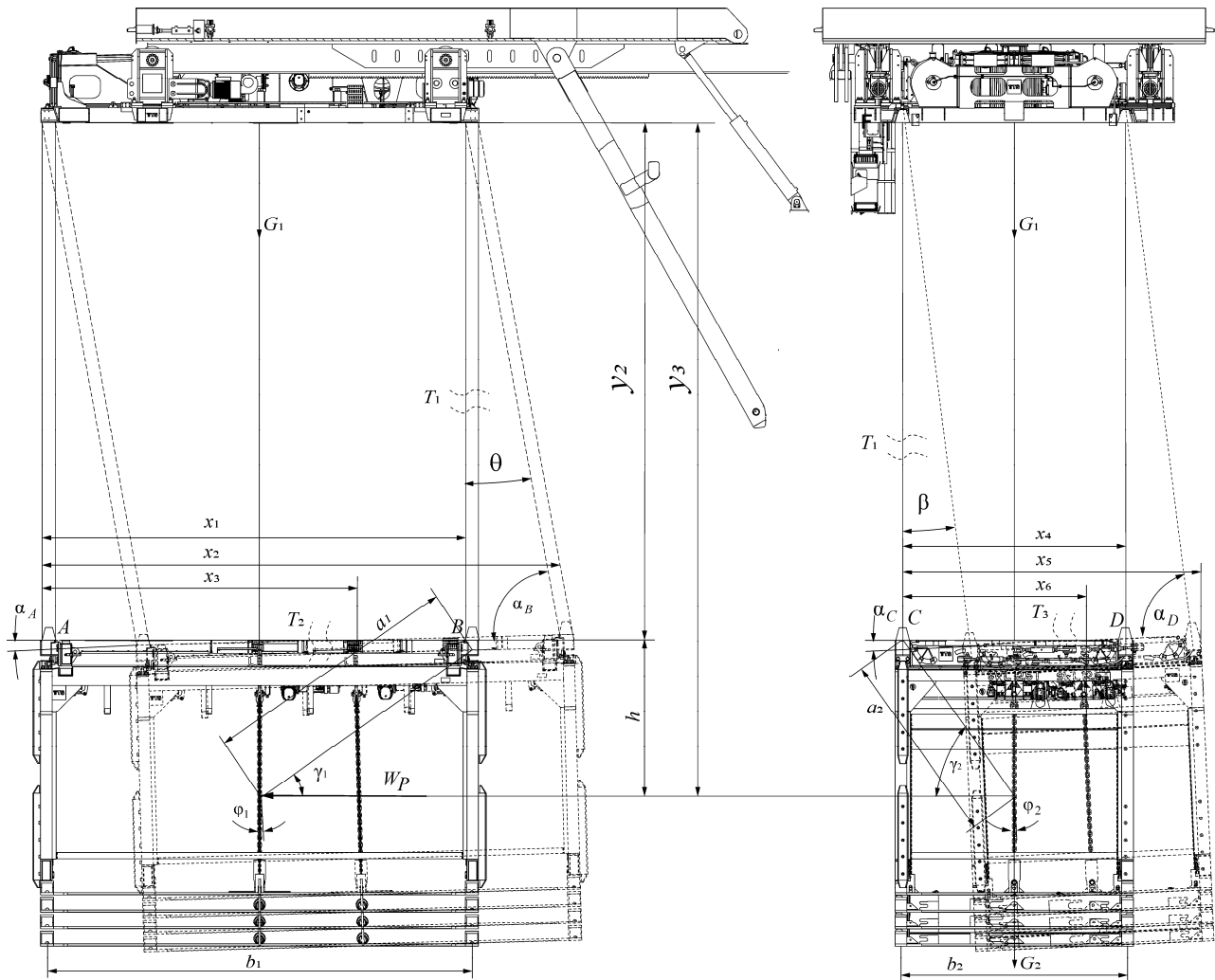


Fig. 2. A diagram of movement dynamics of the lifting mechanism: m_1 – lift carriage mass; F_T – total driving force; W_P – friction force of the carriage movement; T_1 – tension force of the perimeter cables; T_2, T_3 – tension forces of the transverse cables; G_1 – gravity of the lift carriage; G_2 – gravity of the cargo retractor (pallet); G_3 – gravity of the cargo (pallet); $\varphi_{1,2}$ – carriage rotation angle; $\alpha_{A,C}, \alpha_{B,D}$ – angles between cargo and cables; θ, β – deviation angles of corresponding cables from initial position; h – vertical distance between points of cables fixing and cargo center of gravity; $b_{1,2}$ – distances between points of cables fixing; $a_{1,2}$ – distances between points of cables fixing and cargo center of gravity

$$\begin{cases}
 \ddot{x}_{1,4} = \frac{1}{m_1} (-T_{1,4} \times \sin(\theta, \beta) + F_T - W); \\
 \ddot{y}_1 = 0; \\
 \ddot{x}_{2,5} = \frac{1}{m_2} (T_{1,4} \times \sin(\theta, \beta) - T_{2,3} \times \cos(\alpha_A, \alpha_C) + T_{3,2} \times \cos(\alpha_B, \alpha_D)); \\
 \ddot{y}_2 = \frac{1}{m_2} (T_{1,4} \times \cos(\theta, \beta) - T_{2,3} \times \sin(\alpha_A, \alpha_C) - T_{3,2} \times \sin(\alpha_B, \alpha_D) - G_2); \\
 \ddot{x}_{3,6} = \frac{1}{m_3} (T_{2,3} \times \cos(\alpha_A, \alpha_C) - T_{3,4} \times \cos(\alpha_B, \alpha_D) - W_P); \\
 \ddot{y}_3 = \frac{1}{m_3} (T_{2,3} \times \sin(\alpha_A, \alpha_C) + T_{3,2} \times \sin(\alpha_B, \alpha_D) - G_3); \\
 \varphi_{1,2} = \frac{1}{m_3} (T_{2,3} \times a_{1,2} \times \cos(\alpha_A, \alpha_C - \gamma_{1,2}) - T_{3,4} \times a_{1,2} \times \cos(\alpha_B, \alpha_D - \gamma_{1,2}));
 \end{cases} \quad (1)$$

where $T_1 = k \times \Delta l_1 + \beta \times \Delta l_1$ is the tension force of the perimeter cables; $k = \frac{E \times S}{l_1}$ is the cable stiffness coefficient; E is

the absolute module of elasticity of the hanger material; $S = \frac{\pi \times d^2}{4} \times c$ is the sectional area of the cable; d is the cable

diameter; c fill factor of the cable section; $\Delta l_1 = l_1 - l_{10}$ is the perimeter cables expansion; l_1 is the perimeter cables length during movement; l_{10} is the perimeter cables length in the equilibrium state; $\Delta \dot{l}_1 = \frac{(x_1 - x_2) \times (\dot{x}_1 - \dot{x}_2) + (y_1 - y_2) \times (\dot{y}_1 - \dot{y}_2)}{\sqrt{(x_1 - x_2)^2 + (y_1 - y_2)^2}}$ – is the velocity of the perimeter cables length change; β is the coefficient of energy losses; $T_2, T_3 = k \times \Delta l_2, \Delta l_3 + \beta \times \Delta \dot{l}_2, \Delta \dot{l}_3$ is the tension forces of the transverse cables; $\Delta l_2, \Delta l_3, \Delta l_5, \Delta l_6 = l_2, l_3, l_5, l_6 - l_{20}, l_{30}, l_{50}, l_{60}$ is the length change of the transverse cables; $l_2, l_3, l_5, l_6 = \sqrt{(x_{2,5} - x_{A,C}, x_{B,D})^2 + (y_2 - y_{A,C}, y_{B,D})^2}$ is the length of the transverse cables during movement; $l_{20}, l_{30}, l_{50}, l_{60}$ is the length of the transverse cables in the cargo equilibrium state; $\Delta \dot{l}_2, \Delta \dot{l}_3, \Delta \dot{l}_5, \Delta \dot{l}_6 = \frac{(2 \times (x_{2,5} - x_{A,C}, x_{B,D}) \times (\dot{x}_{2,5} - \dot{x}_{A,C}, \dot{x}_{B,D}) + (2 \times (y_2 - y_{A,C}, y_{B,D}) \times (\dot{y}_2 - \dot{y}_{A,C}, \dot{y}_{B,D})))}{2 \times \sqrt{(x_{2,5} - x_{A,C}, x_{B,D})^2 + (y_2 - y_{A,C}, y_{B,D})^2}}$ is the velocity of the transverse cables extension; G_1 is the gravity of the cargo restrainer of the pallet; G_2 is the gravity of the cross bar; m_3 is the pallet mass; $\theta, \beta = \arctan\left(\frac{x_{1,4} - \dot{x}_{1,4}}{x_{2,5} - \dot{x}_{2,5}}\right)$ is the deviation angle of the perimeter cables from the initial position; $\alpha_A, \alpha_C = \arcsin\left(\frac{(x_{2,4} - x_{A,C})(y_{B,D} - y_{A,C}) - (x_{A,C} - x_{B,D})(y_2 - y_{A,C})}{b \times l_2}\right)$ is the angle between the cross bar and cargo; $\alpha_B, \alpha_D = \arcsin\left(\frac{(x_{2,4} - x_{B,C})(y_{A,C} - y_{B,D}) - (x_{B,D} - x_{A,C})(y_2 - y_{B,D})}{b \times l_3}\right)$ is the angle between the diameter ship's plane and cargo; $a_{1,2} = \sqrt{h^2 + \left(\frac{b_{1,2}}{2}\right)^2}$ is the distance between the gravity center and cargo fixing points in the carriage; h is the vertical distance between the center of gravity and points of cargo fixing in the carriage; $b_{1,2}$ are the distances between points of carriage fixing; $W_P = 1000 \times \frac{1}{2} \times \rho \times \dot{x}_{3,6} \times c_A \times n \times b_{1,2} \times h$ is the friction force at the cargo movement; ρ is the environment density; c_A is the coefficient of the aerodynamic force account; n is the overload capacity.

For the synthesis of the model of a two-mass electric lifting drive we used tools of three packages of the *MATLAB* system: basic *Simulink* (controlling and information channel with PID-regulator of speed) as well as specialized *Sim-Power Systems* (virtual blocks of the power channel) and *Simulink Response Optimization* (channel of optimization of built PID-regulators). In developing the model the recommendations and general approaches outlined in [12, 15] (Fig. 3) are taken into account.

Below are functional purposes of block of the model, in parentheses are parameters that are introduced into the fields of windows of elements adjustment: *M* – induction electric motor with squirrel cage (rated power, linear voltage, frequency, active resistance and inductance of stator and rotor windings, mutual inductance, moment of inertia, number of pole pairs); *M_s* – block of load setting (the value of static torque); *VS1...VS6* – thyristors of the thyristor voltage regulator (TVR) included two in each phase and connected back-to-parallel (resistance in the open and closed states, voltage drop on the thyristor); *AVS* – a system of pulse-phase control (SPPC) (network frequency, width of control pulses); *ST* – block of permission (zero signal) or prohibition (single) to the SPPC operation; *Sub* – subsystem forming required range of angles to control TVR thyristors (minimum and maximum values); *AC* – three-phase AC power network (linear voltage, frequency, resistance and inductance of the source); *QF* – circuit breaker (resistance in open and closed states); *AQF* – control unit for the circuit breaker (switch on by a single signal, switch off - zero); *UV* – block of sensors of power supply voltage for synchronization of SPPC operation (linear or phase voltages); *LF* – three-phase current limiting reactor for EMC of the electric drive and electric network (resistance and inductance); *ER* – block of required speed setting (the value of the signal and the time of its

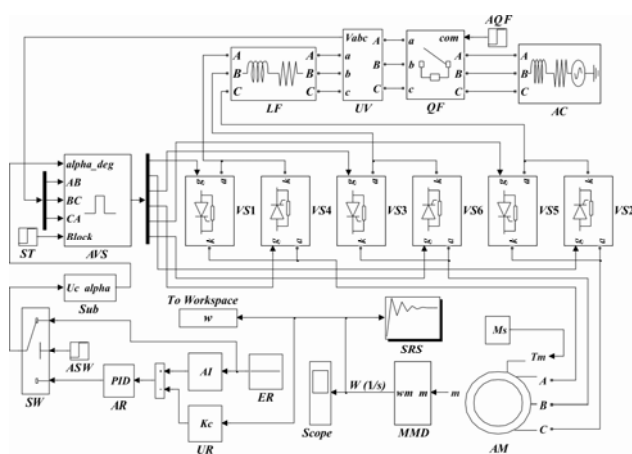


Fig. 3. Computer model of the experimental facility in *Matlab Simulink*

coming); *AI* – setter of intensity to limit the acceleration of the drive (rate of increase of the signal of the set speed); *AR* – PID-regulator of speed (proportional, integral and differential components, limitations of output signal); *UR* – speed sensor to form a negative feedback (gear ratio); *MMD* – block of controlled parameters extraction (speed and torque of the motor); *SRS* – block of optimization of parameters of PID-regulator of speed (required parameters of the transient); *Scope* – oscilloscope for visualization of monitored parameters (number of inputs, modeling time); *To Workspace* – block of speed values output to the working area for further processing (controlled parameter indicator); *SW* – key switching the model operation modes (numerical value of the functioning setup); *ASW* – key control block (single input signal commutes top input, zero - bottom).

To process discrete numerical values of the experimental speed characteristics taken from the working area of the *MatLab* system and to determine factors of the ACS transfer functions tools of the package *Labview* were used. In our case the following values of factors were obtained: $b_0 = 6.2334e^9$, $a_1 = 8726.8$, $a_2 = 0.98763e^7$, $a_3 = 4.31234e^8$ – at approximation by the transient characteristic of the 3rd order; $K = 18$, $a_0 = 8.345e^7$, $a_1 = 0.04567$ – at approximation by the transient characteristic of the 2nd order.

The next step of investigations is determination of dependences to calculate the components of PID-regulator of speed by the gradient-less Powel method in which computation of derivatives is performed by simplified difference formulae which provides increased speed of optimization. Appropriate formulae can be obtained using classical technique similar systems with subordinate regulation of coordinates taking into account the dependences (1).

For the third-order approximately, ignoring the part of the polynomial of the denominator of the third degree:

$$K_P = \frac{a_2}{a_C T_\mu b_0 K_C}, \quad K_I = \frac{a_3}{a_C T_\mu b_0 K_C}, \quad K_D = \frac{a_1}{a_C T_\mu b_0 K_C},$$

$$K_P = \frac{a_1}{a_C T_\mu K K_C}, \quad K_I = \frac{1}{a_C T_\mu K K_C}, \quad K_D = \frac{a_0}{a_C T_\mu K K_C}, \quad (2)$$

In the presented expressions K_C is the coefficient of the negative feedback by speed; T_μ is the time constant taking into account operating speed of the TVR thyristors; a_C is the adjustable parameter of the speed circuit (standard value equals to 2). Calculated components of the PID-regulator of speed are input to the adjustment window of the block *AR* parameters. At modeling of the closed system TVR-IM we commute the lower input by the key *SW*. To obtain results of modeling without regulator's parameters optimization it is necessary to start the process by the button of the model main window.

The main requirements for electric drives of lifting mechanism based on the above analysis are: ensuring start of lifting without an unacceptable shock in the cable, providing cable tension before the lifting, exclusion of re-

peated impact of the lifted load by ship. These requirements can be achieved in two ways.

The first way. The electric drive has two basic speeds, low for the cable tension at the beginning of movement (0.25-0.35 m/s) and high for the load lifting equal to the average rate of the ship's lifting in the direction of the load lifting or exceeds it. The high speed is of 1.5-2 m/s depending on the wavelength of the ship's oscillation. The transition of the electric drive to high speed the control system should carry out when the load will be in the lowest point of the ship's slope at the stretched cable. Here, the load begins to lift along with the beginning of the lifting of the ship and, after a slack of the cable will be chosen, continues to lift at a constant speed until the time of the lift of the ship in the direction of the load movement is over and if the following condition met

$$v_l \geq 1.3 \frac{h_0}{T_l}, \quad (3)$$

where v_l is the speed of the load movement, and

$$1.3 \frac{h_0}{T_l} \approx 1.$$

The adjustment range of speeds for lifting mechanisms operating under this method should be 1/6÷1/8. Obviously, these mechanisms should be used for loads of limited mass (less than 15 t) because at the increasing of power of the electric drive the inertia of the system increases.

The second way. Loading mechanism has a special design with a cable or a mechanical differential and two motors. One of the motors is traction, and another - speed. Traction motor provides selecting the initial cable slack with speed of 0.2 ÷ 0.25 m/s, and then it switches to maximum speed. At the same time high-speed motor switches on connected to the mechanism by overtaking clutch and click. Speed motor should ensure removing the cable at speed of at least $2h_0/T_l - 0.5$ m/s and acceleration time when removing the cable idle no more than $T_l/10$. After reaching the top point of lifting the ship the speed motor stops and traction one continues to run at maximal speed. This speed should be at least 0.5 m/s to avoid dynamic impact even when the ship lifting height will be 40 % above the previous height. Thus, the range of speed control in this system is 1/2÷1/3, and the speed motor can be performed without the speed control device. System with high-speed motor can be used for lifting any loads up to several tens of tons. The disadvantage of such systems is the complexity of the mechanism and low reliability due to the fact that at fault of the handling device of the speed motor the drop of cargo is possible.

Ships during loading and unloading operations feel longitudinal and transverse pitching, period and amplitude of which depend on the degree of agitation, and the design features of ships. Overload operations are carried at vibrations only when they have reasonable parameters. The sum of vertical displacement of the ship is within 2 ÷ 5 m at the period of pitching 6 ÷ 12 s. The condition for safe landing of the load or its overload is to maintain a

constant distance H_0 between the place of loading and load at disconnected load lifting mechanism. The movement of cargo relatively the ship's deck is described by the complicated formula:

$$h_0 = f(h_1, h_2, h_3, t_1, t_2, t_3, \varphi_{max}, \varphi, \varphi_0, l), \quad (4)$$

where h_1, h_2, h_3 are respectively the amplitudes of the vertical ship's displacement and the distance by height from the LTM center of gravity to the ship's center of gravity; t_1, t_2, t_3 are the periods of corresponding ship's orbital movements; $\varphi_{max}, \varphi, \varphi_0$ are the angles corresponding the ship's lurch with pallet restrainer, restrainer inclination and phase shift of the ship's pitching; l is the length of the pallet restrainer boom over the ship's board.

At such a complex movement of the load regarding the ship's deck to maintain the stability h_0 the mechanism is complemented by a special compensating device as to provide tracking using electric drive is practically impossible. The implementation of such devices permits to use for the described mechanisms usual electric drives complemented by the necessary devices for ultimate protection and locking that prevent the movement of the load in the danger zone with no surveillance. There are several ways of reliable compensation of relative movement of ships and cargo. The common feature of these methods is the use of mechanical power sensor of automatic system.

Results of investigations. Fig. 4 shows the charts of the speed of the electric motor using calculated coefficients of the PID-regulator for standard setting by unidentified transfers function of the third (Fig. 4,a) and the second (Fig. 4,b) order.

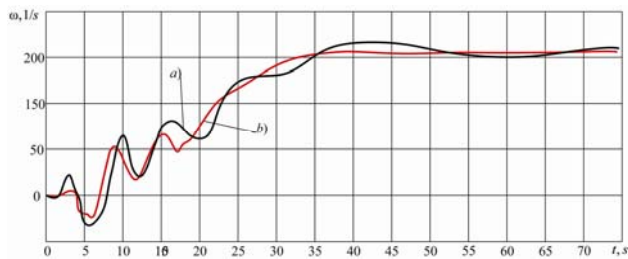


Fig. 4. Charts of the electric drive velocity at the system approximation by transfer functions of the second (a) and the third (b) order

To adjust the components of PID-regulators by optimizing the transients it is necessary to run the model by the button of the settings window of the optimization block SRS (Fig. 3). After optimization we obtain the following results (Fig. 5,a,b).

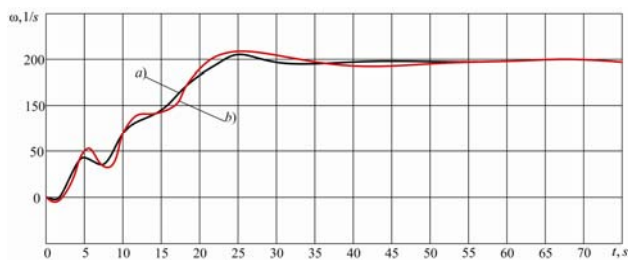


Fig. 5. Charts of the electric drive velocity at optimization by speed for the second (a) and the third (b) order

In order to eliminate vibration processes in the electric drive by adjusting electric control algorithms that ensure the stability of the process of movement of cargo and to confirm the theoretical part, experimental investigations were carried out on a laboratory facility the principal diagram of it is shown in Fig. 6, and external view - in Fig. 7.

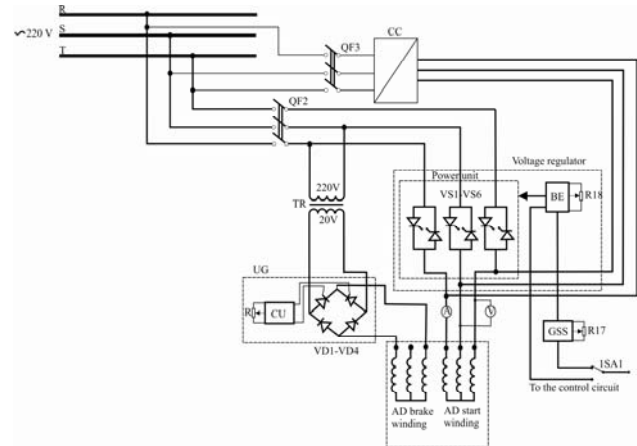


Fig. 6. Principal diagram of the laboratory facility: QF2, QF3 – circuit breakers, CC – frequency converter; AD – double-winding induction motor; TR – step-down transformer; BE – electronic block; GSS – starting signal generator; UG – rectifier; VD1-VD4 – rectifier diodes to supply the braking coil; VS1-VS6 – power thyristors; R – resistor setting the braking torque; R18 – resistor setting voltage on the IM windings; 1SA1 – control methods switch



Fig. 7. External view of laboratory facility: 1 – frequency converter; 2 – double-winding IM; 3 – oscilloscope; 4 – current sensor; 5 – load current adjustment

Fig. 8, 9 show graphs of transients before and after optimization of electric drive control laws on the basis of above theoretical material.

The results of mathematical modeling in *MatLab Simulink* and experimental investigations on laboratory facility confirmed the basic theoretical principles initiated.

Conclusions. In the work solution of actual scientific and technical problem of improvement of efficiency of control process of electric drive of ship's lifting mechanism is carried out. The essence of the research is theoretical generalization of disturbing effects on the movement of the loaded pallet in the most dependent on

the position of the ship plane that essentially define the non-linearity of electromechanical object behavior, thus reducing duration of operational downtimes.

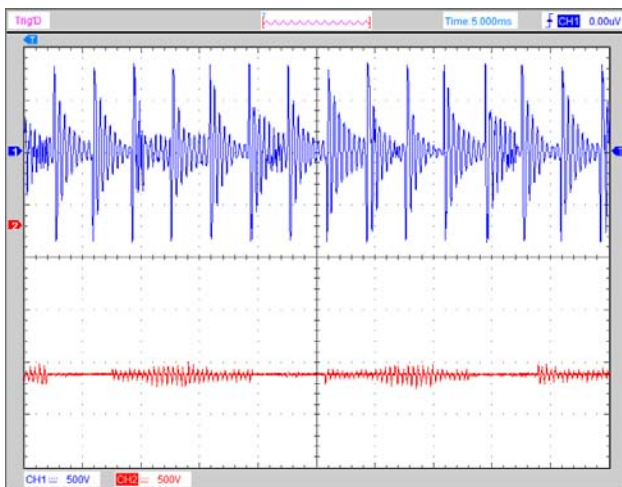


Fig. 8. Dependences of the rotating frequency and current of the IM before optimization

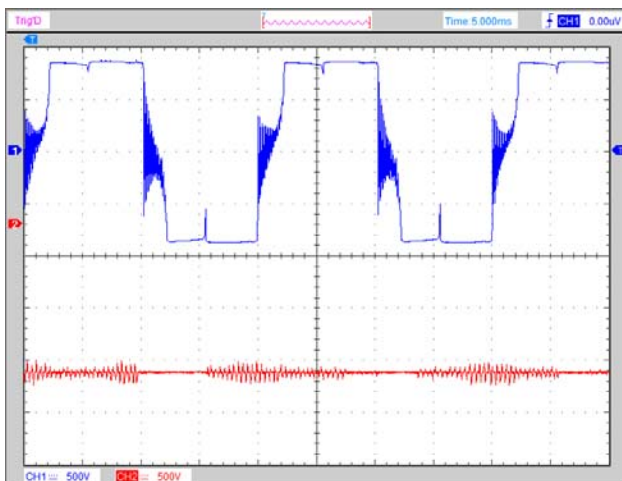


Fig. 9. Dependences of the rotating frequency and current of the IM after optimization

Scientific results, conclusions and recommendations are as follows:

1. Based on analysis of current research it can be concluded that the stability of the electric drive of the lifting mechanism to disturbing torques is provided at the condition of coincidence of zero value of electric drive's electric coordinates and speed of deviation of ship's diametric plane from the vertical position.

2. Criteria for optimizing control system of lifting electric drive are used by mathematical description of its dynamics by differential equations with calculated coefficients derived from the functions of transients.

3. The obtained experimental dependences of coefficients of equations of dynamic object motion under the influence of disturbing forces in the coordinate plane allowed to parameterize characteristic equations to the form providing the solution of the stability problem of

the torque on the shaft of the lifting mechanism electrical motor.

4. The developed functional diagram of the automatic control system eliminates the aperiodic components in the control law in compliance with the criteria of stability and quality of transients by applying the regulator for all modes of coordinate characteristics with forcing of overcoming of the dead zone and increasing the stability of the electric drive as a dynamic object.

5. The carried out complex of investigations may find practical implementation in electric drives of ship's lifting mechanisms that will improve their performance, decrease operational and maintenance downtimes.

REFERENCES

- Hoffmann C., Radisch C., Werner H. Active damping of container crane load swing by hoisting modulation – An LPV approach. *51st IEEE Conference on Decision and Control (CDC)*. IEEE, 2012. doi: [10.1109/cdc.2012.6426889](https://doi.org/10.1109/cdc.2012.6426889).
- Rubar E., Vrančić D. Anti-sway system for ship-to-shore cranes. *Strojniški vestnik (Journal of Mechanical Engineering)*, 2012, vol.58, no.5, pp. 338-344. doi: [10.5545/sv-jme.2010.127](https://doi.org/10.5545/sv-jme.2010.127).
- Skaf J., Boyd S.P. Controller coefficient truncation using Lyapunov performance certificate. *International Journal of Robust and Nonlinear Control*, 2010, vol.21, no.1, pp. 55-78. doi: [10.1002/rnc.1577](https://doi.org/10.1002/rnc.1577).
- Belunce A., Pandolfo V., Roozbahani H., Handroos H. Novel control method for overhead crane's load stability. *Procedia Engineering*, 2015, vol.106, pp. 108-125. doi: [10.1016/j.proeng.2015.06.014](https://doi.org/10.1016/j.proeng.2015.06.014).
- Balachandran B., Li Y.-Y., Fang C.-C. A mechanical filter concept for control of non-linear crane-load oscillation. *Journal of Sound and Vibration*, 1999, vol.228, iss.3, pp. 651-682. doi: [10.1006/jsvi.1999.2440](https://doi.org/10.1006/jsvi.1999.2440).
- Alli H., Singh T. Passive control of overhead cranes. *Journal of Vibration and Control*, 1999, vol.5, no.3, pp. 443-459. doi: [10.1177/107754639900500306](https://doi.org/10.1177/107754639900500306).
- Wua T.-S., Karkoub M., Yu W.-S., Chen C.-T., Her M.-G., Wu K.-W. Anti-sway tracking control of tower cranes with delayed uncertainty using a robust adaptive fuzzy control. *Fuzzy Sets and Systems*, 2016, vol.290, pp 118-137. doi: [10.1016/j.fss.2015.01.010](https://doi.org/10.1016/j.fss.2015.01.010).
- Henry R.J., Masoud Z.N., Nayfeh A.H., Mook D.T. Cargo pendulation reduction on ship-mounted cranes via boom-luff angle actuation. *Journal of Vibration and Control*, 2001, vol.7, no.8, pp. 1253-1264. doi: [10.1177/107754630100700807](https://doi.org/10.1177/107754630100700807).
- Budashko V.V., Onishchenko O.A. Improving management system combined thruster propulsion systems. *Bulletin of NTU «KhPI»*, 2014, no.38(1081), pp. 45-51. (Ukr).
- Budashko V.V., Onishchenko O.A. Mathematical principles of simulation of power plant's control system at drillship. *Bulletin of Kamchatka State Technical University*, 2014, no.29, pp. 6-13. (Rus).
- Budashko V.V., Onishchenko O.A., Yushkov E.A. Physical modeling of multi-propulsion complex. *Collection of scientific works of the Military Academy (Odessa City)*, 2014, no.2 pp. 88-92. (Rus).
- Budashko V.V., Yushkov Y.A. Mathematic modeling of all-range controllers speed of thrusters for ship power plants in combined propulsion complexes. *Electronic Modeling*, 2015, vol.37, no.2, pp. 101-114. (Rus).
- Budashko V.V. Implementation approaches during simulation of energy processes for a dynamically positioned ship. *Electrical Engineering & Electromechanics*, 2015, no.6, pp.14-19. doi: [10.20998/2074-272X.2015.6.02](https://doi.org/10.20998/2074-272X.2015.6.02). (Rus).

14. A.A. Bojko, V.V. Budashko, E.A. Yushkov, Bojko N.A. Synthesis and research of automatic balancing system of voltage converter fed induction motor currents. *Eastern-European Journal of Enterprise Technologies*, 2016, vol.1, no.2(79), pp. 22-34. doi: **10.15587/1729-4061.2016.60544**.

15. Araya H., Kakuzen M., Kinugawa H., Arai T. Level luffing control system for crawler cranes. *Automation in construction*, 2004, vol.13, no.5, pp. 689-697. doi: **10.1016/j.autcon.2004.04.011**.

V.V. Budashko, Candidate of Technical Science, Associate Professor,

Odessa National Maritime Academy,
8, Didrikhson Str., Odessa, 65029.

phone +380 48 7332367, e-mail: bvv@te.net.ua

Received 24.03.2016

How to cite this article:

Budashko V.V. Increasing control's efficiency for the ship's two-mass electric drive. *Electrical engineering & electro-mechanics*, 2016, no.4, pp. 34-42. doi: 10.20998/2074-272X.2016.4.05.

D.V. Tugay

THREE-PHASE ENERGY SUPPLY SYSTEMS SIMULATION FOR THE TOTAL POWER LOSSES COMPONENTS ASSESSMENT

Purpose. The goal is to optimize a structure of Matlab-model of the three-phase energy supply system with power active filter. The mathematical model that describes the energy supply system modes of operation which contains additional losses is proposed. **Methodology.** We have applied concepts of the electrical circuits theory, mathematical modeling elements based on linear algebra and vector calculus, mathematical simulation in Matlab package. **Results.** We have developed two models of three-phase energy supply system. The first one is based on a vector representation, and the second one on the matrix representation of energy processes. Using these models we have solved the problem of maintaining unchanged the average useful power for 279 cases of energy supply system modes of operation. **Originality.** We have developed methods of mathematical analysis of a three-phase energy supply systems with polyharmonic voltages and currents in the symmetric and asymmetric modes. **Practical value.** We have created Matlab-model of a three-phase energy supply system with automated calculation of a correction factor. It allows reducing more than one order the time for energy processes elucidation in multiphase systems. References 11, tables 1, figures 13. **Key words:** energy supply system, power active filter, the minimum possible losses, total losses power, three-dimensional complex vector, Matlab-model of the three-phase energy supply system.

Цель. Целью статьи является оптимизация структуры Matlab-модели трехфазной системы электроснабжения с силовым активным фильтром с помощью математической модели, описывающей режимы работы системы электроснабжения, в которых возникают дополнительные потери. **Методика.** Для проведения исследований использовались положения теории электрических цепей, элементы математического моделирования, основанные на линейной алгебре и векторном исчислении, математическое моделирование в пакете Matlab. **Результаты.** Разработаны две модели трехфазной системы электроснабжения, первая, основанная на векторном представлении, а вторая на матричном представлении энергетических процессов, с помощью которых была решена проблема поддержания неизменной средней полезной мощности нагрузки для 279 случаев работы системы электроснабжения. **Научная новизна.** Получили дальнейшее развитие методы математического анализа режимов работы трехфазных систем электроснабжения с полигармоническими напряжениями и токами в симметричных и несимметричных режимах работы. **Практическое значение.** Создана Matlab-модель трехфазной системы электроснабжения с автоматизированным расчетом поправочного коэффициента, позволяющая более чем на порядок сократить время для исследования энергетических процессов в многофазных системах. Библ. 11, рис. 13, табл. 1.

Ключевые слова: система электроснабжения, силовой активный фильтр, минимально возможные потери, мощность суммарных потерь, трехмерный комплексный вектор, Matlab-модель трехфазной системы электроснабжения.

Introduction. Understanding the operation of three-phase energy supply systems (ESS) allows professionals in the field of power electronics to solve a number of problems related to the electromagnetic compatibility of electric power consumers from the industrial network as well as increasing the energy efficiency of such systems. Complex solution of problems presented in the current conditions based on the use of the active filtering means - power active filters (PAF). In the systems of energy supply of communal consumers, industrial plants, electric vehicles adaptation of PAF of parallel type is increased [1, 2]. Despite the simplicity of the power circuit which is a three-phase voltage inverter on the transistor modules, PAF are complex dynamic systems able to adapt to changes in the configuration and mode of operation of three-phase ESS. The feasibility of using PAF to reduce the losses in the ESS [3, 4] is due to the possibility of a preliminary assessment of the total power losses in the system before and after it is connected. The simplest way to perform such an assessment is a computer simulation of a three-phase ESS with PAF. This paper describes how to create a computer model to investigate diversity of power modes of the three-phase ESS with minimal time overhead.

A complicated extensive three-phase ESS can be replaced by a simple equivalent circuit shown in Fig. 1 [5].

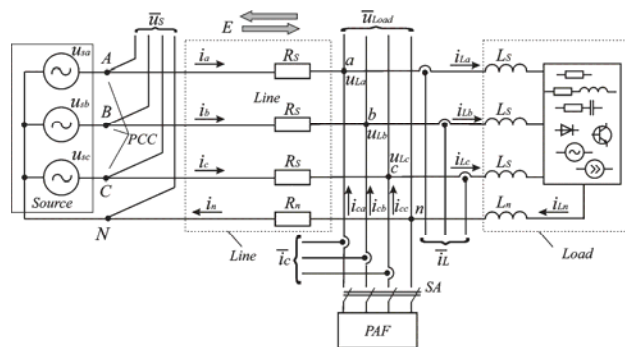


Fig. 1. Equivalent circuit of the three-phase ESS with PAF

The scheme consists of three parts: a three-phase sinusoidal power source of sinusoidal (or nearly sinusoidal) voltages *Source*, a three-phase load *Load* and connecting cable line *Line* with resistance linear wire R_s and neutral wire resistance R_n . The three-phase load in the circuit of Fig. 1 may be any of: resistors, reactors, capacitors batteries, nonlinear consumers, current and voltage sources as well as the possible combinations of the elements listed. It should be noted that the inductances L_s and L_n of the cable line in the equivalent circuit are transferred in the load. Depending on the nature of the load and the operating mode of the ESS three power transmission modes are available: direct – energy is

transmitted from the source to the load, reverse – the energy is transferred from the load to the source, and mixed mode - in the period of recurrence it is possible to combine the first and the second modes. After the contactor *SA* switch on, the power active filter (block *PAF*) is connected parallel to the load.

In [6] a universal formula to determine the total losses power in the three-phase four-wire ESS through its components is proposed

$$\begin{aligned} \Delta P_{\Sigma^*} &= \frac{\Delta P_{\Sigma}}{P_{usf}} = \\ &= \Delta P_{\min^*} + \Delta P_{puls^*} + \Delta P_{q^*} + \Delta P_{n^*} + \Delta P_{mut^*} = \\ &= \Delta P_{\min^*} + \Delta P_{add^*} \left| P_{usf} = const, \right. \end{aligned} \quad (1)$$

where ΔP_{\min^*} is the relative minimum possible power losses determined by the absence of pulsations of the instantaneous active power and the vanishing of the instantaneous reactive power in three-phase ESS; ΔP_{puls^*} is the relative components of additional power losses due to the transient component of the instantaneous power of the three-phase ESS; ΔP_{q^*} is the relative component of additional losses power due to the instantaneous reactive power of the three-phase ESS; ΔP_{n^*} is the relative power losses in the neutral conductor calculated in the period of repeatability caused by current flow in the neutral wire; ΔP_{mut^*} is the relative component of additional losses power due to the mutual influence of the electromagnetic processes in the phase conductors and the neutral wire of the three-phase ESS; ΔP_{add^*} is the relative additional losses power; P_{usf} is the average calculated in the period of repeatability useful load power the amount of which in the course of the experiment must be kept constant.

Calculation of the total power losses components is based on the concepts of modern theories of instantaneous active and reactive power [7-9] on the nature of the electromagnetic processes in three-phase ESS and algorithms of PAF control using matrix transformations of these theories. In the simplest case, if we consider the ideal active filter (with zero internal losses) then when it is connected to the three-phase ESS total losses in the system will be equal to the lowest possible, i.e. the ESS will operate with the highest possible efficiency [10]

$$\eta_{\max} = \frac{1}{2} + \sqrt{\frac{1}{4} - \frac{1}{k_{sc}}}, \quad (2)$$

$$k_{sc} = P_{sc} / P_{usf} \quad (3)$$

is the ratio of power of the three-phase resistive short circuit of the ESS to useful load power.

In above-mentioned publications [5, 6] it was shown that the validation of (1) is possible using the Matlab-model of three-phase four-wire ESS which has properties of universality and allows the calculation of power losses components at different modes of the ESS. Combinations of modes of three-phase voltage source, the nature of three-phase load, the neutral conductor resistance value and direction of the energy flow in the line wires allow to obtain 288 ESS variants, while in 279 ESS variants there are additional losses described by (1). The authors [5, 6] were able to check about 30 ESS variants, the

investigation of which confirmed the validity of (1) but was associated with significant time-consuming.

This work is dedicated to the creation of a universal Matlab-model of the three-phase ESS and optimization of its parameters for an accelerated assessment of the power losses components in any of the 288 possible ESS variants.

The structure of the three-phase ESS model.

Optimization of the structure of the Matlab-model of the three-phase ESS may be carried out at the transition from the circuit on Fig. 1 to the equivalent circuit of Fig. 2.

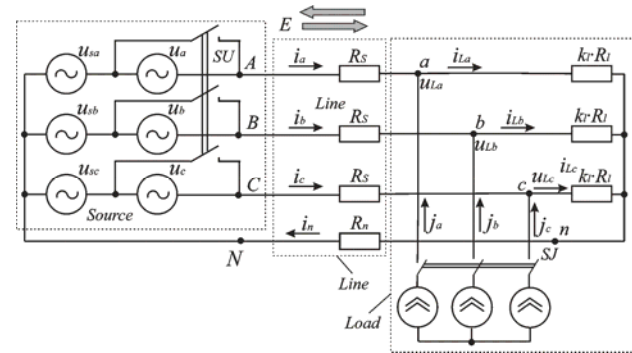


Fig. 2. Equivalent circuit of the three-phase ESS

The three-phase voltage source in this circuit consists of two series-connected sources - symmetrical sinusoidal voltage source u_{sa}, u_{sb}, u_{sc} and additional three-phase voltage source u_a, u_b, u_c which is connected to the ESS by opening the bypass contactor *SU*. With the additional power source it is possible to specify amplitude or phase asymmetry as well as the addition of the higher harmonic components to the range of supply voltage. The three-phase load is modeled by two blocks - a symmetrical three-phase resistive load $k_r R_l$ and regulated three-phase current source j_a, j_b, j_c which is connected in parallel with the symmetrical resistive load after *SJ* contactor closing. Regulated current source provides in linear conductors the necessary current shape that will fit any linear or non-linear load with balanced or unbalanced phases load. The proportionality factor k_l which is multiplied by the active resistances of all three phases is necessary to maintain a constant value of average active useful power of load $P_{usf} = const$ as follows from (1) when making a particular disturbance in the system, and its definition is a separate problem.

Setting variable coefficients that determine the operation mode of the three-phase ESS.

We return to the ESS equivalent circuits on Fig. 1 when the contactor *SA* is open and replace it with a simplified diagram shown in Fig. 3 explaining the cause of the power loss components in accordance with (1). Electrical quantities and parameters in the circuit of Fig. 3 are shown in the vector notation. The circuit consists of a voltage source the phase values of which are described by the vector $\vec{u} = \vec{k}_u \circ \vec{u}_s + \vec{u}_{ns} \circ \vec{k}_{un} \cdot s_u$, resistance of the line $R_s \cdot \vec{v}$, complex linear load resistance for the *i*-th harmonic component of the current which is described by the vector $\vec{z}_{Li} = k_l \cdot R_l \cdot \vec{k}_a + j \cdot (x_{li} \cdot \vec{k}_r + x'_{si} \cdot \vec{v})$, and the

current source modeling the nonlinear load described by the vector $\vec{k}_j \circ \vec{J} \cdot s_j$.

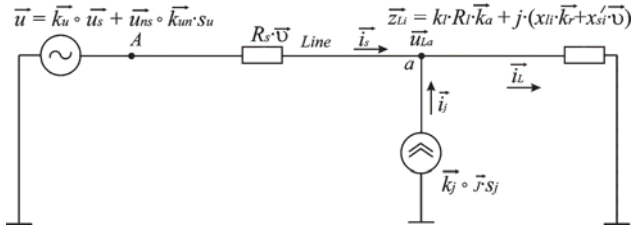


Fig. 3. Simplified circuit of the three-phase ESS for the parameters setting

In Fig. 3 the following notation is used:

- the 3D complex vector of phase symmetrical sinusoidal voltages

$$\vec{u}_s = \begin{bmatrix} U_s \cdot e^{j \cdot 0} \\ U_s \cdot e^{-j \cdot \frac{2\pi}{3}} \\ U_s \cdot e^{-j \cdot \frac{4\pi}{3}} \end{bmatrix} = \begin{bmatrix} \underline{U}_{sa} \\ \underline{U}_{sb} \\ \underline{U}_{sc} \end{bmatrix}, \quad (4)$$

where U_s is the RMS phase voltage of the symmetric source;

- the 3D complex vector of phase voltage of the additional three phase source of non-sinusoidal voltage

$$\vec{u}_{ns} = \begin{bmatrix} \sqrt{\sum_{i=2}^n (U_i \cdot e^{j \cdot \varphi_{uai}})^2} \\ \sqrt{\sum_{i=2}^n (U_i \cdot e^{j \cdot \varphi_{ubi}})^2} \\ \sqrt{\sum_{i=2}^n (U_i \cdot e^{j \cdot \varphi_{uci}})^2} \end{bmatrix} = \begin{bmatrix} \underline{U}_a \\ \underline{U}_b \\ \underline{U}_c \end{bmatrix}, \quad (5)$$

where U_i is the RMS of the i -th harmonic component of phase voltage of three-phase non-symmetric source, n is the number of higher harmonics in the voltage range; φ_{uai} , φ_{ubi} , φ_{uci} are the phases of corresponding i -th harmonic components of phase voltages; s_u is the coefficient taking two values 0 or 1 depending on the switch SU position in Fig. 2; \circ is the operator of element-wise multiplication of elements of vectors and matrices (Hadamard product);

- the 3D complex vector of phase currents of the nonlinear load

$$\vec{J} = \begin{bmatrix} \sqrt{\sum_{i=2}^n (J_i \cdot e^{j \cdot \varphi_{iai}})^2} \\ \sqrt{\sum_{i=2}^n (J_i \cdot e^{j \cdot \varphi_{ibi}})^2} \\ \sqrt{\sum_{i=2}^n (J_i \cdot e^{j \cdot \varphi_{ici}})^2} \end{bmatrix} = \begin{bmatrix} \underline{J}_a \\ \underline{J}_b \\ \underline{J}_c \end{bmatrix}, \quad (6)$$

where J_i is the RMS of the i -th harmonic component of the phase current of the three-phase nonlinear load; φ_{iai} , φ_{ibi} , φ_{ici} are the phases of corresponding i -th harmonic components of phase currents; s_j is the

coefficient taking two values 0 or 1 depending on the switch SJ position in Fig. 2;

- the 3D complex vector of linear load resistances

$$\vec{z}_{Li} = \begin{bmatrix} k_l \cdot R_l \cdot k_{aa} + j \cdot (x_{li} \cdot k_{ra} + x'_{si}) \\ k_l \cdot R_l \cdot k_{ab} + j \cdot (x_{li} \cdot k_{rb} + x'_{si}) \\ k_l \cdot R_l \cdot k_{ac} + j \cdot (x_{li} \cdot k_{rc} + x'_{si}) \end{bmatrix} = \begin{bmatrix} Z_{Lai} \cdot e^{j \cdot \varphi_{zai}} \\ Z_{Lbi} \cdot e^{j \cdot \varphi_{zbi}} \\ Z_{Lci} \cdot e^{j \cdot \varphi_{zci}} \end{bmatrix} = \begin{bmatrix} \underline{Z}_{La} \\ \underline{Z}_{Lb} \\ \underline{Z}_{Lc} \end{bmatrix}, \quad (7)$$

where x_{li} are the reactances for the i -th current harmonic; x'_{si} is the reactance of the cable line for the i -th current harmonic reduced to the load reactance; Z_{Lai} , Z_{Lbi} , Z_{Lci} are the modules of the impedance of linear load phases for the i -th current harmonic; φ_{za} , φ_{zb} , φ_{zc} are the phases of corresponding impedances;

- the 3D vectors which store information about coefficients of amplitude asymmetry of the voltage source and non-linear load current, phase unbalance of active and reactive load as well as the value of the corresponding harmonic component of the input voltage range and a non-linear load current

$$\vec{k}_u = [k_{ua} \quad k_{ub} \quad k_{uc}]^T, \quad (8)$$

$$\vec{k}_{un} = [k_{una} \quad k_{unb} \quad k_{unc}]^T, \quad (9)$$

$$\vec{k}_j = [k_{ja} \quad k_{jb} \quad k_{jc}]^T, \quad (10)$$

$$\vec{k}_a = [k_{aa} \quad k_{ab} \quad k_{ac}]^T, \quad (11)$$

$$\vec{k}_r = [k_{ra} \quad k_{rb} \quad k_{rc}]^T; \quad (12)$$

- the unit vector

$$\vec{v} = [1 \quad 1 \quad 1]^T. \quad (13)$$

By setting the values of s_u , s_j factors and elements of vectors (8) – (12) it is possible to simulate any of 279 modes of operation of the three-phase ESS and calculate the components of the total power losses. To summarize the results of the calculations we assume that the values of the elements of the vectors in (8), (11) are linked by a common regularity

$$k_a^2 + k_b^2 + k_c^2 = 3. \quad (14)$$

The coefficient of the phase A k_a remains unchanged and equal to 1, then

$$k_a = const = 1 \\ k_b = var = 0 \dots \sqrt{2} \quad (15)$$

$$k_c = \sqrt{2 - k_b^2} = \sqrt{2} \dots 0$$

We assume that the values of the elements of the vectors in (9), (10), (12) subject to other regularity

$$k_b = var = 0 \dots \sqrt{2} \\ k_a = k_c = k_b \quad (16)$$

Regularities of change of vector elements values (15) and (16) will be used later to summarize the simulation results for different operation modes of three-phase ESS. Note that these ratios may vary in any arbitrary manner, and the selected regularities (15) and (16) represent the most characteristic changes influences of the three-phase ESS parameters on the total losses.

Fulfillment of the condition $P_{usf} = \text{const}$ at the three-phase energy supply system modeling.

Model representation in the vector form. Changes in the parameters of the elements of the equivalent circuit of three-phase ESS changes the value of the average active useful load power. Returning its initial value, as previously mentioned, is carried out by varying the coefficient k_l . Obtaining the analytical expressions for determination of k_l is a difficult problem. It is easier to use the software for calculations. For automated calculation of the coefficient k_l it is necessary to build the equation for the useful load power as shown in Fig. 3. There are two forms of this equation – in the vector and matrix form. We consider the first method.

We use the method of the current superposition. In the circuit of Fig. 3 we leave the voltage source. We define the vector of three-phase ESS conductivities for the i -th current harmonic

$$\vec{y}_i = \frac{1}{\vec{z}_{Li} + R_s \cdot \vec{v}} \quad (17)$$

The total conductivity of the three-phase four-wire ESS for the i -th current harmonic

$$y_{si} = \vec{y}_i \cdot \vec{v} + R_n^{-1} \quad (18)$$

We write the dependence for the neutral voltage displacement for the main harmonic of the three-phase voltage source

$$\underline{U}_{01} = \vec{y}_1 \cdot y_{s1}^{-1} \cdot (\vec{u}_s \circ \vec{k}_u) \quad (19)$$

Vector of partial currents created by main voltage harmonic of the linear source in the ESS linear wires

$$\vec{i}_{e1} = (\vec{u}_s - \underline{U}_{01} \cdot \vec{v}) \circ \vec{y}_1 \quad (20)$$

If the higher harmonics (coefficient $s_u = 1$) are in the input voltage curve, the procedure for calculating the vectors of the partial currents created by the three-phase voltage source must be repeated for each harmonic component using (7), (17) – (20). The total vector of the partial currents created by the three-phase voltage source in the ESS line wires in this mode is described by the relation

$$\vec{i}_e = \sqrt{(\vec{i}_{e1})^2 + \sum_{i=2}^n (\vec{i}_{ei})^2} \quad (21)$$

where \vec{i}_{ei} is the partial current vector of the i -th harmonic component in the circuit with three-phase voltage source.

In the circuit of Fig. 3 we leave the current source pre-shortening the voltage source, and define the vector of partial linear load current in the circuit with three-phase current source

$$\vec{i}_{Lj} = \left[\begin{array}{c} \sqrt{\sum_{i=2}^n \left(J_i \cdot Y_{ai} \cdot R_s \cdot e^{j(\varphi_{iai} + \varphi_{yai})} \right)^2} \\ \sqrt{\sum_{i=2}^n \left(J_i \cdot Y_{bi} \cdot R_s \cdot e^{j(\varphi_{ibi} + \varphi_{ybi})} \right)^2} \\ \sqrt{\sum_{i=2}^n \left(J_i \cdot Y_{ci} \cdot R_s \cdot e^{j(\varphi_{ici} + \varphi_{yci})} \right)^2} \end{array} \right] \circ \quad (22)$$

$$\circ \vec{k}_j = \sqrt{\sum_{i=2}^n (\vec{i}_{Lji})^2} = \left[\begin{array}{c} \underline{I}_{aLj} \\ \underline{I}_{bLj} \\ \underline{I}_{cLj} \end{array} \right]$$

where Y_{ai} , Y_{bi} , Y_{ci} are the modules of total load phase conductivities for the i -th current harmonics; φ_{yai} , φ_{ybi} , φ_{yci} are the initial phases of corresponding conductivities.

We find the vector of partial current created by the three-phase current source in ESS linear wires by the first Kirchhoff law

$$\vec{i}_{sj} = \vec{J} - \vec{i}_{Lj} \quad (23)$$

We determine the current vector in the linear load circuit

$$\vec{i}_L = \sqrt{(\vec{i}_e)^2 + (\vec{i}_{Lj})^2} \quad (24)$$

and find the voltage vector on the load terminals

$$\vec{u}_L = \sqrt{(\vec{i}_{e1} \circ \vec{z}_{L1})^2 + \sum_{i=2}^n (\vec{i}_{ei} \circ \vec{z}_{Li})^2 + \sum_{i=2}^n (\vec{i}_{Lji} \circ \vec{z}_{Li})^2} \quad (25)$$

Average active useful power

$$P_{usf} = \text{Re} \left(\vec{u}_L \cdot \sqrt{(\vec{i}_e)^2 + (\vec{i}_{sj})^2} - (J)^2 \right) = \text{Re} \left(\vec{u}_L \cdot \sqrt{(\vec{i}_L)^2} - 2 \cdot (\vec{J} \circ \vec{i}_{Lj}) \right) \quad (26)$$

Model representation in the matrix form. Vector form for three-phase models of ESS has some disadvantage manifests itself at polyharmonic shape of the supply voltage. With this it is difficult to describe the mutual influence of the higher voltage harmonic components of the three-phase source and higher current harmonics flowing in the non-linear load phases. In such a case it is convenient to use the matrix form of the model description.

Let's set the voltage at the three-phase source terminal by the matrix size $n \times 3$

$$\mathbf{u} = \left\| \begin{array}{ccc} \underline{U}_{a1} & \underline{U}_{b1} & \underline{U}_{c1} \\ \vdots & \vdots & \vdots \\ \underline{U}_{an} & \underline{U}_{bn} & \underline{U}_{cn} \end{array} \right\| \quad (27)$$

Similarly, we write the matrix of the three-phase current source

$$\mathbf{j} = \left\| \begin{array}{ccc} \underline{J}_{a2} & \underline{J}_{b2} & \underline{J}_{c2} \\ \vdots & \vdots & \vdots \\ \underline{J}_{an} & \underline{J}_{bn} & \underline{J}_{cn} \end{array} \right\| \quad (28)$$

Separately, we define a matrix of complex load impedances for the three-phase voltage source currents and three-phase current source

$$\mathbf{z}_u = \begin{pmatrix} \underline{z}_{au1} & \underline{z}_{bu1} & \underline{z}_{cu1} \\ \vdots & \vdots & \vdots \\ \underline{z}_{aun} & \underline{z}_{bun} & \underline{z}_{cun} \end{pmatrix}, \quad (29)$$

$$\mathbf{z}_j = \begin{pmatrix} \underline{z}_{aj2} & \underline{z}_{bj2} & \underline{z}_{cj2} \\ \vdots & \vdots & \vdots \\ \underline{z}_{ajn} & \underline{z}_{bjn} & \underline{z}_{cjn} \end{pmatrix}. \quad (30)$$

We express the complex matrix of phase conductivities for three-phase voltage source currents

$$\mathbf{y}_u = \frac{\mathbf{M}_u}{\mathbf{z}_u + R_s}, \quad (31)$$

where \mathbf{M}_u is the matrix of states size $n \times 3$ whose rows are taking the unit values in the case of presence of corresponding harmonic components in the range of the three-phase voltage source.

We write the vector of total complex impedances of the three-phase four-wire system

$$\vec{y}_s = \mathbf{y}_u \cdot \vec{v} + R_n^{-1}. \quad (32)$$

We represent the current in the neutral wire due to the higher harmonic components multiple three of the three-phase current source, as a vector of the length n

$$\vec{i}_{3j} = \mathbf{j} \circ \frac{\mathbf{z}_j}{R_s + 3 \cdot R_n + \mathbf{z}_j} \cdot \vec{v}. \quad (33)$$

The displacement voltage at the neutral at polyharmonic supply voltage and polyharmonic current is represented as a vector of the length n

$$\vec{u}_0 = \frac{\mathbf{y}_u \circ \mathbf{u}}{\vec{y}_s} \cdot \vec{v} - \vec{i}_{3j} \cdot R_n. \quad (34)$$

The line currents matrix in the circuit with three-phase voltage source

$$\mathbf{i}_e = (\mathbf{u} - \vec{u}_0 \cdot \vec{v}^T) \circ \mathbf{y}_u. \quad (35)$$

Using matrix relations (28) and (30) we express the partial currents of the three-phase current source, respectively, in the load and linear wires

$$\mathbf{i}_{Lj} = \mathbf{j} \circ \frac{R_s}{R_s + \mathbf{z}_j}, \quad (36)$$

$$\mathbf{i}_{sj} = \mathbf{j} - \mathbf{i}_{Lj}. \quad (37)$$

We determine total line current and total current in the linear load phases

$$\mathbf{i}_s = \mathbf{i}_e - \mathbf{i}_{sj}, \quad (38)$$

$$\mathbf{i}_L = \mathbf{i}_e + \mathbf{i}_{Lj} \quad (39)$$

And find the voltage on the load terminals

$$\mathbf{u}_L = \mathbf{i}_e \circ \mathbf{z}_u + \mathbf{i}_{Lj} \circ \mathbf{z}_j. \quad (40)$$

Average active useful load power

$$P_{usf} = (\mathbf{u}_L \circ (|\mathbf{i}_L| - |\mathbf{j}|))^T \cdot \mathbf{M}_u^{(1)} \cdot \vec{v}. \quad (41)$$

Both described models allow to relatively simply calculate the value of the correction factor k_l returning the original value of the average load useful power even

when using standard MathCad tools (*Given* block and *Find* function). After that it is possible to determine components of the power losses and the comparison of calculation results at ESS different modes of operation.

As an example, we consider a three-phase ESS with a ratio of three-phase power of resistive short circuit to load active power $k_{sc} = 20$. The RMS of the phase sinusoidal voltage of the three-phase symmetric source $U_s = 220$ V. If the useful load power at the mode of minimum of losses equal to $P_{usf} = 400.1$ kW, then $R_s = 0.01815 \Omega$, $R_l = 0.3256 \Omega$. According to (8) - (12) we consider separately 5 modes of ESS operation, each of which is caused by one factor influencing the occurrence of additional losses:

1. Voltage unbalance.
2. Resistive load unbalance.
3. Symmetric active-inductive load at $\varphi_L = 15^\circ$ ($L = 0.2777$ mH).
4. Higher harmonics in the supply voltage curve (odd harmonics whose amplitudes vary inversely their serial number U_m/n , where $n=2i-1$, $i = 2, 3 \dots 19$).
5. The symmetrical non-linear load resulting in the higher current harmonics (odd harmonics, the amplitudes of which vary inversely their serial number $U_m/(n \cdot (R_s + R_l))$, where $n=2i-1$, $i = 2, 3 \dots 19$).

Changing the ratio k_b by (15) or (16) determine the alteration of the corresponding known power indicator: asymmetry coefficient by reverse sequence K_2 , the power factor $\cos\varphi$, THD of voltage THD_u and current THD_i . Fig. 4 illustrates the relationship of these power indicators with regularity of k_b factor changes.

Fig. 5 shows the dependences of the correction factor k_l on the k_b factor which sets the pattern of changes of the asymmetrical operation mode of the three-phase three-wire ESS by (15). The values of the coefficient k_l at $k_b = 0$ and at $k_b = \sqrt{2}$ correspond to the three-phase ESS emergency operation mode at breakage of the line wire. The value of the coefficient k_l at $k_b = 1$ corresponds to the three-phase symmetrical operation at which the total power losses are equal to the lowest possible power losses.

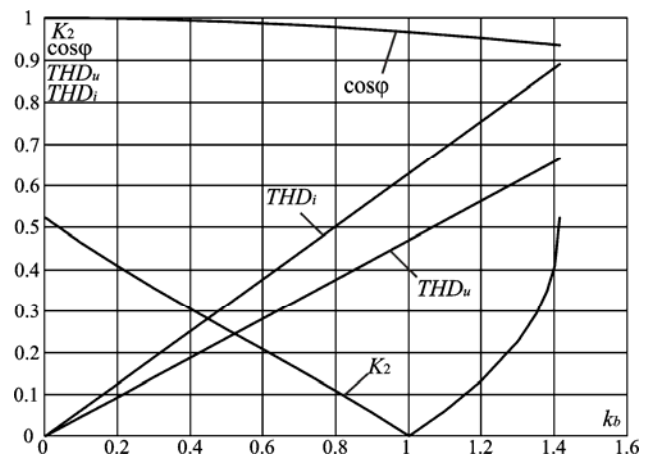


Fig. 4. Dependence of power indicators vs coefficient k_b

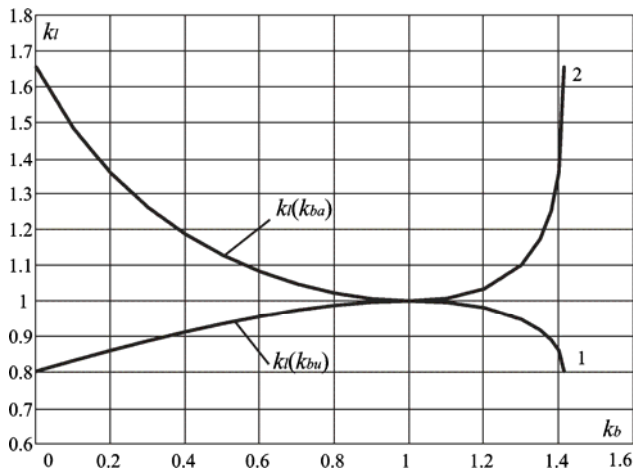


Fig. 5. Dependences $k_l = f(k_b)$ for three-phase ESS unbalanced modes: 1 – three-phase source unbalance; 2 – resistive load unbalance

Fig. 6 shows the dependence of the correction factor k_l on the k_b factor which sets the pattern of change of power factor and amplitudes of voltage and current higher harmonic of the three-phase four-wire ESS at $R_n = R_s$ by (16).

Additional power losses determination. Deviation of the operation conditions of the three-phase ESS from the conditions in which the power losses correspond to the minimum possible value, leads to additional losses [10]. Developed mathematical models allow us to calculate the value of power the additional losses in any of 279 modes of operation of the three-phase ESS. Fig. 7 shows the dependences of the relative, as a fraction of the average load useful power, power of additional losses on the k_b factor for five considered ESS modes of operation.

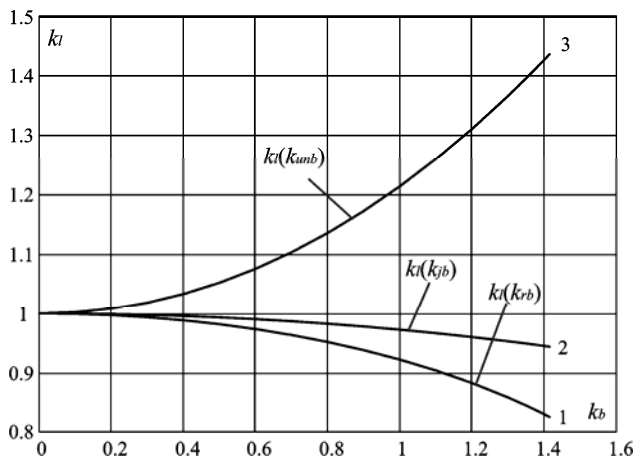


Fig. 6. Dependences $k_l = f(k_b)$ at: 1 – active-inductive load; 2 – symmetric nonlinear load; 3 – three-phase voltage source higher harmonics

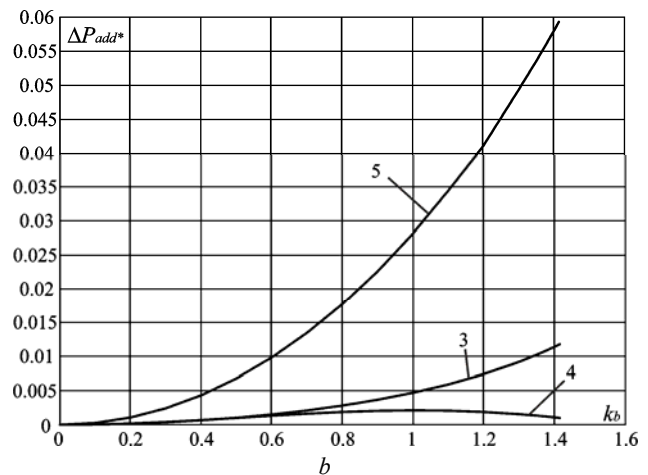
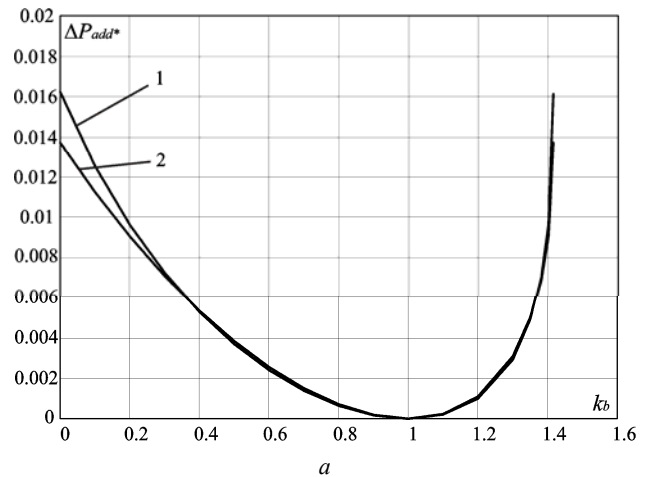


Fig. 7. Dependence of the relative additional power losses on the factor k_b

Analysis of the dependences in Fig. 7 shows that additional power losses in three-phase ESS at $k_{sc} = 20$ can range from a few tenths to a few percent of the average load useful power. The three-phase ESS with non-linear load have the smallest power efficiency. A combination of factors causing additional losses decreases energy efficiency of three-phase ESS.

Analytical data obtained on the developed model (27) – (41) for five of considered cases are presented in Table 1.

Table 1

Calculation of correcting factors and power indicators for five operation modes of the three-phase ESS

k_b	Mode 1			Mode 2			Mode 3			Mode 4			Mode 5		
	k_{lu}	K_{2U}	ΔP_{add*}	k_{la}	K_{2I}	ΔP_{add*}	k_{lr}	$\cos\varphi$	ΔP_{add*}	k_{lun}	THD_u	ΔP_{add*}	k_{lj}	THD_i	ΔP_{add*}
0	0.8028	0.522	0.0137	1.6551	0.522	0.01612	1	1	0	1	0	0	1	0	0
0.1	0.8324	0.462	0.0112	1.4839	0.462	0.01251	0.9993	1	0.00004	1.0021	0.047	0.00005	0.9997	0.041	0.0003
0.2	0.8608	0.407	0.009	1.3576	0.407	0.0096	0.9971	0.999	0.00016	1.0084	0.094	0.0002	0.9989	0.082	0.0011
0.3	0.8877	0.354	0.0071	1.2615	0.354	0.0072	0.9935	0.997	0.00037	1.0188	0.141	0.0004	0.9975	0.123	0.0024
0.4	0.9129	0.304	0.0053	1.1868	0.304	0.0053	0.9883	0.994	0.00066	1.0336	0.188	0.0007	0.9957	0.164	0.0044
0.5	0.9359	0.254	0.0038	1.1282	0.254	0.0037	0.9816	0.991	0.00104	1.0526	0.235	0.00101	0.9932	0.205	0.0068
0.6	0.9564	0.206	0.0025	1.0824	0.206	0.0024	0.9733	0.987	0.00153	1.0759	0.282	0.00134	0.9902	0.246	0.0099
0.7	0.9738	0.157	0.0015	1.0473	0.157	0.0014	0.9634	0.983	0.00212	1.1037	0.329	0.00164	0.9866	0.287	0.0135
0.8	0.9875	0.107	0.0007	1.0218	0.107	0.00064	0.9516	0.978	0.00284	1.1359	0.367	0.0019	0.9825	0.328	0.0178
0.9	0.9966	0.055	0.0002	1.0058	0.055	0.00017	0.9378	0.972	0.0037	1.1726	0.423	0.0021	0.9778	0.368	0.0227
1.0	1	0	0	1	0	0	0.9219	0.966	0.0047	1.214	0.47	0.00213	0.9725	0.409	0.0283
1.1	0.9958	0.061	0.00023	1.0071	0.061	0.00021	0.9035	0.959	0.00595	1.26	0.517	0.0021	0.9665	0.45	0.0345
1.2	0.9808	0.133	0.0011	1.0338	0.133	0.001	0.8825	0.952	0.00743	1.3109	0.564	0.0019	0.96	0.491	0.0415
1.3	0.9479	0.227	0.0031	1.1008	0.227	0.0029	0.8581	0.944	0.00922	1.3665	0.611	0.00156	0.9525	0.532	0.0494
1.35	0.918	0.293	0.0049	1.1731	0.293	0.0049	0.8445	0.94	0.01027	1.3962	0.634	0.00135	0.949	0.553	0.0536
1.38	0.8901	0.35	0.0069	1.2538	0.35	0.007	0.8358	0.938	0.01095	1.4145	0.648	0.0012	0.9466	0.565	0.0562
1.4	0.8608	0.407	0.009	1.3576	0.407	0.0096	0.8298	0.936	0.01144	1.427	0.657	0.0011	0.945	0.573	0.058
1.414	0.8028	0.522	0.0137	1.6551	0.522	0.0161	0.8254	0.935	0.0118	1.436	0.664	0.00101	0.9438	0.579	0.0593

Three-phase ESS Matlab-model. In accordance with the equivalent circuit of Fig. 2 and matrix mathematical model (27) – (41) a Matlab-model of the three-phase ESS shown in Fig. 8 was created. It differs from the previously developed models [5, 6, 11] by the presence of optimized load structure which is divided into a symmetric resistive load and a adjustable symmetrical three-phase current source and a block of automated calculation of the correction factor k_l (kl Calculation). The model allows at setting the values of the elements of the vectors (8) – (12) without an operator to automatically calculate the coefficient k_l and calculate the values of the total power losses components taking into account the calculated ratio.

The Matlab-model consists of:

- the power circuit configured by Fig. 2 and included:
 - the three-phase source of symmetric sinusoidal voltages U_{sa} , U_{sb} , U_{sc} ;
 - the three-phase source of non-sinusoidal voltages U_a , U_b , U_c ;
 - the symmetrical resistive load R_{la} , R_{lb} , R_{lc} ;
 - the three-phase current source J_a , J_b , J_c ;
 - the active resistances of the four-wire line R_a , R_b , R_c , R_n ;
 - the power active filter configured on three adjustable current sources SAF.
- the current and voltage sensors connected to the model's power circuit.
- the subsystems of the measured data processing:
 - the subsystem of the total power losses components calculation by (1) Calculation 1 (Fig. 9);
 - the Subsystem of the total power losses components

calculation in p-q-r coordinates Calculation 2 (Fig. 10);

- the subsystem of load useful power harmonic composition calculation Calculation 3;
 - the subsystem of the total power losses components calculation by coefficients of direct, reverse and zero consequences Calculation 4 (Fig. 11);
 - the subsystem of calculation and indication of measured information on instantaneous values of electrical quantities and three-phase ESS parameters Measurements 1;
 - the subsystem of calculation and indication of measured information on average and RMS values of electrical quantities and three-phase ESS parameters Measurements 2 (Fig. 12).
- the subsystems of the ESS state control and monitoring:
 - the PAF control system SAF Controller (Fig. 13);
 - the subsystem for setting control signals for the three-phase current source and three-phase non-sinusoidal voltage source Control System;
 - the subsystem of the correcting factor k_l calculation kl Calculation;
 - the block for the PAF connection to the ESS PAF Connection.

5. the virtual measured devices.

The developed Matlab-model can be used to analyze the three-phase energy supply systems and for assessment the energy efficiency at to a power system of the active power filter at any of 288 possible modes of operation.

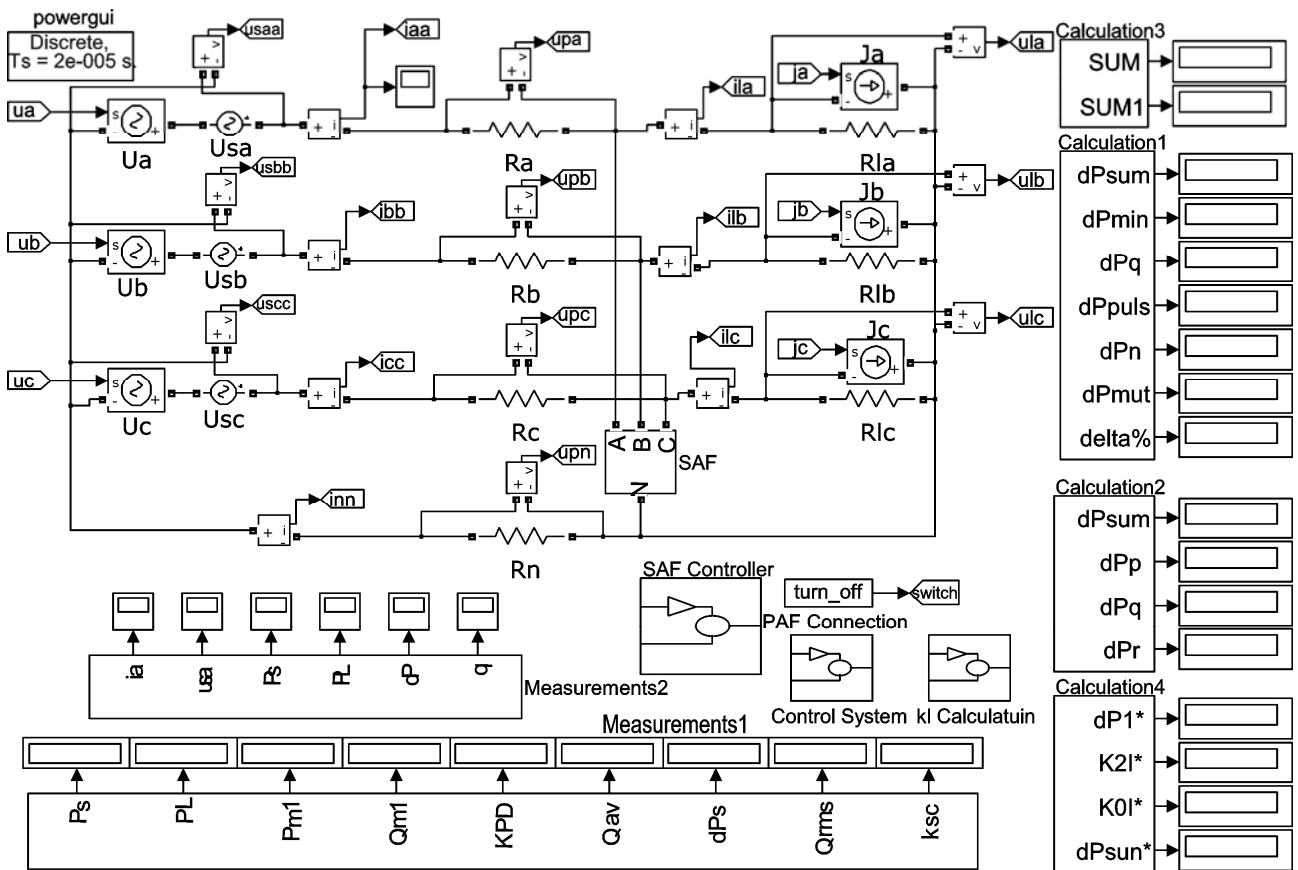


Fig. 8. Matlab-model of the three-phase ESS with PAF

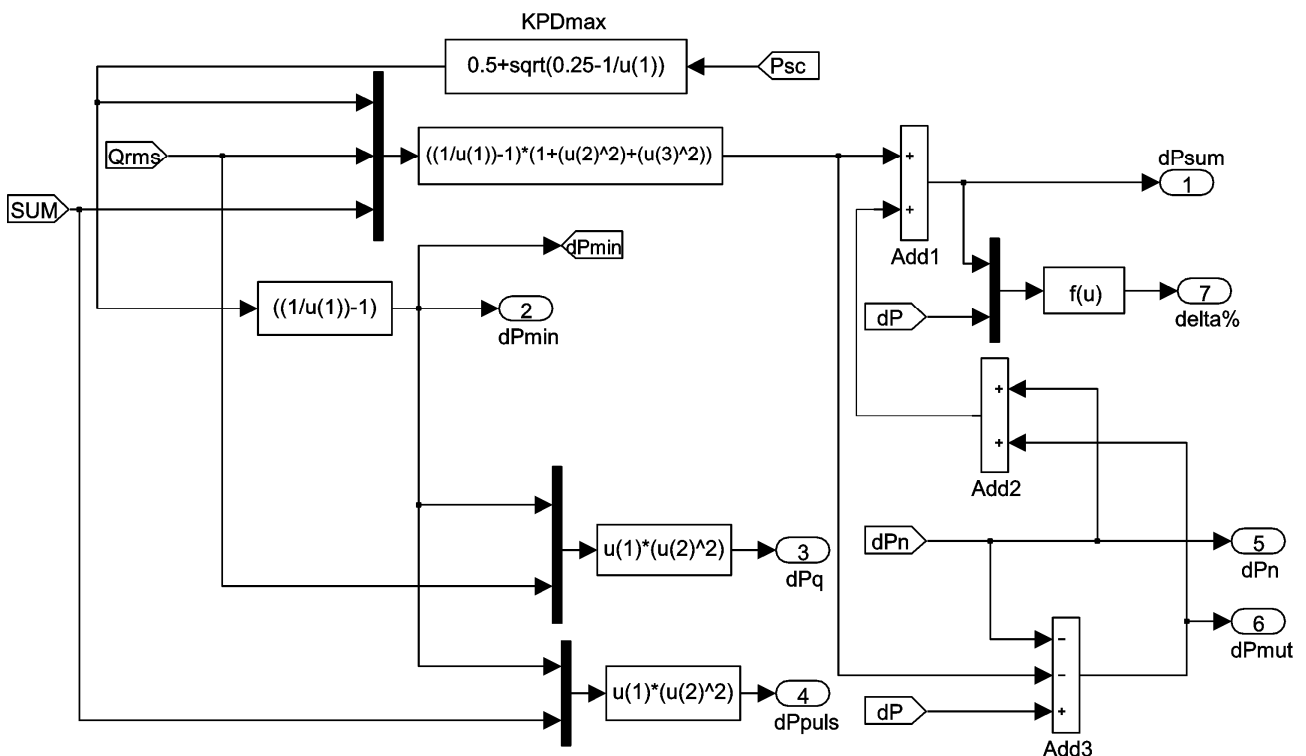


Fig. 9. Subsystem of the total power losses components calculation by (1) Calculation 1

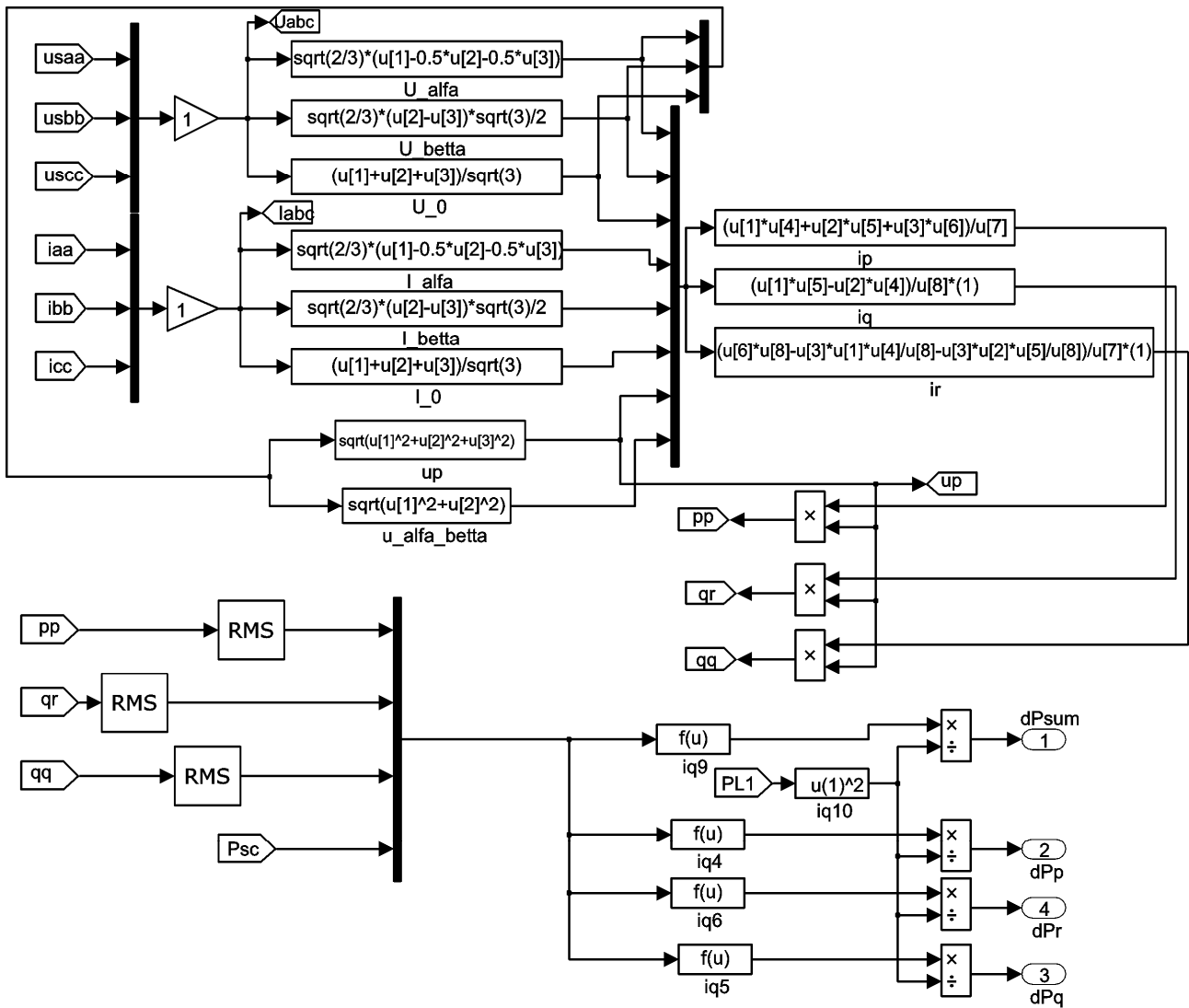


Fig. 10. Subsystem of the total power losses components calculation in p-q-r coordinates Calculation 2

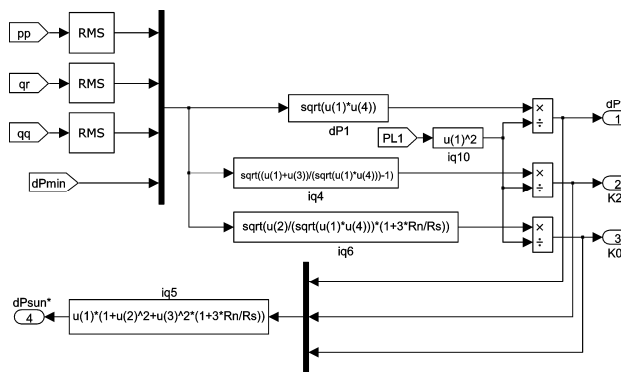


Fig. 11. Subsystem of the total power losses components calculation by coefficients of direct, reverse and zero consequences Calculation 4

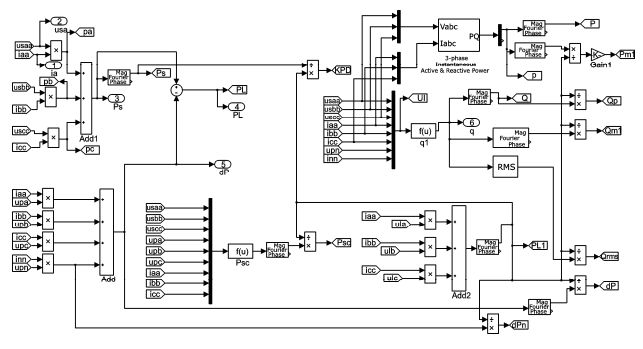


Fig. 12. Subsystem of calculation and indication of measured information on average and RMS values of electrical quantities and three-phase ESS parameters Measurements 2

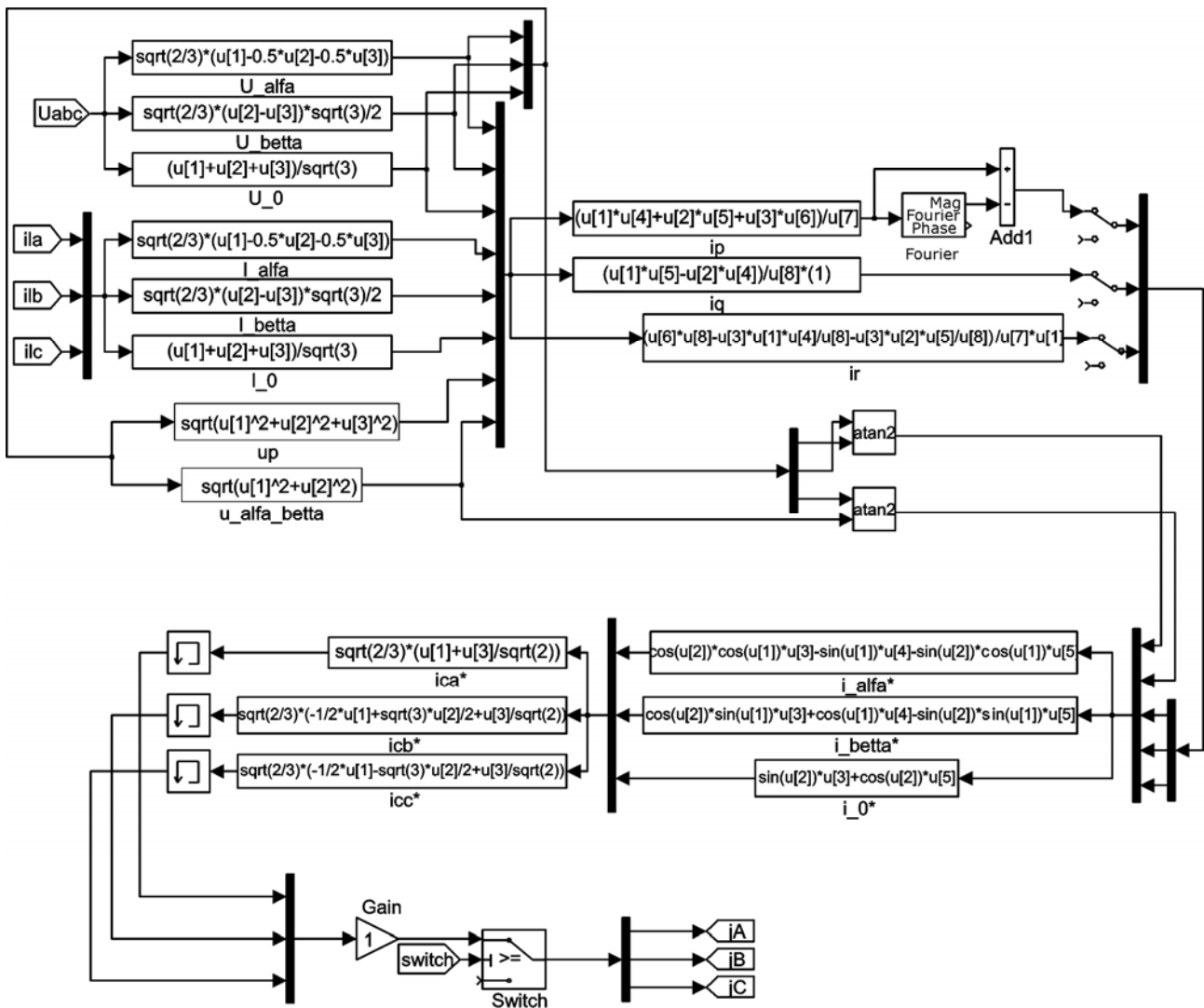


Fig. 13. PAF control system SAF Controller

Conclusions.

1. We proposed two ways to create a mathematical model of the three-phase ESS, the first one is based on the vector form, and the second one is based on the matrix representation of power processes in multiphase systems. It allows solving the problem of maintaining of constant values of average active load power in the ESS operation at different modes.

2. Based on the analysis of the results of modeling of five operating modes of the three-phase ESS, at each of which a unique factor that causes the appearance of additional losses in the system is involved, it was concluded that the maximum reduction of power efficiency corresponds the ESS with non-linear load.

3. Using the developed mathematical models the operation of the MATLAB-model of the three-phase ESS with PAF is optimized. The possibility of the automated calculation of the correction factor k_f is realized which is more than an order reduced the working time with model at investigation of the ESS operating modes at which additional losses arise

REFERENCES

1. Akagi H., Kanazawa Y., Nabae A. Instantaneous reactive power compensators comprising switching devices without energy storage components. *IEEE Transactions on Industry Applications*, 1984, vol. IA-20, no.3, pp. 625-630. doi: [10.1109/TIA.1984.4504460](https://doi.org/10.1109/TIA.1984.4504460).
2. Wong M.-C., Dai N.-Y., Lam C.-S. «Active Power Filters», *Parallel Power Electronics Filters in Three-Phase Four-Wire Systems*. Springer Singapore, 2016. pp. 59-165. doi: [10.1007/978-981-10-1530-4_3](https://doi.org/10.1007/978-981-10-1530-4_3).
3. Artemenko M.Yu., Batrak L.M., Mykhalskiy V.M., Polishchuk S.Y. Analysis of possibility to increase the efficiency of three-phase four-wire power system by means of shunt active filter. *Tekhnichna elektrodynamika*, 2015, no.6, pp. 12-18. (Ukr).
4. Artemenko M.Yu., Batrak L.M., Polishchuk S.Y., Mykhalskiy V.M., Shapoval I.A. The effect of load power factor on the efficiency of three-phase four-wire power system with shunt active filter. *2016 IEEE 36th International Conference on Electronics and Nanotechnology (ELNANO)*, IEEE, 2016. pp. 277-282. doi: [10.1109/ELNANO.2016.7493067](https://doi.org/10.1109/ELNANO.2016.7493067).
5. Zhemerov G.G., Tugay D.V. Physical meaning of the «reactive power» concept applied to three-phase energy supply systems with non-linear load. *Electrical engineering & electromechanics*, 2015, no.6, pp. 36-42. (Rus). doi: [10.20998/2074-272X.2015.6.06](https://doi.org/10.20998/2074-272X.2015.6.06).

6. Zhemerov G.G., Tugay D.V. An universal formula clarification to determine the power losses in the three-phase energy supply systems. *Bulletin of NTU «KhPI»*, 2015, no.12, pp. 339-343. (Rus).
7. Peng F.Z., Ott G.W., Adams D.J. Harmonic and reactive power compensation based on the generalized instantaneous reactive power theory for three-phase four-wire systems. *IEEE Transactions on Power Electronics*, 1998, vol.13, no.6, pp. 1174-1181. doi: **10.1109/63.728344**.
8. Afonso J., Couto C., Martins J. Active filters with control based on p-q theory. *IEEE Industrial Electronics Society Newsletter*, 2000, vol.47, no.3, pp. 5-10.
9. Kim H.S., Akagi H. The instantaneous power theory on the rotating p-q-r reference frames. *Proceedings of the IEEE 1999 International Conference on Power Electronics and Drive Systems. PEDS'99 (Cat. No.99TH8475)*, 1999, pp. 422-427. doi: **10.1109/PEDS.1999.794600**.
10. G. Zhemerov, N. Ilina, D. Tugay. The Theorem of Minimum Energy Losses in Three-Phase Four-Wire Energy Supply System. *2016 2nd IEEE International Conference on*

Intelligent Energy and Power Systems (IEPS-2016). June 07-11, 2016, Kyiv, Ukraine, pp. 52-54. doi: **10.1109/IEPS.2016.7521889**.
 11. Zhemerov G.G., Tugay D.V. Components of total electric energy losses power in pqr spatial coordinates. *Electrical engineering & electromechanics*, 2016, no.2, pp. 11-19. (Rus). doi: **10.20998/2074-272X.2016.2.02**.

Received 01.06.2016

D.V. Tugay, Candidate of Technical Science, Associate Professor,
 O.M. Beketov National University of Urban Economy in Kharkiv,
 12, Revolution Str., Kharkiv, 61002, Ukraine.
 phone +38 057 7073111, e-mail: tugaydv@yandex.ua

How to cite this article:

Tugay D.V. Three-phase energy supply systems simulation for the total power losses components assessment. *Electrical engineering & electromechanics*, 2016, no.4, pp. 43-53. doi: 10.20998/2074-272X.2016.4.06.

Yu.V. Batygin, E.A. Chaplygin, O.S. Sabokar

MAGNETIC-PULSE CAR BODY PANELS FLATTENING. THEORETICAL ASPECTS AND PRACTICAL RESULTS

The aim of the article is to provide theoretical and experimental studying of the «induction system with an attractive screen» practical effectiveness with the excited magnetic pulse attractive forces numerical estimation. Originality. For the first time, the theoretical analysis of the electrodynamic process for the «inductor system with attractive screen» at the low frequent assumption were conducted. Methodology of the analysis applied is based on the classic electrodynamic circuits theory. All of the resulted carried out, were obtained as the Maxwell's differential equation solutions and its behavior was analyzed analytically. Results. The electrodynamic process was analyzed and the principle efficiency of the «induction system with an attractive screen» as an effective tool for magnetic pulse forming of the thin sheet metals was substantiated. The axis distributions of the attractive forces based on the relations been obtained were illuminated graphically. The results of experimental testing of the system in the engineering operation of the external non-contact dents removing on the car body panels samples were presented. Practical value. According to the results of the calculation analyses the fundamental workability of the «inductor system with attractive shield» as an effective magnetic pulse sheet metal part attraction tool was proved. It was shown that the not deep metal surface damages could be worked up by magnetic pulses technologies with a high performance in a short time. References 12, figures 4.

Keywords: magnetic-pulse forming, inductor system, field tension, induced current density, electromagnetic processes.

Проведен анализ электродинамических процессов и обоснована принципиальная работоспособность «индукторной системы с притягивающим экраном», как эффективного инструмента магнитно-импульсной рихтовки тонкостенных листовых металлов. Представлены результаты экспериментальной апробации системы в производственной операции по внешнему бесконтактному удалению вмятин в образцах кузовных панелей автомобилей. Библи. 12, рис. 4.

Ключевые слова: магнитно-импульсная рихтовка, индукторная система, напряженность поля, плотность индуцированных токов, электромагнитные процессы.

Introduction and publications analysis. The applying of magnetic fields for metals engineering is widely used [1]. Now, the contemporary technologies allow to make production available and technically simple of the complexes for electromagnetic-pulse metals forming (EMF). Currently EMF technology got widespread throughout the world [2]. Therefore, firms like «Boeing», «Electroimpact» and «Flextronic» use this technology for repair namely to remove dents on the fuselage of the aircraft [3, 4]. We should note so company like «Betag Innovation» (last «Beule Technik AG») that has the practice-approved experience at the area of the development of various systems for the car body panels dents removing [5].

In the laboratory of the electromagnetic technologies at the Kharkiv National Automobile and Highway University (KhNAHU) the developments in the area of the magnetic pulse metal forming (MPMF) takes a place.

The complex (prototype) for the external magnetic-pulse car body panels flattening, that is consist of the power source and the magnetic-pulse tool series for dents removing was developed and made [6].

The power source that in special literature called like magnetic pulse plant (MPP) is a universal devise in its essence, withal, the tools – the magnetic field sources, that are called inductor systems, must satisfy the carrying out operations correctly [1, 2].

In particular, the main purpose of the magnetic-pulse metal processing consists in the external non-contact car body metal flattening. The detailed enough review of these tools, repairing technologies, its appearance and historical development aspects in the treaties [7] are presented.

According to the work principle, all tools can be divided in two big groups. So, the performance of the first group is based on the sheet metal attraction, that is caused

by curtain magnetic properties under such condition as low frequency of the action field [8, 9]. The effectiveness of the second group tools, that have an author's name «inductor system with an attractive shield (ISAS)», is determined by conductors forced attraction, that have same directional induced Fouke's currents and is described by Ampere's law. This system consists constructively of the field source– inductor that is placed between two sheet metal conductors. One of them – is the auxiliary attractive shield, another one is the sheet metal simple, the current area of which is subjected to the attractive magnetic pulse influence [8-10].

One of the ISAS constructions is proposed by authors of the patent [11]. It supposes circle inductor, conductive auxiliary shield and sheet metal sample layer-to-layer placing. Respectively, such construction of the inductor system can be an effective enough tool for the contemporary technologies of the automobile body panel dents removing [12].

Purpose of the article is theoretical and experimental studying of the ISAS practical effectiveness with the excited magnetic pulse attractive forces numerical estimation. The ISAS practical testing as a tool for new method of external car bodies flattening with protective paintwork saving. The description of the external non-contact magnetic pulse flattening technological route.

Theory, calculated ratio. The accepted calculated model of the cylindrical inductor system (tool) design for the magnetic-pulse flattening with equal thin-walled non-magnetic sheet metals and the flat circular one-coil solenoid that placed above the attractive shield surface is presented in fig. 1.

According to the articles [2, 8-10] the mathematical assumptions were accepted.

For the calculated model fig. 1 Maxwell's equations were composed, solution of which gives us the induced

© Yu.V. Batygin, E.A. Chaplygin, O.S. Sabokar

currents time form. (Detail calculation sequence can be reviewed in [1, 2, 7-10]). At the low frequency work mode for the action fields, currents can be presented in the next form.

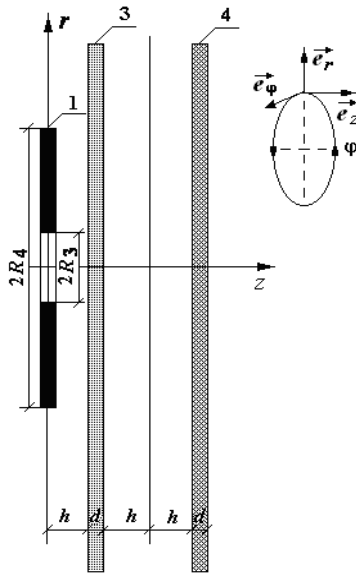


Fig. 1. The calculated model in a cylindrical coordinate system:
1 – multicoil inductor; 2 – shield; 3 – sample; d – thickness;
 R_3, R_4 – inner and outer radii; h – the distance from the inductor to the shield, $2h$ – the distance between the shield and the metal sample; $\vec{e}_r, \vec{e}_\varphi, \vec{e}_z$ – directing vectors

The excited signal in the auxiliary shield:

$$J_\phi^{(s)}(\psi, r) = -J_m \cdot \int_0^\infty f(x) \cdot \frac{e^{-x \frac{h}{d}} (1 - e^{-x})}{x} J_1\left(x \cdot \frac{r}{d}\right) dx, \quad (1)$$

where $J_m = \left(\frac{I_m}{R_4 - R_3} \right) \cdot \frac{\omega \tau}{2} \cdot \frac{dg(\psi)}{d\psi}$ – the «conditional»

induced signal amplitude, I_m and $g(\psi) = e^{-\delta_0 \psi} \cdot \sin(\psi)$ – the amplitude and the phase relation of the excited current in the solenoid; $\psi = \omega \cdot t$ – phase, t – time,

$$f(x) = \frac{1}{x^2} \cdot \int_{\frac{x R_3}{d}}^{\frac{x R_4}{d}} y \cdot J_1(y) dy.$$

The linear current density that is excited in the sheet metal sample:

$$J_\phi^{(p)}(\psi, r) = -J_m \cdot \int_0^\infty f(x) \cdot e^{-x \left(\frac{3h}{d} + 1 \right)} \cdot \frac{(1 - e^{-x})}{x} J_1\left(x \frac{r}{d}\right) dx. \quad (2)$$

At the consider low frequency mode, as there have been shown before, the attractive forces integral efficiency tends to zero value [2, 10].

Under conditions of the hard auxiliary shield fixation, the sample will be subjected only to the attractive forces influence. The attractive forces (Ampere's forces) dependence that presents in the terms of the inductor current phase takes the next form [10].

$$F_{attr}(\psi, r) = \mu_0 \cdot J_\phi^{(s)}(\psi, r) \cdot J_\phi^{(p)}(\psi, r) \cdot \frac{r}{(2h)}. \quad (3)$$

The numerical estimations were made according to the next initial data that is typical for the magnetic pulse metal processing [1, 2]: $I_m = 120$ kA, $\omega = 2\pi \cdot 1500$ Hz, $R_3 = 0.005$ m, $R_4 = 0.05$ m, $d = 0.001$ m, $h = 0.005$ m.

Calculation results in the fig. 2 are presented.

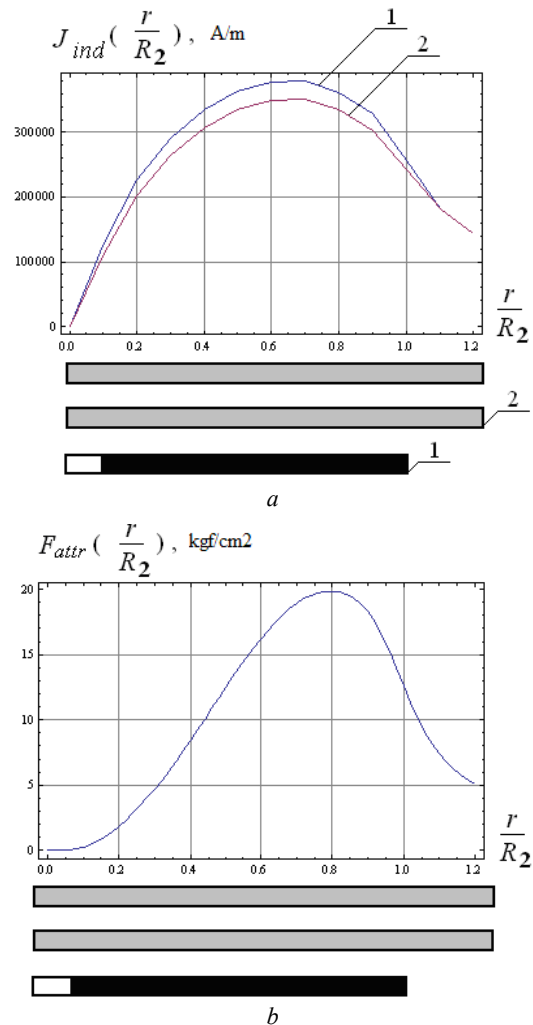


Fig. 2. Spatial excited currents and attractive forces distribution:
a) the currents induced in the auxiliary shield metal – 1 and sheet metal sample – 2;
b) is the radial attractive forces distribution

On the calculated dependences in the fig. 2 it is obtained that achieved attractive forces can reach up to 20 Atm. in the researched ISAS system.

The averaged surface forced impact is equal to 10 Atm. It is necessary to attend, that insignificant increase of the current, e.g., up to 150 kA, (that is real enough practically) gives us more than 2 times attractive forces value increase. As the practice of magnetic-pulse metals processing, this forced impact value is enough for effective deformation of the thin walled conductors. Ultimately, the main result of the analysis of electrodynamic processes is the conclusion about the practical effectiveness of the proposed ISAS construction.

Experimental testing and the main results. The ISAS principal construction that is used in experiments and coincides with its calculated model.

Actually, based on the forced impact results, the proposed «inductor system with attractive shield» is

analogical to the well-known electromagnet, fig 3,*b*. However, unlike the last, there can be realized the attraction not only for ferromagnetic, but also for metal of any physical nature.

In the fig. 3 the magnetic pulse flattening complex and the experimental ISAS prototype are presented. The winding of the exciting coil is connected to the power source – magnetic pulse plant МНУС-2, that was designed and developed in the Laboratory of electromagnetic technology KhNAHU, fig 3,*a* [6]. Its distinguishing feature consists of the serial pulse work mode. It means continuously predetermined number of charge current pulses repetition, that eventually are transformed into the power attraction pulses of the metal dents to the working shield surface.

As experimental samples there were taken galvanized steel sheet metal samples and car body metal samples so Automobile mark like «Subaru» and «Citroen». The samples thickness was $\sim 0.0008\dots 0.001$ m. The damages, that were made in each sample were $\sim 0.0018\dots 0.002$ m and external diameter was 0.05 m.

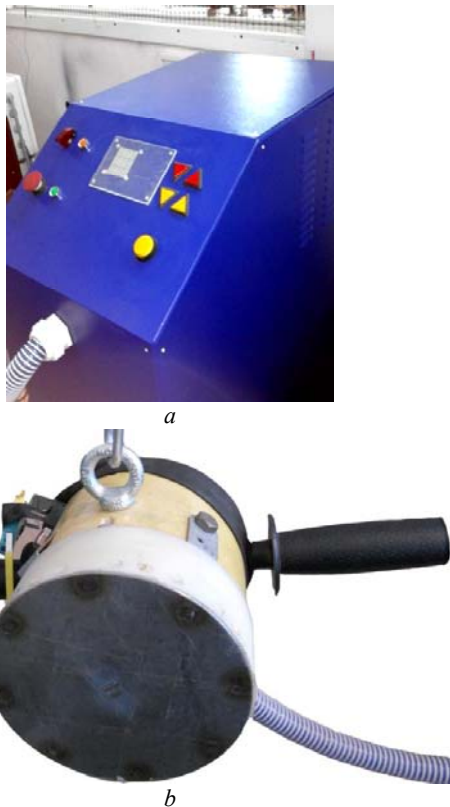


Fig. 3. The external magnetic pulse flattening complex (1 – magnetic pulse flattening tool – ISAS); 2 – the cable connection; 3 – magnetic pulse plant МНУС2):
a – common complex view; *b* – ISAS

The technological operations was carried out under the following terms:

- stored energy and the voltage of the capacitive storage ~ 2.4 kJ and 1500 V, respectively;
- working frequency and the current pulse amplitude ~ 1500 Hz and ~ 12 kA, respectively;
- current pulses frequency ~ 5 Hz;
- power attraction pulses number, that provides alignment of the sheet sample with a dent $\sim 18\dots 20$.

In the fig. 4 there are presented the experimental samples that illustrate examples of effective external non-contact magnetic pulse dents removing in samples of cars body panels of the Japanese and European production. It is necessary to note about the safety of the protective cover lay.

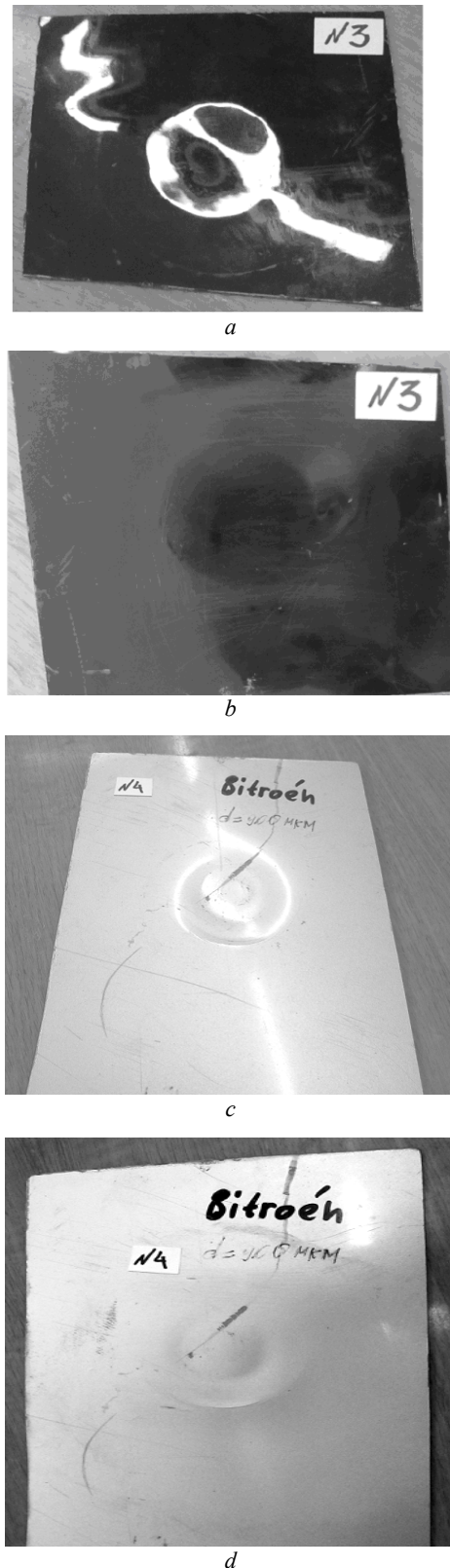


Fig. 4. The experimental samples variety of automotive steels: «Subaru» (*a* – before the power impact, *b* – after attraction); «Citroen» (*c* – before the power impact, *d* – after attraction)

Conclusions.

1. At the low frequent assumption, the theoretical analysis of the electrodynamic process for the «inductor system with attractive shield» with the external one coil circle inductor exciting were conducted.

2. The fundamental workability of the «inductor system with attractive shield» as an effective magnetic pulse sheet metal part attraction tool was proved.

3. The successful experimental testing of the «inductor system with attractive shield» and external exciting for the actual external non-contact dent removing operation in the European and Japan car body samples was conducted.

4. The external magnetic pulse flattening technical route was disclosed and described.

5. The experiment results showed us the efficiency of the proposed magnetic pulse flattening tool in the practical realization for the principally new flattening method with a paintwork covering saving.

REFERENCES

1. Psyk V., Risch D., Kinsey B.L., Tekkayaa A.E., Kleiner M. Electromagnetic forming – A review. *Journal of Materials Processing Technology*, 2011, vol.211, no.5, pp.787-829. doi: **10.1016/j.jmatprotec.2010.12.012**.
2. Batygin Yu.V., Lavinskiy V.I., Khimenko L.T. *Impul'snyye magnitnyye polya dlya progressivnykh tekhnologiy. Tom 1. Izdaniye vtoroye, pererabotannoye i dopolnennoye*. [Pulsed magnetic fields for advanced technologies. Vol.1. 2nd edition, revised and enlarged.] Kharkov, MOST-Tornado Publ., 2003. 284 p. (Rus).
3. *Electromagnetic Dent Removal*. Available at: <http://www.electroimpact.com/EMAGDR/overview.asp> (accessed 25 May 2014).
4. *Need an electromagnetic dent remover on hand. Fluxtronic offers the best: the Portable Flux 3 dent remover*. Available at: <http://www.fluxtronic.com/product.php> (accessed 07 August 2014).
5. *Welcome to BETAG Innovation*. Available at: <http://www.betaginnovation.com> (accessed 16 June 2014).
6. *Laboratoriia elektromagnitnykh tekhnologii* (Laboratory of Electromagnetic Technology) Available at: <http://electromagnetic.comoj.com> (accessed 10 July 2014).
7. Yuriy V. Batygin, Sergey F. Golovashchenko, Andrey V. Gnatov. Pulsed electromagnetic attraction of sheet metals – fundamentals and perspective applications. *Journal of Materials Processing Technology*, 2013, vol.213, no.3, pp. 444-452. doi: **10.1016/j.jmatprotec.2012.10.003**.
8. Batygin Yu.V., Gnatov A.V. Magnetic-pulse attraction and repulsion of thin-walled sheet ferromagnetics. *Electrical Technology Russia*, 2012, no.8, pp. 58-65. (Rus).
9. Batygin Yuri V., Sergey F. Golovashchenko, Andrey V. Gnatov. Pulsed electromagnetic attraction of nonmagnetic sheet metals. *Journal of Materials Processing Technology*, 2014, vol.214, iss.2, pp. 390-401. doi: **10.1016/j.jmatprotec.2013.09.018**.
10. Batygin Yu.V., Golovashhenko S.F., Chaplygin E.A. Magnetic-pulse attraction of nonmagnetic metals. *Electrical Technology Russia*, 2014, no.2, pp. 40-52. (Rus).
11. Batygin Yu.V., Gnatov A.V., Chaplygin E.O., Trunova I.S., Gopko A.V., Sabokar O.S. *Sposib magnitno-impul'snogo prityagannya metalevikh zagotivok odnovitkovim krugovim induktorom, roztashovanim nad dopomizhnim ekranom* [Method of the magnetic-pulse attraction metal workpieces single-turn circular inductor located on the auxiliary screen]. Patent UA, no.77579, 2013. (Ukr).
12. Batygin Yu.V. Experimental test of the tool for the external EMF removing dents on a car body. *International Journal of Energy and Power Engineering*, 2014, vol.3, no.4, pp. 204-208. doi: **10.11648/j.ijpe.20140304.14**.

Received 25.03.2016

Yu.V. Batygin¹, Doctor of Technical Science, Professor,
E.A. Chaplygin¹, Candidate of Technical Science, Associate
Professor,
O.S. Sabokar¹,
¹Kharkov National Automobile and Highway University,
25, Petrovskogo Str., Kharkov, 61002, Ukraine.
phone +38 057 7073727, e-mail: batygin48@mail.ru,
chapygin.e.a@gmail.com, o.s.sabokar@gmail.com

How to cite this article:

Batygin Yu.V., Chaplygin E.A., Sabokar O.S. Magnetic-pulse car body panels flattening. Theoretical aspects and practical results. *Electrical engineering & electromechanics*, 2016, no.4, pp. 54-57. doi: 10.20998/2074-272X.2016.4.07.

L.A. Shchebeniuk, T.Yu. Antonets

INVESTIGATION OF LOSSES IN INSULATION OF HIGH-VOLTAGE CABLES WITH XLPE INSULATION

In this paper the authors calculate the losses in insulation system cable with XLPE-polyethylene as a solid dielectric insulation and with semiconductor polyethylene used as a conductor screen and a insulation screen. The paper is devoted to the investigation of losses in the insulation system of high-voltage XLPE-cables. The line of XLPE-cables in group running horizontally, provided that the cables are of equal diameter and emit equal losses. It is limited to the following: the air flow around the cables may be necessary restricted by proximity to next cables. The dielectric losses are voltage depended and related to the insulation system materials being used. All current in this insulation system are complex quantities containing both real ($Re(I)$) and imaginary ($Im(I)$) parts. Values of the loss factor of the insulation system at power frequency $tg\delta$ are given as $tg\delta = Re(I)/Im(I)$. It was proposed the quantities criterion of the loss factor of the insulation system to high voltage XLPE-cables. The work is devoted to creation of a method for calculation of the current rating of high-voltage cables in conditions function. References 7, figures 2.

Key words: power cable, XLPE-cable, insulation losses, insulation system, loss factor.

Рассмотрен современный нормативный подход к определению потерь в изоляции силовых высоковольтных кабелей. В стационарном режиме нагрузки (100 % -ный коэффициент нагрузки) в соответствии с действующим международным стандартом (IEC 60287-1-1) диэлектрические потери зависят только от напряжения и от использованного изоляционного материала. Силовые высоковольтные кабели с изоляцией из сшитого полиэтилена (СПЭ-кабели) имеют безусловные преимущества перед традиционными, что обусловило их широкое использование во всех развитых странах и заметное сокращение использования других типов кабелей. Ряд существенных особенностей СПЭ-кабелей, которые влияют на температуру в элементах конструкции кабеля и, соответственно, на потери в них как в рабочих, так и в аварийных режимах эксплуатации, а именно: 1) большие, чем у традиционных маслом наполненных кабелей, значения площади сечения жил и толщины изоляции; 2) большая, чем у традиционных маслом наполненных кабелей, допустимая температура изоляции (90 °C); 3) большие, чем у традиционных маслом наполненных кабелей, значения толщины полупроводящих экранов по жиле и по изоляции; 4) существенная зависимость теплопроводности и теплоемкости полиэтиленовой изоляции от температуры; 5) наличие элементов конструкции с высоким удельным тепловым сопротивлением (до 50 °C·м/Вт), что существенно влияет на температуру в элементах конструкции СПЭ-кабеля и, соответственно, на потери в них. Представлены данные о потерях в системе, состоящей из изоляции и полупроводящих экранов по жиле и по изоляции СПЭ-кабеля на напряжение 110 кВ для электрофизических и конструктивных характеристик материалов системы изоляции конкретного кабеля на основе схемы замещения. Ток в этой изоляционной системе является комплексной величиной, и значение тангенса угла ее диэлектрических потерь при промышленной частоте определено как отношение действительного тока к реактивному. В работе выполнен расчет потерь в системе изоляции, состоящей из изоляции из сшитого полиэтилена, экрана по жиле и экрана по изоляции из полупроводящего полиэтилена. Работа нацелена на разработку метода оценки пропускной способности СПЭ-кабелей в конкретных условиях испытаний и эксплуатации. Библ. 7, рис. 2.

Ключевые слова: силовой кабель, СПЭ-кабель, потери в изоляции, система изоляции, тангенс угла диэлектрических потерь.

Problem definition. High-voltage XLPE-cables have a number of essential peculiarities influencing the temperature mode in working as well as in emergency operation mode:

- more than for traditional oil-filled cables, values of wires sectional area and thickness of the insulation causing significant dependence of the cable heating process on wires and insulation heat capacity and losses in it;
- more than for traditional oil-filled cables, insulation permissible temperature (90 °C) that firstly, causes high

values of allowable current [1]; secondly, increases losses in structural parts of the cable that requires a separate consideration of losses in insulation [2];

- substantial dependence of thermal conductivity and heat capacity of polyethylene insulation on temperature (e.g., specific heat capacity of polyethylene at temperature of 20 °C is 2300 J/kg·°C and at 80 °C – 3750 J/kg·°C) and the presence of elements of design with high specific thermal resistance (till 50 °C·m/W) which changes the

thermal conditions of insulation compared to the operation mode of the traditional oil-filled cables.

Therefore, investigation of losses in insulation of high-voltage cables with cross-linked polyethylene insulation is necessary for decision-making regarding their technical capacity and overload capacity.

Analysis of literature sources. The combination of high working intensity of the electric field (up to 8 kV/mm or more) with long-term high insulation temperature (up to 90 °C or more) lead to the use of long-term and expensive tests [3] at which XLPE-cables are exposed hundreds of heating cycles (every of 8 hours) with simultaneous action of high voltage $1.7U$; during the cycles of heating all the major parameters are checked:

- electrical (dielectric loss tangent, the level of partial discharges);
- thermal (temperature in cable design elements and on its surface).

At the same time, the capacity of power cables is determined solely by calculation in nominal terms, i.e. at steady load (100% load factor matched) [4]. Accordingly, the rated current I_n is infinitely long-term at which the maximum wire temperature is set at nominal conditions environment. Practically applied computational models to determine I_n must include the calculation of losses in the insulation of high-voltage cables [4].

Since the losses in the elements of the design of cable indirectly affect the losses in insulation but in operation the cable is almost never works in a steady maximum allowable mode, to verify specific cables use or special laboratory [5, 6] cable or take the manufacturer's warranty. This means the need to investigate the manufacturer specific losses in insulation cables. Obviously, standardized calculations are necessary. But for innovative products, which differs significantly from the traditional use only standardized methods are inadequate. For example, in [7] the method we use universal and unified computational models of processes of heat and mass transfer in high-voltage cables with plastic isolation to study their capacity through interval parameter estimation models. It is shown that for calculating high-capacity power cable with plastic insulation necessary joint resolution models that describe structural, electrical, thermal and economic parameters of the cable. A solution for a single-cable with cross-section of 625 mm² for voltage of 220 kV is presented. It was established that the optimal range of insulation thickness from 9.5 mm to 10.5 mm and further reducing the thickness of the insulation capacity of the cable is reduced.

The goal of the work is to estimate the losses power in the system of insulation of the XLPE cable

for the voltage of 110 kV at the nominal load mode using equivalent circuits.

Results of investigations. In the basis of calculation of losses in insulation of high-voltage XLPE-cable an analogy of processes of heat and mass transfer, including charges transfer processes and heat transfer process is laid. Appropriate models are identical in structure, they include both basic potential difference (electrical or thermal), flow, resistance, conductivity. Accordingly, all other elements of models describing a particular process are derived from these values, and mathematical description of a process in a system of differential equations is fairly universal and unified [2, 3].

In cylindrical coordinates (r, θ, z) the most suitable to describe the processes of heat transfer in cables for potential we use Poisson equation which, if the potential φ depends only on the radius r (radial field in a homogeneous substance), a potential gradient is inversely proportional to radius:

$$-d\varphi/dr = \varphi_0/[r \cdot \ln(r_2/r_1)], \quad (1)$$

where r_1, r_2 are the radii of equipotential lines between which there is a radial field in a homogeneous substance, $r_1 < r_2$; $\varphi = \varphi_0$ at $r = r_1$, and $\varphi = 0$ at $r = r_2$.

This model is the main calculation model used in cable technology for the describing stationary processes of charges or heat transfer through a homogeneous substance in a radial field.

Since the potential depends on the radius only if infinitely long cable and a substance which is the process of transferring, in one way or another is heterogeneous, the application model (1) causes the error, the smaller the aforementioned conditions closer to reality. To avoid significant error we need to perform calculations for intervals of possible values of parameters and compare calculation results with the results arising from real experience.

For example, when calculating the dielectric losses in cables with polyethylene insulation we should use interval values of specific thermal insulation resistance, since this parameter depends on temperature [7]. Using a similar process of charge transfer and heat transfer to determine the distribution of the field strength in the elements of structure of the XLPE-cable if the transfer process is **stationary** (process parameters are independent of time) and **linear**, relation corresponding motion potential difference (for example, the temperature difference τ , K) to intensity of flow (for heat flow P , J/s) is constant. Then for flow through any uniform cable design element:

$$\tau = P \cdot S, \quad (2)$$

where S is the resistance of the cable design element.

If the flow of heat and radial, the thermal insulation resistance **per unit length of the cable** is determined by formula:

$$S_i = \sigma_i \ln(r_2/r_1)/2\pi, \quad (3)$$

where r_1, r_2 are the radii of equipotential lines of the radial field for wire and insulation, respectively; σ_i is the specific thermal resistance of insulation.

The system of the XLPE-cable insulation consists of successive layers of different materials: a semiconductor screen for wire, insulation and a semiconductor screen for insulation. So, to calculate the charge transfer process at DC in such a system we should take into account different values of resistivity of all three elements.

Semiconductor screens for wire and for insulation consist of composite material - XLPE filled with acetylene soot. This material structure and characteristics can be seen as imperfect dielectric, conducting electric current. For approximate estimation of power energy dissipation in semiconductor structures of specific cable structures' screens we can use different equivalent circuits of the system «semiconductor screen for wire – insulation – semiconductor screen for insulation», for example, a known parallel equivalent circuit for each element of the system shown in Fig. 1.

If equivalent circuit parameters C_1, C_2, C_3 and R_1, R_2, R_3 are determined by known formulae for the radial electric field:

$$C = 2\pi \cdot \varepsilon \cdot \varepsilon_0 / \ln(r_2/r_1), \quad (4)$$

where ε_0 is the electric constant, ε is the relative dielectric constant of insulation; $\varepsilon_0 = 1/\mu_0 \cdot c_0^2 = 8.85 \cdot 10^{-12}$ F/m; $c_0 = 2.99 \dots \times 10^8$ m/s is the speed of light in vacuum; $\mu_0 = 4\pi \cdot 10^{-7}$ H/m is the magnetic constant;

$$R = (2\pi \cdot \gamma)^{-1} \cdot \ln(r_2/r_1), \quad (5)$$

where γ is the electrical conductivity of the element's material, then corresponding complex impedances of these elements are determined by the common formula (6).

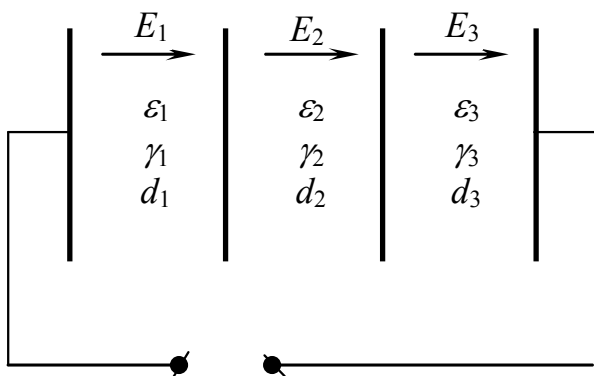


Fig. 1. A circuit of the system «semiconductor screen for wire – insulation – semiconductor screen for insulation»: $\varepsilon_1, \varepsilon_2, \varepsilon_3$ – relative dielectric constants of the elements' material; $\gamma_1, \gamma_2, \gamma_3$ – electrical conductivities of the elements' material; d_1, d_2, d_3 – thicknesses of the system's elements

Complex impedances of the insulation system's elements:

$$Z = -jX_c \cdot R / (R - jX_c), \quad (6)$$

where R, X_c are the active and reactive resistances of the corresponding system's element, $X_c = (\omega C)^{-1} = (2\pi f C)^{-1}$; f is the frequency; C is the capacitance of the insulation system's element.

Current that flows through the insulation and the cable semiconductor screens is defined phase cable voltage U and the sum of complex impedances of cable insulation system's elements:

$$I = U / (Z_1 + Z_2 + Z_3). \quad (7)$$

Voltage on the system's elements and active losses on it are determined by formulae:

$$U_1 = I \cdot Z_1; \quad P_1 = U_1 \cdot [\text{Re}(I) - j\text{Im}(I)]; \quad (8)$$

$$U_2 = I \cdot Z_2; \quad P_2 = U_2 \cdot [\text{Re}(I) - j\text{Im}(I)]; \quad (9)$$

$$U_3 = I \cdot Z_3; \quad P_3 = U_3 \cdot [\text{Re}(I) - j\text{Im}(I)]. \quad (10)$$

Losses in the insulation system are determined by formula:

$$P = U \cdot [\text{Re}(I) - j\text{Im}(I)]. \quad (11)$$

Thus, the losses in the insulation system P depend on the voltage associated with the electrical characteristics of the used material (relative dielectric constant ε , specific conductivity γ) and the geometric dimensions of the insulation system's elements.

On the other hand, practically applicable and recommended by the corresponding International Standard [2] the formula by which we determine P_d losses in dielectric of power high-voltage cables, is the ratio, including the value of the dielectric losses tangent $\text{tg}\delta$:

$$P_d = \omega C U^2 \text{tg}\delta, \quad (12)$$

where ω is the angular frequency, $\omega = 2\pi f$; C is the capacitance per unit length; U is the phase voltage.

Values of the dielectric losses tangent are determined experimentally. For high-voltage XLPE cables in [2] the value $\text{tg}\delta = 0.0015$ is indicated. Losses power P_d in the dielectric of the cable АПВБВНГД 1×500 of 110 kV by (12) is $P_d = 0.33$ W/m.

The value of power losses in the insulation system calculated by (11) for this cable is $P = 0.34$ W/m with at dielectric conductivity of 10^{-11} S/m and conductivity of semiconductor screens material ranging from 10^{-1} S/m to 10^1 S/m. Obviously, the use of more complex circuits of the system «semiconductor screen for wire - insulation - semiconductor screen for insulation» can provide more accurate calculations. But compliance of P_d and P values are sufficient to address through this equivalent circuit of the problem, namely - a rough estimate of losses in semiconductor high-voltage cable screens compared to losses in its insulation.

Using (7) the dissipation factor of the insulation system can be defined as the ratio of real current to reactive:

$$tg\delta = Re(I)/Im(I). \quad (13)$$

Fig. 2 shows an illustration of the results of calculations by (13) in the form of dependence of dissipation factor of the insulation system of the XLPE cable for voltage of 110 kV on the conductivity of the material of the screen. These data, first, indicate that the reduction of the electrical conductivity of the material of the screen causes increase of losses in the screen, but in a fairly wide range of values of conductivity of the material of the screen which includes real values in the appropriate cable constructions, namely from 10^{-3} S/m to 10^2 S/m, power losses in the semiconductor screens are negligible compared to the power losses in insulation.

Second, maximum on the dependence of the dissipation factor of the insulation system of the XLPE cable for the voltage of 110 kV on the screen material conductivity γ_e for any value of relative dielectric constant of the material of the screen is far from the real values γ_e (at least five orders) therefore this maximum has no practical value.

Third, at real values of relative dielectric constant of the material of semiconductor screens of high-voltage XLPE cables insulation (at least 100 at frequency of 50 Hz) the maximum $tg\delta$ approaching to normative ($tg\delta = 0.0015$). This demonstrates the acceptability of the equivalent circuit as a serial connection of complex impedances of three elements of the insulation system. All elements are represented as a parallel connection of active and reactive resistance.

Maximum on the dependence of the dissipation factor of the XLPE cable insulation system takes place under condition of equality of the absolute values of active and reactive resistance of semiconductor screens:

$$Re(Z_1) = -Im(Z_1); \quad (14)$$

$$Re(Z_3) = -Im(Z_3), \quad (15)$$

which reflects the mainly capacitive nature of current through the semiconductor screen at real values of electrophysical characteristics of semiconductor material of the screen.

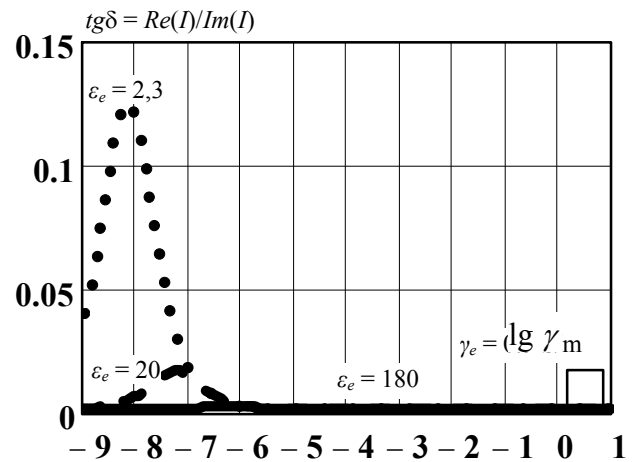


Fig. 2. Dependencies of the dissipation factor of the XLPE cable insulation system for voltage of 110 kV on the conductivity of the material of the screen at different relative permittivity of the material of the screen ϵ_e (results obtained for cable with insulation thickness of 16 mm are shown)

Conclusions.

1. Using an equivalent circuit analysis the power losses in the XLPE cable insulation system for the voltage of 110 kV at the nominal load mode is determined.

2. Based on the fact that the value $tg\delta$ XLPE by Standards IEC is 0.0015 it is determined that the power losses in the insulation system of the cable АПВБНГД 1×500 for 110 kV is 0.33 W/m. The value of the power losses in the insulation system calculated by the equivalent circuit for the same cable is 0.34 W/m at dielectric conductivity of 10^{-11} S/m and conductivity of semiconductor screens material ranging from 10^{-1} S/m to 10^1 S/m.

3. Current flowing through the insulation and the cable semiconductor screens is determined by phase voltage and the sum of complex impedances of these structural elements of the cable. The criterion of correctness of calculations by the equivalent circuit is beneficial coincidence of these results with international regulations data. Therefore, it can be concluded that calculations by the adopted equivalent circuit can be used to approximate estimates of the need to take into account losses in semiconductor screens of the high-voltage cable compared to losses in its insulation.

4. In the sufficiently wide range of values of conductivity of the material of the screen which includes real values in the appropriate cable designs, in particular from 10^{-3} S/m to 10^2 S/m, power losses in the semiconductor screens are negligible compared to the power losses in insulation.

5. Reduce of the conductivity of the material of the screen causes the increase of losses in the cable insulation system. Accordingly, on the dependence of the dissipation factor of the insulation system of the high-voltage XLPE

cable the maximum is observed. The value of the electrical conductivity of the material of the screen γ_e at which the maximum of losses:

- is far from the real values γ_e (at least five orders) that has no practical value;
- at the real values of the relative permittivity of the semiconductor screens material in the insulation system of high-voltage XLPE cables (at least 100), the maximum $tg\delta$ approaches to the regulatory value ($tg\delta = 0.0015$);
- maximum on the dependence of the dissipation factor of the insulation system of the XLPE cable takes place under condition of equality of the absolute values of active and reactive resistances of semiconductor screens that are property of the adopted equivalent circuit.

REFERENCES

1. Karpushenko V.P., Shchebeniuk L.A., Antonets Yu.O., Naumenko O.A. *Sylovi kabeli nyz'koyi ta seredn'oyi napruhy. Konstruyuvannya, tekhnolohiya, yakist'* [Power cables of low and medium voltage. Designing, technology, quality]. Kharkiv, Region-inform Publ., 2000. 376 p. (Ukr).
2. IEC 60287-1-1: 2001. Electric cables. Calculation of the current rating. Part 1-1: Current rating equations (100 % load factor) and calculation of losses – General. – 65 p.
3. SIGRE № 303 «Revision of qualification procedures for high voltage and extra high voltage AC extruded underground cable systems», 2006.

How to cite this article:

Shchebeniuk L.A., Antonets T.Yu. Investigation of losses in insulation of high-voltage cables with XLPE insulation. *Electrical engineering & electromechanics*, 2016, no.4, pp. 58-62. doi: 10.20998/2074-272X.2016.4.08.

4. IEC 60287-2-1: 2001. Electric cables. Calculation of the current rating. Part 2-1: Thermal resistance – Calculation of thermal resistance. – 84 p.
5. IEC 62067: Ed. 1.1b: 2006. Power cables with extruded insulation and their accessories for rated voltages above 150 kV ($U_m = 170$ kV) up to 500 kV ($U_m = 550$ kV) – Test methods and requirements. – 90 p.
6. HD 632 S1: 1998. Power cables with extruded insulation and their accessories for rated voltages above 36 kV ($U_m = 42$ kV) up to 150 kV ($U_m = 170$ kV) Part 2: Additional test methods.
7. Shchebeniuk L.A., Antonets T.Yu. To determine the capacity of high-voltage power cables with plastic insulation. *Visnyk NTU «KhPI» – Bulletin of NTU «KhPI»*, 2011, no.3, pp. 152-157. (Ukr).

Received 05.05.2016

L.A. Shchebeniuk¹, Candidate of Technical Science, Professor,
T.Yu. Antonets¹, Postgraduate Student,
¹National Technical University «Kharkiv Polytechnic Institute»,
21, Kyrpychova Str., Kharkiv, 61002, Ukraine.
e-mail: agurin@kpi.kharkov.ua

R.V. Zaitsev, M.V. Kyrychenko, A.V. Kholod, L.V. Zaitseva, D.S. Prokopenko, G.S. Khrypunov

CALCULATION OF OPERATING PARAMETERS OF HIGH-VOLTAGE POWER TAKE-OFF SYSTEM FOR THE PHOTOVOLTAIC FACILITY

Purpose. To ensure maximum production of electric power by photovoltaic facilities, in addition to using highly efficient photovoltaic modules equipped with solar radiation concentrators must use a highly effective power take-off system. This paper is inscribed to solving the problem of a highly efficient and economic power take-off system development. *Methodology.* To solving the problem, we implemented three stages. On the first stage examines the dependence of electrical power from the intensity of the incident solar radiation. Based on this, the second stage is calculated the DC-DC converter resonant circuit and its working parameters, and developed circuit diagram of DC-DC converter. On the third stage, we carry out an analysis of power take-off system with step up DC-DC converter working. *Results.* In this paper, we carry out the analysis of working efficiency for photovoltaic facility power take-off system with step-up boost converter. The result of such analysis show that the efficiency of such system in a wide range of photovoltaic energy module illumination power is at 0.92, whereas the efficiency of classic power take-off systems does not exceed 0.70. Achieved results allow designing a circuit scheme of a controlled bridge resonant step-up converter with digital control. Proposed scheme will ensure reliable operation, fast and accurate location point of maximum power and conversion efficiency up to 0.96. *Originality.* Novelty of proposed power take-off system solution constitute in implementation of circuit with DC-DC converters, which as it shown by results of carrying out modeling is the most effective. *Practical value.* Practical implementation of proposed power take-off system design will allow reducing losses in connective wires and increasing the efficiency of such a system up to 92.5 % in wide range of photovoltaic energy modules illumination. References 7, tables 3, figures 4.

Key words: photovoltaic module, step-up converter, power take-off system, photovoltaic facility, efficiency.

Проведен анализ работы системы отбора мощности фотоэлектрической станции с использованием повышающего преобразователя. Показано, что коэффициент полезного действия такой системы в широком диапазоне освещенности фотоэлектрического модуля находится на уровне 0,92, тогда как эффективность классических систем отбора мощности не превышает 0,70. Разработана принципиальная электрическая схема регулируемого мостового резонансного повышающего преобразователя с цифровым управлением, обеспечивающая надежность работы, быстрое и точное нахождение точки максимальной мощности и эффективность преобразования до 0,96. Библ. 7, табл. 3, рис. 4.

Ключевые слова: фотоэнергетический модуль, повышающий преобразователь, система отбора мощности, фотоэлектрическая станция, коэффициент полезного действия.

Introduction. To ensure maximum production of photovoltaic facility (PVF), in addition to using highly efficient photovoltaic modules (PVM) equipped with solar radiation concentrators it is necessary to use a highly effective power take-off system (PTOS) [1]. The most important part of the PTOS is a DC-DC converter which enhances increase of DC voltage generated in the operation of PVM for its further high-efficiency transmission and transformation [2, 3]. Here, because depending on the daily change of solar radiation the electrical power produced by PVM also changes, the structural optimization solutions of DC-DC converters and PTOS should be made taking into account the full range of electrical power that is converted. Optimization of constructive and technological solutions of all components of system converting solar energy into electricity of power frequency will increase the efficiency of PVF and by cumulative energy and economic indicators to achieve its competitiveness in the domestic and global market.

Problem definition. Based on the above, the aim of the work is to develop a circuit and constructive decisions and calculation of the operating parameters of high-voltage power take-off system of photovoltaic facility. In the first phase the dependence of electrical power of PVM on the intensity of the solar radiation is investigated. Based on this, in the second phase calculation of the resonance circuit of a DC-DC converter

and the parameters of its work is conducted, a circuit diagram of a DC-DC converter is developed. In the third stage analysis of operation of the PTOS using a DC-DC step-up converter is carried out.

The experimental technique. Measurements of short circuit current (I_{SC}), open circuit voltage (U_{OC}), working (I_W) and maximum (P_{MAX}) electrical power and efficiency of standard industrial designs of PVM of Chinese production are carried out at power of solar radiation from 1000 to 2000 W/m² that permits to simulate their performance when using concentrators. Measuring these quantities was conducted by the method of loading lighting current-voltage characteristics using the developed and produced stand, block diagram and external view of which are shown in Fig. 1.

Stand for PVM investigations includes: investigated PVM (1), control unit (2), pulse lighter based on xenon flash lamps (3), store of the load resistance (4) with electronic commutation using MOSFET-transistors, and digital oscilloscope to record experimental data (5).

For use as a load resistance a shop of load resistance was designed and manufactured switching individual resistors in which is carried out by using modern MOSFET transistors IRFZ48Z type which have in the open state very small (0.011-0.012 Ω) and stable resistance of the channel, and do not make thus a significant error in the value of the load resistance, even when measuring the short-circuit current. Registration of

voltage drop on the load resistance was carried out with a digital oscilloscope RIGOL DS1052E which has the ability to connect directly to a PC.

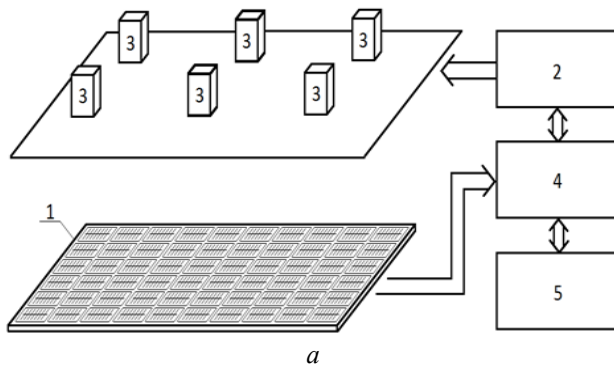


Fig. 1. Block diagram (a) and external view (b) of the stand for PVM investigations

The operation principle of this stand is as follows. At pulse irradiation from lighter the PVM generates a photocurrent, the duration of amplitude value of its force approximately corresponds to the length of the main phase of the lamp-flash combustion which is about 1 ms. Photocurrent amplitude value dividing into diode component flowing through the shunt resistance value, and amplitude of the current flowing in the load resistance 4 generates the voltage drop in the load resistance which is registered by a memory digital oscilloscope 5, which operates in sweep waiting mode.

To check the temperature of the PVM in the process of measurements directly to PVM a thermocouple were connected. Determination and adjustment of the radiation power on the front surface of the PVM in the range 1000-2000 W/m² was carried out using a standard photoelectric converter that has a known value of short circuit current at the radiation power of 1000 W/m². Investigation by the described technique was consistently performed for the values of the radiation power: 1100, 1200, 1300, 1400, 1500, 1600 1700, 1800, 1900, 2000 W/m² and repeated for three experimental samples of PVM.

Results and discussion.

1. The influence of radiation power on the efficiency of the power module.

Typical results of investigations of experimental samples of PVM are presented in Table 1. Fig. 2 shows built on the basis of the obtained data compiled charts of dependencies of open circuit voltage, short circuit current,

maximum power and efficiency on the radiation power on the front surface of PVM. From the results of investigations of experimental samples of PVM it can be concluded that for the investigated samples at the radiation intensity 1500-1800 W/m² the typical value of the open circuit voltage is 37.5 V, short circuit current value is 11-13 A, value of maximum power up to 440 W at voltage in the operating point at least 33 V providing the photovoltaic module efficiency of at least 16.8 %.

Table 1
Output parameters which are characteristic for investigated PVM samples determined at different radiation power (P_I) on the front surface of PVM

P_I , W/m ²	U_{OC} , V	I_{SC} , A	I_W , A	P_{MAX} , W	Efficiency, %
1000	36.99	7.68	7.37	241.49	16.54
1100	37.12	8.45	8.11	266.65	16.60
1200	37.24	9.21	8.85	291.80	16.65
1300	37.39	9.98	9.58	317.08	16.71
1400	37.51	10.76	10.33	342.96	16.78
1500	37.60	11.54	11.08	368.99	16.84
1600	37.74	12.29	11.80	394.48	16.88
1700	37.86	13.03	12.50	419.16	16.89
1800	37.59	13.83	13.28	441.97	16.81
1900	37.28	14.60	14.01	462.45	16.67
2000	36.98	15.33	14.71	481.61	16.50

It should be noted that the use of experimental models of PVM at low concentrated solar radiation is justified because it is at the radiation power 1700 W/m² investigated PVM reach maximum efficiency of 16.89 %. An additional advantage of using low concentrated radiation is to increase the maximum power produced by PVM to 419 W which is 1.7 times more than the value of specified characteristic of the classic solar panels.

Use of low concentrated solar radiation is also an additional argument in favor of equipping each PVM by a step-up DC-DC converter at the development of PTOS as the operating current of PVM at radiation power 1700 W/m² reaches 13 A almost twice exceeding the same value at the radiation power 1000 W/m² which if operation of PTOS in traditional way will cause additional losses in the connecting cables or lead to the need of significant investment to equip a photovoltaic facility by cables of enlarged section.

2. Development of a step-up DC-DC converter for the high effective PTOS.

In developing a step-up DC-DC converter as reference parameters obtained in the study of series of PVM are used (Table 1).

2.1. Calculation of a resonant DC-DC circuit and operating parameters of converter.

Conversion gain of the adjustable bridge resonant converter:

$$G = K \cdot n, \quad (1)$$

where K is the conversion gain of the resonant LLC circuit; n is ratio of secondary winding turns to the number of turns of the primary winding of the transformer TR1.

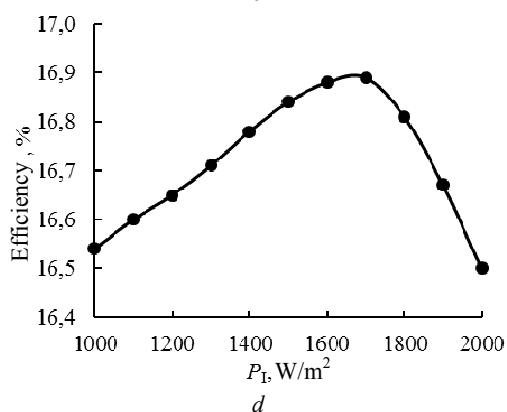
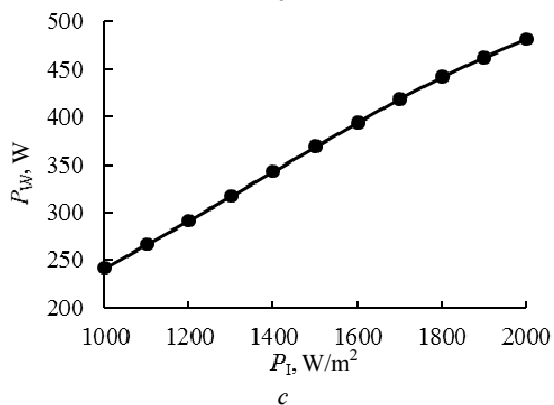
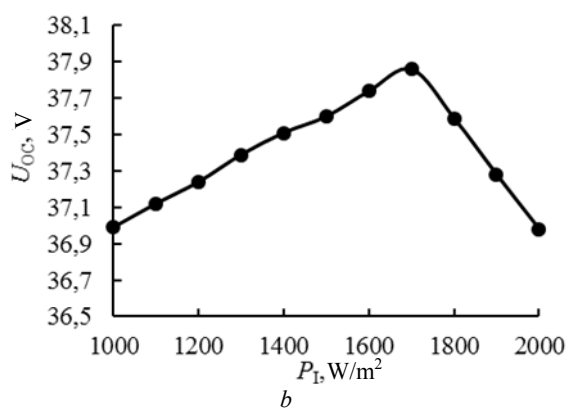
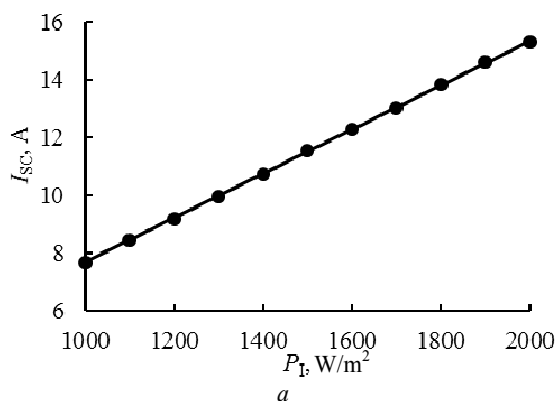


Fig. 2. Typical dependency graphs of short-circuit current (a), open circuit voltage (b), maximum power (c) and efficiency (d) of investigated PVM on radiation power on the front surface

Since the resonant converter has a maximum efficiency at $K = 1$, we calculate n from the condition of maximum efficiency in nominal operation mode of the converter:

$$n = \frac{U_{in.nom.}}{U_{out.nom.}} = \frac{30}{630} = \frac{1}{21}, \quad (2)$$

where $U_{in.nom.}$ is the nominal input voltage of the converter; $U_{out.nom.}$ is the nominal output voltage of the converter.

Conversion gain of the resonant LLC circuit should have maximal value $K_{max.}$ at the combination of the minimal input ($U_{in.min.}$) and maximal output ($U_{out.max.}$) voltage, and minimal value $K_{min.}$ at the combination of maximal input ($U_{in.max.}$) and minimal output ($U_{out.min.}$) voltage:

$$K_{max} = n \cdot \frac{U_{out.max.}}{U_{in.min.}} = \frac{1}{21} \cdot \frac{700}{23} \approx 1,45; \quad (3)$$

$$K_{min} = n \cdot \frac{U_{out.min.}}{U_{in.max.}} = \frac{1}{21} \cdot \frac{600}{42} \approx 0,68. \quad (4)$$

To calculate the parameters of the resonant LLC circuit we use the equivalent circuit of the resonant circuit [3-5]. For the presented equivalent circuit the conversion gain of the resonant LLC circuit is described by:

$$K = \left| \frac{U_{in}}{U_{out}} \right| = \frac{F_x^2(m-1)}{\sqrt{(mF_x^2-1) + F_x^2(F_x^2-1)^2(m-1)^2 Q^2}}, \quad (5)$$

where

$Q = \frac{\sqrt{L_r}}{R_{ac} C_r}$ is the quality factor; $R_{ac} = \frac{8}{\pi^2} n^{-2} \frac{U_{out}}{I_{out}}$ is the superficial load resistance; U_{in} is the input voltage of the converter; U_{out} is the output voltage of the converter;

I_{out} is the output current of the converter; $F_x = \frac{f_s}{f_r}$ is the normalized frequency of switching transistors; f_s is the frequency of switching transistors of the converter;

$f_r = \frac{1}{2\pi\sqrt{L_r C_r}}$ is the resonant frequency of the circuit L_r

, C_r ; L_r is the resonant inductance; C_r is the resonant capacitance; $m = \frac{L_r + L_m}{L_r}$ is the ratio of the total input

inductance of the circuit to the resonant inductance; L_m is the inductance of the transformer magnetization.

Minimum superficial load resistance $R_{ac.min.}$ corresponds to the minimum output voltage and maximum output power ($P_{in.max.}$) at the maximum expected efficiency of 98%:

Minimum superficial load resistance $R_{ac.min.}$ corresponds to the minimum output voltage and maximum output power ($P_{in.max.}$) at the maximum expected efficiency of 98%:

$$R_{ac.min.} = \frac{8}{\pi^2} n^2 \frac{U_{out.min.}^2}{P_{in.max.} \cdot \eta} = \frac{8}{3,14^2} \cdot 0,047619^2 \cdot \frac{600^2}{300 \cdot 0,98} \approx 2,25 \Omega. \quad (6)$$

The correct calculation of the resonance circuit allows to obtain optimal characteristics of the converter. The algorithm allows for multiple iterations to calculate

the required parameters of the LLC resonant circuit. Using approximate calculation and refine it using simulations we can obtain quite faithful results at considerable time savings.

Maximum input voltage of the DC-DC converter meets maximal temperature of the PVM, illumination 200 W/m², i.e. input power ($P_{in,min.}$) not more than:

$$P_{in,min.}(23V) \leq 23V \cdot I_{in,nom.} \cdot \frac{200 \text{ W}}{1000 \text{ m}^2} = 37,6 \text{ W}. \quad (7)$$

The maximum value of Q corresponds to the maximum output current. Output current takes maximum value at minimum output voltage and maximum output power. The value of the superficial minimum load resistance $R_{ac,min.} = 2.25 \Omega$ corresponds to the maximum Q of the LLC circuit, and the maximum conversion gain of the resonant circuit $K_{max} = 1,45$ is required at the input power of 50 W and output voltage of 700 V. According to the expression for R_{ac} , the value of minimal superficial load resistance $R_{ac,min.}$ is determined for the input voltage of 23 V:

$$R_{ac,min.}(23V) = \frac{8}{3,14^2} \cdot 0,047619^2 \cdot \frac{600^2}{50 \cdot 0,98} \approx 13,5 \Omega. \quad (8)$$

Data for the resonance frequency of 100 kHz obtained by the algorithm calculating the parameters of the resonance circuit in several iterations with test computer modeling are presented in Table 2. The value of the ratio of the total input inductance to resonance one $m = 11$.

Table 2

Resonance circuit parameters

U_{in}, V	P_{in}, W	K_{max}	K	$R_{ac,max.}, \Omega$	Q_{max}	F_x
23	50	1.45	3.13	13,5	0.113	0.33
30	230	1.11	1.134	3,995*	0.383*	0.48*
33	300	1.01	1.026	2,25	0.68	0.86
42	300	0.79	1.026	2,25	0.68	0.972

* Value of $R_{ac,min.}$ corresponds to maximum output voltage and K_{max} .

Choosing the resonant capacitance of 0.94 μF at the resonance frequency $F_r = 110.7 \text{ kHz}$ we obtain the resonant inductance value $L_r = 2.2 \mu\text{H}$ and at $m = 10.1$ the transformer inductance of magnetization value $L_m = 20 \mu\text{H}$.

2.2 Development of schematic diagram of the DC-DC converter.

Fig. 3 shows the functional diagram of the DC-DC converter. Photovoltaic module voltage comes to the input of the DC-DC converter. Formation of converter parameters r and switching transistors are carried out by using a digital microcontroller MC. The control signal comes to gates of transistors VT1 – VT4 from the MC by drivers Dr.1 – Dr.4. Transistors within each arm of the bridge are switched simultaneously. Drivers and microcontrollers supply is carried out through a stabilized step-down DC converter of own needs. MC measures output current of the PVM using shunt R3 and amplifier, output voltage of the FEM through divider on the resistors R1 – R2. MC at the outputs G1 and G2 forms two counter-phase meanders for switching transistor with the

required frequency and time delay between switching diagonals of the bridge («dead» time). Voltage of the midpoint of the half-bridge of transistors VT1 and VT2 is used in determining of adaptive «dead» time (minimum required one) for maximum efficiency of the converter through divider on the resistors R4 and R5 enters to the comparator of MC. Additional transformer winding N3 connected to the rectifier bridge VD1 is used to control the output voltage and, together with the signal voltage of the midpoint of the half-bridge, is involved in the detection algorithm of approach to the capacitive current character of the resonant LLC circuit. Detection of approaching to the capacitive current character of the resonance circuit is essential when starting of the converter, as well as at relatively sharp changes of voltage on the output converter – a DC network 600 – 700 V.

The resonant LLC circuit is formed by a choke L1, a capacitor C1 and a transformer T1. The resonant inductance includes the inductance of the choke L1 and scattering inductance of the transformer T1. The output voltage from the transformer enters to the rectifier formed by added diode VD2 and the capacitor C3. Output voltage of the rectifier is the output voltage of the converter.

Tracking the point of maximum power of the PVM is carried out by microcontroller using the algorithm «Perturbations and monitoring» [6]. The microcontroller calculates the input power of the converter, then for a small amount it changes the input resistance by the change of the frequency of switching transistors, thus the input voltage changes, and calculates the power, and if the power increases – the controller continues to change the voltage in the same direction until the power stops growing. Digital converter control enables to realize an algorithm of maximum power point tracking «Perturbations and surveillance», forming the adaptive «dead» time, current detection of capacitive nature of the bridge load. With the microcontroller implementation of an information cable or wireless network, for example, RS-485 or ZigBee for monitoring of parameters of PVM converters, providing timely information about the failure, and so on becomes possible.

2.3 A schematic diagram of the DC-DC converter.

The converter consists of three functional blocks.

Source of power supply for own needs (SON) is designed to form a stabilized supply voltage 3.3 V and voltage of converter's transistors drivers supply 12 V. SON consists of two consecutive stages of step-down pulse DC converters without galvanic isolation. SON has high efficiency and stabilizes the output voltage in a wide input voltage range.

Controller. As a microcontroller a 32-bit ARM Cortex M-4 is used. Feedback signals after the conversion of levels filtering enter to the ADC of the microcontroller. The signal of current from the shunt is increased by the differential amplifier to the required level and then supplied to the ADC. On the chip DA6 the ADC voltage reference voltage is performed. Comparators are made on high-speed integrated circuits LMV7235M5. Transistors' control signals come to the circuit G1 and G2 on drivers inputs.

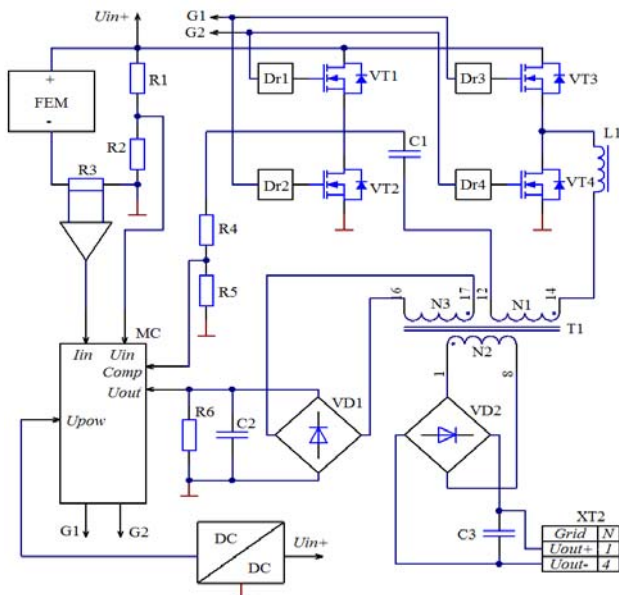


Fig. 3. Functional electric circuit of the DC-DC converter

The converter consists of: four transistors MOSFET VT1 – VT4; two drivers of a half-bridge on chips DA7, DA8; capacitors of a supply circuit; RLC resonant circuit on the choke L4, transformer T1, capacitors C46, C47; signal rectifier on diodes VD – VD12; output rectifier on diodes VD13 – VD16 and capacitors S52, S53. As a transistor bridge high-speed MOSFET transistors with low gate charge and open channel resistance of 2.8 mΩ are used. In the input rectifier diodes based on silicon carbide are used which allows significantly increase efficiency in the frequency range of switching transistors above resonance frequency value due to the absence of losses on reverse recovery of diodes based on silicon carbide.

3. Analysis of the power take-off system operation with DC-DC converter utilization.

To significantly reducing power losses [7] in PTOS utilization in its composition previously developed DC-DC converters that will reduce the currents flowing within the PTOS and, accordingly, proportionally the square of the current, decrease power losses, can lead. In the case of the PTOS development using DC-DC converters, the system will be divided into the following areas, which will experience losses in PTOS:

- area of the cable connection of the PVM and DC-DC converter ($P_{loss.PVM-DC}$);
- directly DC-DC converter ($P_{loss.DC}$);
- area of the cable connection of the DC-DC converter and inverter ($P_{loss.DC-Inv}$);
- inverter ($P_{loss.Inv}$).

Calculated losses for each of areas and calculated efficiency of the PTOS ($Efficiency_{PTOS}$) as a dependence o the PVM current (I_{PVM}) are presented in Table 3 and Fig. 4.

Table 3
Parameters of power losses and efficiency calculated for PTOS with utilization of the DC-DC converter

I_{PVM} , A	$P_{loss.PVM-DC}$, W	$P_{loss.DC}$, W	$P_{loss.DC-Inv}$, W	$P_{loss.Inv}$, W	$Efficiency_{PTOS}$, %
7.68	0.57	10.72	4.78	351.86	92.68
8.45	0.69	11.83	5.92	388.35	92.66
9.21	0.82	12.94	6.84	424.83	92.63
9.98	0.96	14.06	8.24	461.52	92.61
10.76	1.11	15.21	9.72	499.36	92.59
11.54	1.27	16.34	10.92	536.37	92.57
12.29	1.45	17.48	12.64	573.68	92.54
13.03	1.64	18.58	14.46	609.94	92.52
13.83	1.84	19.57	15.92	642.34	92.49
14.60	2.05	20.45	17.46	671.29	92.46
15.33	2.27	21.27	18.48	697.98	92.44

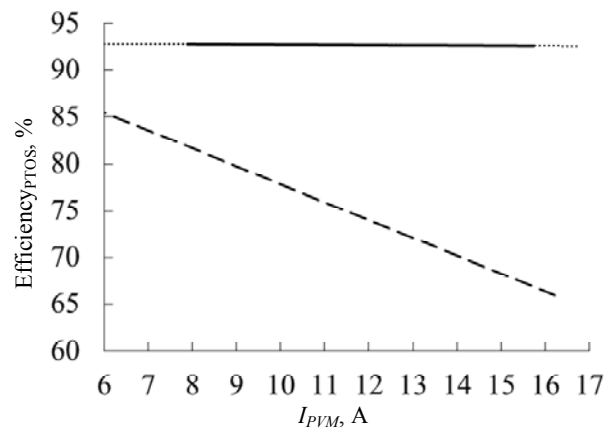


Fig. 4. Dependence of the calculated efficiency of the PTOS of the PVF with utilization of the DC-DC converters (solid line) in the comparison with PVF without DC-DC converters (dotted line)

Conclusions.

1. From the results of the experimental investigations of photovoltaic modules on the intensity of solar radiation it is found that at the radiation power of 1700 W/m² the investigated PVM reach maximum efficiency of 16.89 % and maximum power produced by photovoltaic modules reaches 419 W that 1.7 times more that the indicated value which is character for the classic solar panels.

2. Based on experimental data, the calculation of the resonance circuit of the DC-DC converter for use in high voltage power take-off system of the photovoltaic facility and the parameters of its operation. The main features of the developed schematic diagram of the DC-DC converter circuit is controlled using the bridge resonant converter and allows utilization of digital control that permits to achieve a conversion efficiency of 95.8 %.

3. The carried out analysis of the system for selecting the photovoltaic facility power using developed DC-DC converters has shown that the efficiency of the system in a wide range of illumination of the PVM is about 92 %, that is significantly more than for the classical power take-off systems, whose effectiveness is about 70 %.

REFERENCES

1. Kriukov Yu.A., Zaitsev A.Ye., Feshchenko A.A., Gorshkov A.V. Influence of operating temperature on efficiency of silicon photovoltaic devices. *International Journal of Applied Engineering Research*, 2015, vol.10, no.15, p.35446-35450.
2. Rozanov Yu.K., Baranov N.N., Antonov B.M., Efimov E.N., Solomatin A.V. Power electronics in systems with non-traditional power sources. *Electrical Technology Russia*, 2002, no.3, pp. 20-28.
3. Melyoshin V., Ovchinikov D. *Upravlenie tranzistornymi preobrazovatelayami elektroenergii* [Management transistor power converters]. Moscow, Technosfera Publ., 2011. 576 p. (Rus).
4. Yilei Gu, Lijun Hang, Huirning Chen, Jun Li, Zhaoming Qian, Jun Li. A simple structure of LLC resonant DC-DC converter for multi-output applications. *Twentieth Annual IEEE Applied Power Electronics Conference and Exposition*, 2005, vol.3, pp.1485-1490. doi: 10.1109/apec.2005.1453229.
5. Abdel-Rahman S. Resonant LLC converter: Operation and Design 250W 33Vin 400Vout Design Example. *Infineon Technologies Application Note AN 2012-09 VI.0*, 2012.
6. Freeman D. Introduction to photovoltaic systems maximum power point tracking. *Texas Instruments Application Report SLVA446*, 2010.
7. Bogatyirev N.I., Grigorash O.V., Kurzin N.N., Strelkov Yu.I., Telnov G.V., Tropin V.V. *Preobrazovateli elektricheskoy energii: osnovyi teorii, rascheta i proektirovaniya* [Converters

of electric power: the basic theory, calculation and design]. Krasnodar, BI Publ., 2002. 358 p. (Rus).

Received 21.01.2015

R.V. Zaitsev¹, Candidate of Technical Science, Associate Professor,
M.V. Kyrychenko¹, Candidate of Technical Science, Senior Research Scientist
A.V. Kholod², Senior Engineer,
L.V. Zaitseva³, Candidate of Technical Science, Senior Instructor,
D.S. Prokopenko¹, Master of Science,
G.S. Khrypunov¹, Doctor of Technical Science, Professor,
¹National Technical University «Kharkiv Polytechnic Institute», 21, Kyrpychova Str., Kharkiv, 61002, Ukraine.
e-mail: zaitsev.poman@gmail.com, kirichenko.mv@gmail.com
²Company «ELAKS»,
1, build. 12, Ac. Proskura Str., Kharkiv, 61085, Ukraine.
e-mail: underholod@mail.ru
³Zhukovsky National Aerospace University «Kharkiv Aviation Institute»,
17, Chkalova Str., Kharkiv, 61000, Ukraine.

How to cite this article:

Zaitsev R.V., Kyrychenko M.V., Kholod A.V., Zaitseva L.V., Prokopenko D.S., Khrypunov G.S. Calculation of operating parameters of high-voltage power take-off system for the photovoltaic facility. *Electrical engineering & electromechanics*, 2016, no.4, pp. 63-68. doi: 10.20998/2074-272X.2016.4.09.

V.S. Petrushin

METHODICS, SOFTWARE AND LABORATORY EQUIPMENT FOR AN INNOVATIVE ELECTRICAL ENGINEERING DISCIPLINE

Purpose. Development of innovative electrical engineering discipline «Electric Machines in Mechatronic Systems» in order to improve the training of specialists of electrical engineering specialty. Methodology. The proposed project concerns the educational reforms that promote the intensification of the educational process. Results. The structure of interactive educational and training complex, which is a computer learning tool in the form of software and methodical support, as well as data and knowledge bases and consists of functionally related multimedia learning systems, interactive learning, automated control of the learning process. Originality. To offer online training and research facilities, guidelines for laboratory and computational and graphic works. Practical value. Increase the knowledge of students of educational material related to the discipline of innovation «Electric Machines in Mechatronic Systems». References 11.

Key words: innovative electrical engineering discipline, sections of the academic discipline, guidelines for calculation and graphic works.

Предлагается инновационная электротехническая дисциплина «Электрические машины в мехатронных системах». Обосновывается необходимость изучения дисциплины студентами электротехнической специальности. Приведены разделы и объем дисциплины, а также методическое, программное и лабораторное обеспечение, способствующее качественному усвоению учебного материала. Перечислены разработанные мероприятия и методические указания к расчетно-графическим работам данной дисциплине. Библ. 11.

Ключевые слова: инновационная электротехническая дисциплина, разделы учебной дисциплины, методические указания к расчетно-графическим работам.

Currently the educational process concerning the majority of technical disciplines, including electrical engineering, is not keeping pace with the rapid development of the industry. To overcome this drawback, it is advisable to introduce into the educational process of topical subjects, most meet the needs of today, in particular the discipline «Electric Machines in Mechatronic Systems». Sections of discipline are: semiconductor converters of mechatronic systems; features of the induction motors in adjustable electric drives, valve drives, design of regulated induction and brushless motors, DC motors work in regulated electric drives, transformers for mechatronic systems, especially of synchronous generators to the converter load.

The use of variable speed drives (VSD) which are the basis of modern high technology in all sectors of industry and transport makes it possible to improve the manufacturing processes, provides comprehensive mechanization and automation of production, enhances the quality of products, reduce its production costs, increase productivity, improve the reliability and life of the equipment. Widespread use has led to VSD what a modern electric drive is not only energy-power basis capable of supporting production mechanisms necessary mechanical energy, but also a means of process control as well as tasks for the implementation of the quality of production processes currently in the majority of cases are assigned to the adjustable control system ac-

tuators in conjunction with systems technological automation. Of particular importance is the use of energy-saving aspects of the VSD. In connection with the increase in energy prices, in particular for electricity, and limited increase in power generating capacity problem of energy saving systems, including the reduction of power consumption, it is of particular relevance. Energy conservation has become one of the priority directions of technical policy in all developed countries. This is due, firstly, to the limited and non-renewable primary energy, and secondly, with the continuously increasing complexity of production and the value in the third to global environmental problems.

Electromechanical systems with adjustable induction (IM) and electronic (EM) motors in which the union of energy and information processes takes place, ensure maximum use of the opportunities and achievements of electronics for converting electrical energy into mechanical energy. This is achieved by increasing the service life of equipment, reducing operating losses, high reliability.

Insufficient knowledge of the operation of the main unit controlled electric drive - IM or EM - does not allow the drive to improve due to the modernization of this link. A comprehensive analysis of IM and EM in VSD systems based on a systems approach and systems analysis methods makes it possible to design a special adjustable IM and EM with improved adjusting, launchers, dynamic and

vibroacoustic performance, reduced mass, size and cost characteristics. The demand for professionals possessing knowledge gained in the process of studying the discipline is observed in all areas of industry and transport, which are used electromechanical energy conversion devices. Particular influence is expected in the electrical industry, engaged in the design and manufacture of motors under consideration [1].

The proposed project concerns the educational reforms that promote the intensification of the educational process, in terms of the development of courses for a bachelor's degree. Academic discipline «Electric Machines in Mechatronic Systems» can be introduced into the educational process on the basis of the principles stipulated by the European Credit Transfer System (ECTS). Formation of individual student's educational plan provides a choice of this discipline, respectively structural and logical scheme of training. Workload in the discipline of four ECTS credits in one semester. It provides 30 hours of lectures, 15 hours of laboratory exercises. In the process of studying this discipline students perform independent course work. Control of Learning is carried out with the use of modern methods and techniques and recorded estimates ECTS scale. The discipline can be taught in the traditional mode and in remote mode.

Modern teaching techniques should be adapted to the new principles of the organization of educational process is provided by the introduction of the industry has problems raising the level of preparation of students to engineering. Fixed assets should include measures for the development and implementation of information technology education, the development of research and scientific and technological activities in the education system. Innovative engineering discipline should be provided with modern methodological and software development, allowing not only the conduct of full-time, but also in absentia, remote, post-graduate training. Using the European educational trends in Ukraine will bring the national standards of teaching to the standards of European education. One result is the establishment of a working relationship between the training activities, scientific research, production and social practice.

To solve the above was carried out as follows:

- satisfied formation (development) of innovative technical discipline, training material that is the most relevant topics, and that topicality confirmed the latest developments in the electrical industry. The relevance of the discipline «Electric Motors in Mechatronic Systems» supported by the extensive use of VSD in all branches of industry and transport for sustainable management process while minimizing energy consumption;

- carried out the development of the structure of interactive educational and training complex for this innova-

tive discipline, which is a computer learning tool in the form of software and methodical support, as well as data and knowledge bases and consists of functionally related multimedia learning systems, interactive learning, automated control of the learning process;

- made the development of multimedia teaching system comprising electronic textbooks and teaching aids for the course in the form of media, as well as various manuals;

- carried out the development of interactive learning system, which is a computer simulator, with which you can perform a number of settlement-graphic (analysis of the serial general-purpose IM in different systems of VSD, designing special controlled IM and EM to work in VSD) and virtual labs for study It features the work of IM and IM in different systems of VSD. To perform an interactive learning system developed by multi-level software, allows the analysis of electromagnetic electromechanical, power, thermal, mechanical, vibro-acoustic processes in the engine and on the basis of this analysis, to carry out an automated selection and design optimization motors of VSD. The opportunity of communication developed software with other commonly used in the industry and computing facilities;

- made the development of an automated control system, which serves for the input, current and final control, and includes testing programs, a database of test questions and answers, registration and accounting log, temporary training statistics in graphic form;

- providing support to developing individual educational trajectories, using the system, open and distance education in remote access via the global Internet network, which has interactive and differentiated approach to learning;

- quality education is possible by this innovative technology discipline everyone access to all comers methodical and program materials;

- possible formation of an active dialogue between the users in the study of this discipline and communities with an interest in this technical discipline;

- data can be provided and the sharing of knowledge required for new educational and research approaches for the presentation and dissemination of results, preparation of research presentations.

Computer code DIMAS-Drive [2] performs mathematical modeling of physical (electromagnetic, electromechanical, thermal, mechanical, vibro-acoustic) processes in static and dynamic modes of induction motors, regulated electric drives with matching transformers and gearboxes, with semiconductor converters, different types, species and management methods, frequency control laws. Mathematical models take into account the structural features of the motors (closed and secure ver-

sion) and cooling (self-cooling and independent cooling, ventilation ducts), squirrel cage design. Taken into account the impact on the physical processes of magnetic circuit saturation, displacement currents in the windings, the presence of the highest space-time harmonics. We consider the mechanical and vibro-acoustic performance in dynamic conditions. On the basis of multiple targeted simulation taking into account the nature, size and mode of operation of load in a certain range of control is carried out design (structural and parametric optimization) special controlled asynchronous motors with different formulations of the problems (designing a predetermined control range, design, taking into account the duration of the work on specific speeds, projecting a predetermined tachogram considering transitions).

Developed guidelines [3-11]: for laboratory work on the experimental stands or virtual laboratory works; to the settlement and graphic works: a study of electromechanical and power characteristics of the controlled induction motors; analysis of the thermal state of the controlled induction motors; analysis of the vibro-acoustic performance of controlled induction motors; Study the performance of electric rolling stock traction with induction motors; analysis of electronic motors.

Performing by students laboratory work on experimental stands or virtual labs to study the characteristics of motors and drives at the phase and frequency control makes it possible to fix in practice theoretical principles.

The knowledge gained as a result of studying the discipline «Electric Machines in Mechatronic Systems» can be used when the final works on the Bachelor and Master levels.

Implementation of a large number of educational projects (traction induction motors of electric locomotives and urban electric transport, motors of pumping and ventilation systems controlled performance, conveyors and transporters, roller conveyors, geared and gearless elevator winches, etc.) showed that as a result of the design could reduce the power required frequency converters and reduce the size of motors at constant capacity or increase their power at constant dimensions in agreement converter settings and design motors for these settings.

REFERENCES

1. Petrushin V.S. *Asinhronnye dvigateli v reguliruemom elektroprivode: Uchebnoe posobie* [Induction motors in adjustable electric: Textbook]. Odessa, Nauka i tehnika Publ., 2006. 320 p. (Rus). Available at: <https://books.google.com/books?isbn=966833549x>.
2. Petrushin V.S., Rjabinin S.V., Yakimets, A.M. *Programnyj produkt «DIMASDrive». Programma analiza raboty, vybora i proektirovaniya asinhronnyh korotkozamknutyh dvigatelej sistem reguliruemogo elektroprivoda* [Program performance analysis, selection and design of asynchronous cage motors controlled drive systems]. Patent UA, no.4065. (Ukr).

3. Petrushin V.S., Yakimets, A.M. *Metodichni vkazivki do rozrakhunkovo-grafichnoi roboti z distsiplini «Elektrichni mashini v regul'ovanomu privodi» dlia studentiv napriamku «Elektromekhaniki»* [Guidance for calculation-graphic work on the subject «Electric machines in a regulated drive» for students of direction «Electromechanics»]. Odessa, ONPU Publ., 2007. 33 p. (Ukr). Available at: <http://memos.library.opu.ua:8080/memos/jsp/materials.iface?mId=7556>.
4. Petrushin V.S., Yakimets A.M., Lysenko S.I. *Metodichni vkazivki do rozrakhunkovo-grafichnoi roboti z distsiplini «Elektromekhanotronika»* [Guidance for calculation-graphic work on the subject «Elektromekhanotronika»]. Odessa, ONPU Publ., 2008. 13 p. (Ukr). Available at: <http://memos.library.opu.ua:8080/memos/jsp/materials.iface?mId=10594>.
5. Petrushin V.S., Yakimets A.M., Grusha A.V. *Metodichni vkazivki do laboratornykh robot z doslidzhennia kharakteristik asinhronnykh dviguniv pri fazovomu ta chastotnomu reguluvanniakh z distsiplini «Elektrichni mashini v regul'ovanomu privodi» dlia spetsialistiv i magistriv za fakhom «Elektrichni mashini ta aparati» ta «Elektrichnii transport»* [Guidance for laboratory works on research performance phase asynchronous motors with frequency regulation and discipline «Electric machines in a regulated drive « for specialists and masters in the specialty «Electrical machines and apparatus « and «Electric transport»]. Odessa, ONPU, Publ., 2008. 34 p. (Ukr). Available at: <http://memos.library.opu.ua:8080/memos/jsp/materials.iface?mId=11945>.
6. Petrushin V.S., Yakimets A.M., Barbiniagra M.P. *Metodichni vkazivki do laboratornykh robot z doslidzhennia teplovikh kharakteristik asinhronnykh dviguniv z distsiplini «Teplovi ta ventiliatsiini rozrakhunki elektrichnykh mashin» dlia spetsialistiv i magistriv za fakhom «Elektrichni mashini ta aparati» ta «Elektrichnii transport»* [Guidance for laboratory works on the study of thermal characteristics of asynchronous motors with the subject «Heating and ventilation calculations electric machines» for specialists and masters in specialty «Electrical machines and apparatus» and «Electric Transport»]. Odessa, ONPU Publ., 2011. 28 p. (Ukr). Available at: <http://memos.library.opu.ua:8080/memos/jsp/materials.iface?mId=15442>.
7. Petrushin V.S., Yakimets A.M. *Metodichni vkazivki do laboratornykh robot z doslidzhennia kharakteristik asinhronnykh dviguniv pri zhivlenni vid chastotnogo peretvoriuvacha z riznimi nalashtuvanniymi z distsiplini «Elektromekhanotronika» dlia magistriv za fakhom «Elektrichni mashini ta aparati» ta «Elektrichnii transport»* [Guidance for laboratory works on research performance asynchronous motors with power from the frequency converter with different settings on discipline «Elektromekhanotronika» for masters in specialty «Electrical machines and apparatus» and «Electric Transport»]. Odessa, ONPU Publ., 2011. 25 p. (Ukr). Available at: <http://memos.library.opu.ua:8080/memos/jsp/materials.iface?mId=15445>.
8. Petrushin V.S., Yakimets A.M., Pirkovskii S.M. *Metodichni vkazivki do rozrakhunkovo-grafichnoi roboti z distsiplini «Osnovi elektrichnoi tiagi» dlia studentiv napriamku «Elektromekhaniki»* [Guidance for calculation-graphic work on the subject

«Fundamentals of electric traction» for students of direction «Electromechanics»]. Odesa, ONPU Publ., 2012. 36 p. (Ukr). Available at: <http://memos.library.opu.ua:8080/memos/jsp/materials.iface?mId=17537>.

9. Petrushin V.S. *Metodichni vказivki do rozrakhunkovo-grafichnoi roboti z distsiplini «Vibratsiia ta shum elektrichnikh mashin» dlia studentiv napriamku «Elektromekhaniki»* [Guidance for calculation-graphic work on the subject «The vibration and noise of electrical machines» for students of direction «Electromechanics»]. Odesa, ONPU Publ., 2015. 27 p. (Ukr). Available at: <http://memos.library.opu.ua:8080/memos/jsp/materials.iface?mId=25120>.

10. Rymsha V.V., Yakimets A.M. *Modeliuvannia ventil'no-reaktivnikh dviguniv. Doslidzhennia kharakteristik. Metodichni vказivki do vikonannia rozrakhunkovo-grafichnoi roboti pri pidgotovtsi fakhivtsiv za napriamkom 0922 – «Elektromekhanika»* [Simulation of valve-jet engines. Research characteristics. Guidance for calculation-graphic work at the direction of training 0922 – «Electromechanics»]. Odesa, ONPU Publ., 2006. 26 p. (Ukr). Available at: <http://memos.library.opu.ua:8080/memos/jsp/materials.iface?mId=6923>.

11. Petrushin V.S. *Metodichni vказivki do virtual'nikh laboratornikh robot z doslidzhennia kharakteristik asinkhronnikh dviguniv pri fazovomu ta chastotnomu reguliuvanniakh z distsiplini «Elektrichni mashini v regul'ovanomu privodi» dlia spetsialistiv i magistriv za fakhom «Elektrichni mashini ta aparati» ta «Elektrichnii transport»* [Guidance for virtual lab works on research performance phase asynchronous motors with frequency regulation and discipline «Electric cars drive in a regulated» for specialists and masters in «Electrical machines and apparatus» and «Electric Transport»]. Odesa, ONPU Publ., 2016. 19 p. (Ukr). Available at: <http://memos.library.opu.ua:8080/memos/jsp/materials.iface?mId=26860>.

Received 17.03.2016

V.S. Petrushin, Doctor of Technical Science, Professor,
Odessa National Polytechnic University,
1, Shevchenko Avenue, Odessa, 65044, Ukraine.
phone +380 048 7058494, e-mail: victor_petrushin@ukr.net

How to cite this article:

Petrushin V.S. Methodics, software and laboratory equipment for an innovative electrical engineering discipline. *Electrical engineering & electromechanics*, 2016, no.4, pp. 69-72. doi: 10.20998/2074-272X.2016.4.10.